MICROMECHANICS OF
FIBER-REINFORCED COMPOSITES

E. L. Alexander
A. A. Caputo
M. E. Prado
J. E. Hilzinger

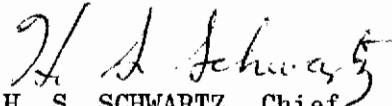Distribution of Document Unlimited

FOREWORD

This technical report, covering a program to investigate the micromechanics of fiber-reinforced composites, is submitted to the Plastics and Composites Branch, Nonmetallic Materials Division, Air Force Materials Laboratory, Wright-Patterson AFB, Ohio, in compliance with Contract AF33(615)-1627. Mr. M. Hennessey is the project engineer for the United States Air Force.

This report was prepared by the Research Department of Rocketdyne, a Division of North American Aviation, Inc., and covers the 12-month period ending on 30 June 1965.

This report was submitted by the authors on 5 November 1965. The Rocketdyne number assigned to this report is R-6260. This technical report has been reviewed and is approved.

H. S. SCHWARTZ . Chief
Plastics & Composites Branch
Nonmetallic Materials Division

ACKNOWLEDGMENT

The authors wish to thank the following individuals of the Rocketdyne Research Department for their special contributions to this investigation:

F. P. Hollenbach--Photoelastic Model Fabrication

J. R. Fulton and D. A. Shipley--Photography

R. S. Goldberg--Work on the initial phase of the program

The assistance of Mr. H. S. Schwartz, Capt. B. Riley and the program monitor Mr. M. Hennessey of the Air Force Materials Laboratory in providing research guidance and frequent discussions relating to problems in the field of micromechanics is acknowledged.

ABSTRACT

Research on the micromechanical behavior of composites
reinforced with boron and other fibers is reported. A
wide variety of reinforcing elements were used in photo-
elastic matrix materials to form beams, plates, and
three-dimensional microspecimens of varied configura-
tions. The effects of reinforcing element modulus and
elongation were investigated in beams in four- and
three-point loading. The degree of stiffening derived
from various filament reinforcing materials was defined,
and different failure mechanisms were investigated.

Reinforced plates were biaxially tested, and fiber
unbonding, buckling, and the subsequent stress redis-
tribution were observed photoelastically.

Significant advances in microphotoelasticity are
reported. Very small specimens were loaded, and
sharp microscopic photoelastic stress patterns
(including induced flaw points) were photographed.
The filament configurations represent typical lami-
nate geometries, and small flaws were seen to have
a remarkably wide field of influence.

CONTENTS

LIST OF ILLUSTRATIONS

INTRODUCTION

The various divisions of North American Aviation, Inc., have been interested for some time in the design and use of many types of filament-reinforced composite structures. Glass-filament-wound structures were fabricated for use in propellant expulsion tanks as early as 1947 and for thrust chambers somewhat later. Since then, work on filament-reinforced composites has continued, including ablative thrust chambers, advanced filament-wound rocket nozzles, fiberglass pressure vessels and rocket motor cases, wire-reinforced propellants, and fiberglass airplane structures. The most recent research includes boron-filament-reinforced test panels with a titanium matrix which are being investigated for advanced high-temperature, high-specific-strength (and modulus) applications by the Los Angeles Division.

The Research Department of the Rocketdyne Division has been particularly interested in a unique wire-reinforced type of solid propellant. Several contractually supported research programs have been active in the reinforced propellant area during the past four years. A significant level of research activity has also been maintained on glass-filament-wound rocket motor cases, advanced filament-wound nozzles, and new materials such as beryllium wire, boron filaments, and high-strength whiskers.

Because of the diverse combinations of filaments and matrix materials that are being investigated at Rocketdyne and on a wider basis in the various divisions of North American Aviation, Inc., the need for unifying concepts to explain the mechanical behavior of a variety of filament-reinforced composites became apparent.

The necessity to develop more fundamental knowledge of reinforced composite mechanical properties led to a series of research programs to obtain structural design knowledge for wire-reinforced propellants. An

1

outgrowth of these programs was a photostress technique to examine fiber-matrix strain interactions. Methods of measuring filament strain and local strain in reinforced composites were also developed using strain-gage wire and X-ray techniques.

At the time this research program was initiated in July 1964, some complex strain patterns had been observed surrounding reinforcing fibers in a photoelastic matrix, and success was achieved in explaining many of the observed features of the strain pattern with a mathematical model (Ref. 1). Strain-wire measurements in internally pressurized filament-wound cylinders had quantitatively confirmed the extreme anisotropy which was suspected in this type of structure.

A major problem in investigating internal mechanics of reinforced plastic composites is as follows: It has not been possible to obtain knowledge of the true properties of the resin in the immediate vicinity of the rein-forcing elements. There has also been no good method of observing and measuring mechanical interactions between filaments and matrix at the microscopic level inside filament-reinforced structures. The Rocketdyne investigators proposed that the techniques of using internal strain wires and a variety of photoelastic matrix materials should be appropriate to investigate in situ filament-matrix interactions in intimate detail. The necessary techniques to obtain this type of information are now available. Observations and measurements can be made on the microscopic level inside filament-reinforced composites to investigate sources of structural inefficiency and the role of defects or flaws.

In planning this program, attention was focused on investigating the fine detail of strain fields that had been observed surrounding reinforcing elements in a birefringent plastic matrix. It was also apparent that a fundamental understanding of the mechanical response of filament-reinforced composites should involve formulation of mathematical models at a suffi-ciently sophisticated level to account for the strain patterns that were experimentally observed. Although quantitative measurements are not easily

2

made on complex photoelastic models, it was important to extend this aspect of the phtoelastic model observations as far as possible. Useful mathematical models require quantitative knowledge as well as guidance with respect to the general form of the expected solutions. The analytical and experimental aspects of the program were intimately linked together. Preliminary photoelastic observations had revealed strain patterns of such complexity that the mathematician could not hope to hypothesize a corresponding model without first observing the general form expected for solutions in the photoelastic model. However, simple observation of strain patterns in a photoelastic specimen does little to advance fundamental knowledge unless results of the experimental work can be fitted into a logical hypothesis (the mathematical model).

The plan for developing better fundamental knowledge of reinforced composites was as follows:

1. Characterize the mechanical properties of materials to be used in experimental models to the degree necessary.

2. Choose geometrically simple experimental models for initial observations.

3. Verify results with simple models (filament-reinforced beams) in relation to existing mechanical response theory.

4. Extend knowledge gained in testing simple structures to more complex configurations and refine observation techniques.

5. Obtain quantitative measurements to the degree possible with more complex structures.

6. Use known mathematical solutions and impose results of observations as perturbations due to the influence of reinforcing elements.

7. Create new mathematical models where existing concepts prove inadequate.

8. Define the consequences of analysis and experimental observations in relation to useful knowledge of filament-reinforced composites.

3

SUMMARY AND DISCUSSION

The value of this investigation of micromechanics of filament—reinforced composite materials depends largely on relating results of this work to the design and use of reinforced composite structures. Some of the approaches to the structural problem and details of techniques for observing filament—matrix stress phenomena may be useful in suggesting other ways in which the efficiency of filament—reinforced composite structures might be improved.

The work reported herein covers a large number of topics ranging from mechanical properties of polymeric matrix materials and various reinforcing filaments to reinforced beams, plates, and a number of microspecimens with a varied geometry.

Photoelastic techniques are used extensively, but not exclusively, in investigating details of the state of stress in mechanically loaded composite specimens. The approach to photoelastic analysis may be unusual to the degree that a quantitative stress analysis is the ultimate objective in examining most of the reinforced specimens. This approach is usually not required in photostress analysis of homogeneous structural models. In the latter case, mechanical loads imposed on a photoelastic model quickly reveal critical stress concentrations in a structural part. The designer can simply change the shape of the part to obtain a more even stress distribution, and knowledge of absolute stress values is neither desired nor required. However, in filament—reinforced composites, the overall geometric shape of the specimen (in this investigation) was of less interest than knowledge of how stress is distributed between fibers and matrix at local points in the specimen. A quantitative stress analysis such as the one reported for filament compression is most useful in the study of stress transfer mechanisms.

Prior to describing specific results of this investigation, it should be
mentioned that the work represents a survey which could not possibly
explore in detail all of the topics which are covered. It was not
intended that any phase of the research should dominate the remainder
of the program. However, the most recent observations of microscopic
strain patterns are perhaps the outstanding highlights of the program.
The microphotoelastic pictures serve to stimulate the imaginative
resources of the materials investigator.

By refining techniques to obtain much improved optical resolution with
microspecimens, a technical breakthrough has been achieved in this pro-
gram in support of the experimental science of micromechanics of rein-
forced composite materials. Photographs of microstrain fields which show
several orders of sharp photoelastic fringe lines in a space considerably
less than the 0.005-inch diameter of reinforcing elements are reproduced
in this report. With this resolving power, it becomes feasible to obtain
a quantitative analysis of strain fields at the microscopic level. An
example of this type of analysis for a reinforcing filament in compres-
sion loading is presented in this report.

In general, the theoretical and experimental aspects of micromechanics
research on reinforced composites must be brought together in some
manner to achieve useful results. It would appear that the theory-
experimental interface must involve prediction of numerical values of
strain (at the microlevel) and verification by measured experimental
results. This concept is expanded in relation to specific experiments
throughout this report.

FLAWS AND FAILURE MECHANISMS

A study of failure mechanisms was one of the objectives of this research. The investigators were particularly interested in extending experimental techniques for obtaining stress in reinforced composites as far as possible to analysis at the microscopic level. A microanalytical capability was desired for several reasons:

1. The region in the matrix immediately surrounding the fibers in a reinforced composite is considered by many investigators to have an important influence on mechanical properties of the composite.

2. Flaws most probably originate at the filament-matrix interface; therefore, the ability to observe and measure local strains in this region could be of value in understanding reasons for structural failure and in evaluating improved matrix materials.

3. Preliminary observations had indicated that a nonuniformly stressed sheath of matrix material might exist in the neighborhood of fibers under certain load conditions. Under such conditions, maximum local stress points are of greater interest than average values, and a detailed study in the region of the filament might explain structural behavior which could not be interpreted in the large.

It proved possible by careful preparation of microspecimens to observe birefringent strain patterns at a magnification as high as 320X in this research program. In two specimens which were observed at high magnification under compressive force microscopic flaws were observed at inception. It was of interest that of two possible flaw locations, both were observed. In one case, failure initiated in the matrix and traveled partially around a 5-mil boron filament. The crack did not extend more than 1 mil from the surface of the filament. Several photoelastic fringe

7

lines converging at the crack indicated a state of high local stress. In the other case, failure occurred in a boron filament and many fringe lines were clearly evident in a distance considerably less than the diameter of the filament.

In addition to high-fringe resolution, the observed strain pattern demonstrated extremely large areas of influence exerted by each of these relatively small flaw regions. Both of the microspecimens were cut from plates and contained end views as well as longitudinal profiles of other fibers. There was a high degree of geometric symmetry in the arrangement of the reinforcing elements and also in the fringe lines emerging from areas where compressive loading was applied. The flaws clearly caused major changes in the symmetrical strain field at a distance sufficient to involve neighboring reinforcing elements which were several fiber diameters removed.

Another type of flaw, consisting of unbonding along the surface of boron filaments, was observed at high stress in testing reinforced beams. The influence of the unbonded region also extends for a considerable distance.

Distinctly different types of failure depending on the number (volume density) and kind of reinforcing elements were observed with filament-reinforced beams. With no more than two reinforcing elements, a branched crack initiated at the tension (bottom) side of the beam and traveled in symmetrical, curved paths, terminating again at the tension side of the beam. With high-modulus reinforcing elements, the beams failed by cracking perpendicular to the bottom edge. Lower-modulus reinforcing elements appeared to yield a failure mechanism intermediate between the two extremes. Frequently, a crack would start perpendicular to the bottom edge of the beam but it would branch to either side along a curved path until a reinforcing element was encountered. Depending on the angle of encounter, the crack would break the reinforcing fiber or follow the fiber for a distance before branching off on a new curved path.

8

REINFORCED BEAMS AND PLATES

A simple geometric pattern of parallel reinforcing wires in a beam was selected to check experimental techniques and to start analysis of photoelastic stress patterns to compare with a known solution for non-reinforced beams (Ref. 2). Measurements at low load levels confirmed that the reinforced beams behaved as theory predicts and, therefore, that methods used to prepare the specimens did not introduce aberrations in mechanical properties.

It was not possible to position all of the reinforcing fibers in the beam specimens symmetrically and in a perfectly accurate pattern. However, measurements of the actual fiber locations in each specimen with an optical comparator gave a set of dimensions from which a section modulus could be calculated. Comparisons between beam specimens were made taking individual beam dimensions into account.

The experiments with reinforced beams included measurements of stress inside the reinforcing filaments as well as the surrounding stress in the photoelastic matrix. This was accomplished by using strain gage wire for the reinforcing elements and a Wheatstone bridge to measure change in resistance of the reinforcing wires located at varying distances from the neutral axis. The measured strains were in agreement with theoretical calculations. The feasibility of refining the technique involving strain gage wires by butt welding leads with higher electrical conductivity to a shorter length of gage wire was established. More accurate gage lengths and more localized filament strain measurements would be obtained with the improved technique.

Photoelastic strain patterns in relatively wide plates in a strip biaxial tensile test were photographed in color and with monochromatic plane polarized light. A nonreinforced plate and plates with boron and high-modulus steel reinforcing filaments were investigated. A bidirectional

9

pattern of reinforcing filaments with a 60-degree crossover angle was selected to hold the specimen width to 7 inches which was convenient for use in conjunction with the analysis apparatus.

The plate tests were informative at two levels: At low loads the reinforcing elements were very effective in evenly distributing loads from the clamped edges of the plate. At higher loads an extremely interesting incremental stress redistribution process was observed. This appeared to be a "stick-slip" phenomenon analogous to seismic events where strain energy is accumulated in the earth's crust and then released suddenly in slippage at fault lines. It has not been established whether this behavior of the reinforced plates is beneficial from the structural viewpoint. However, a logical line of reasoning can be advanced based on the assumption that structural degradation should be delayed if strain energy is dissipated in stepwise fashion.

Photoelastic patterns resulting from residual stress in the filament-reinforced plates (after failure) were extremely complex, indicating unbonding especially at crossover points. However, the strain patterns at low loads were relatively simple. This test is an excellent illustration of the value of the photoelastic technique in following a single reinforced composite specimen through a region of simple mechanical response to very complex strain distributions at high loads. It is obvious when examining photographs of strain patterns under increasing loads that a simple mathematical model might explain initial mechanical response, but a very sophisticated model would be required to represent the structure just before failure.

The observations on filament-reinforced plates indicate that problem areas in using similar filament-reinforced panel structures will center around methods of introducing loads evenly at the edges. One of the test plates was not loaded evenly, but the filaments apparently compensated for this in the space required to transmit strain to the central region of the plate. The complex concentrated strain patterns appeared first at the clamped edges in both reinforced plate tests. Although a mathematical analysis in this region may be virtually impossible, it

10

appears quite feasible to use photoelastic techniques to study the merits
of various designs for joining filament-reinforced panels.

QUANTITATIVE ANALYSIS OF PHOTOSTRESS PATTERNS

The analysis of reinforced composite photoelastic models of interest is
likely to be tedious and difficult. However, it is highly desirable that
principal stress contours be found for several reasons:

1. The model may contain different materials than the structure
    that it is to simulate. In this case, it would be important
    to establish (if possible) numerical scale factors relating
    stress in corresponding parts of a photoelastic model and the
    simulated structure.

2. Extrapolations may be desirable in working with photoelastic
    models. For example, knowledge of stress distribution at
    high fiber density may be needed, but this information is
    obscured by the presence of a large number of fibers. A suit-
    able solution might be approached by analysis of a series of
    models with decreasing space between filaments. Stress in
    critical regions could be plotted against interfiber distance
    and cautiously extrapolated to the desired filament density.

3. The utility of mathematical models is curtailed to the degree
    that simplifying assumptions may oversimplify the problem to
    be solved. The analysis of photoelastic models yields a wealth
    of quantitative detail which would not otherwise be available.
    Better mathematical models should be feasible on the basis of
    additional information.

4. If the composite components are strained beyond the yield point,
    it may be important to determine where nonlinear deformation is
    taking place. Numerical strain values would be useful to
    investigate this possibility.

As a result of the quantitative analysis of photoelastic reinforced composites for this program, it has been found that it might be feasible to program a large part of the detailed repetitious operations for a computer solution. If the burdensome aspects of the analysis can be transferred to the computer, it should be possible to analyze several important situations such as flaws and unbonded regions near the surface of reinforcing fibers.

COMPONENT PROPERTIES

REINFORCING ELEMENT ANALYSIS

The characterization of reinforcing filaments was directed primarily to
the tensile testing of materials under conditions considered pertinent
to the evaluation of composite reinforced beams and other model photo-
elastic structures to be studied in this program. The specific filaments
evaluated under uniaxial tension conditions produced a broad spectrum of
mechanical behavior. These materials included: (1) boron, (2) E-glass,
(3) tungsten, (4) annealed beryllium, (5) high-strength steel, (6) René 41,
(7) two types of strain-gage wire, and (8) as-received and annealed
aluminum.

Although the effects of several strain rates and gage lengths were exam-
ined, the majority of the tests were conducted at a strain rate of approx-
imately 0.02 in./in./min. to achieve an effective specimen gage length
comparable to the conditions existing in the reinforcing beam analysis.

Experimental Techniques

All tests were performed with an Instron testing machine equipped with
pneumatic gripping devices. Rubber-faced flat jaws operating at 85 to
90 psi were found to be the most reliable vise-type grips applicable to
all the materials tested in the ambient 75 ±5°F temperature range.

A problem exists in determining modulus values from fiber tensile test
data. The modulus is derived as a ratio of two parameters, force and
elongation measured on the testing machine and therefore cannot be more
precise than either of these variables. Moreover, the experimental error
of measurement of cross sectional area of the specimen is necessarily
included in the derived modulus value.

13

With good quality testing equipment the statistical variance of force measurements and area measurements can generally be less than the elongation variance measured by the testing machine. The elongation measurement can be made more precisely by placing fiducial marks on the specimen and recording strain photographically during load application. This is generally too costly a procedure except for very critical characterization work. Therefore, a simple correction procedure, consisting of a "zero elongation" series of tests, usually provides adequate estimates of observed strain. Basically, the zero elongation tests provide a graphic estimate of filament elongation which is transmitted back into the portion of the specimen being restrained by the gripping devices. This is used to obtain an effective gage length which is greater than the actual distance of jaw separation. This method was applied to all filaments on this program, and resulted in effective gage lengths ranging from 10.5 to 12.3 inches for an apparent gage length (initial grip separation) of 10 inches. A typical application of this technique is shown for tungsten wire in Appendix A. A comparison of elongation derived from the use of the plotted effective gage length and also from the point-to-point correction for "zero" gage length jaw effects is also shown.

Experimental Results

The performance of 10 filament materials is shown in Fig. 1 through 3 and tabulated in Table 1. Figure 1 compares the high-modulus ductile materials with more brittle materials. The glass fiber tensile performance is also shown in Fig. 2 for comparison with aluminum filaments which demonstrated a similar modulus of elasticity. Strain-gage wire results are shown separately in Fig. 3.

Boron exhibits the highest elastic modulus, slightly greater than that of tungsten, followed by beryllium and the steels, in decreasing order. The steel filaments, however, display the highest tensile strength, with boron

14

FILAMENT TYPE	DIAMETER (AVE.–IN.)	MODULUS PSI X 10^{-6}
BERYLLIUM	.00520	45.5
BORON	.00501	56.7
E GLASS	.00462	11.8
HS STEEL	.00398	29.4
RENE' 41	.00398	31.8
TUNGSTEN	.00508	54.7
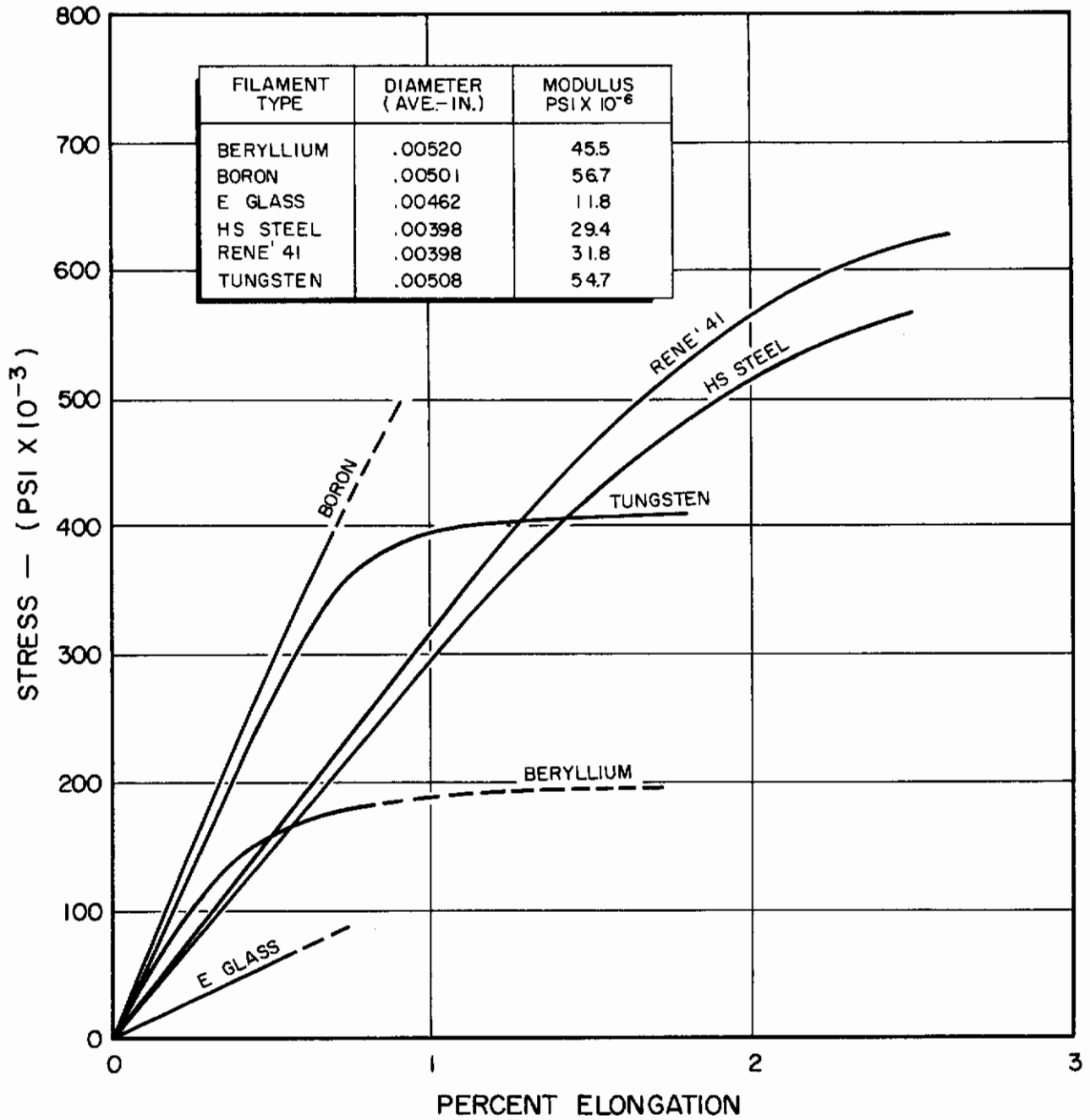
Figure 1. High–Modulus Reinforcement

15
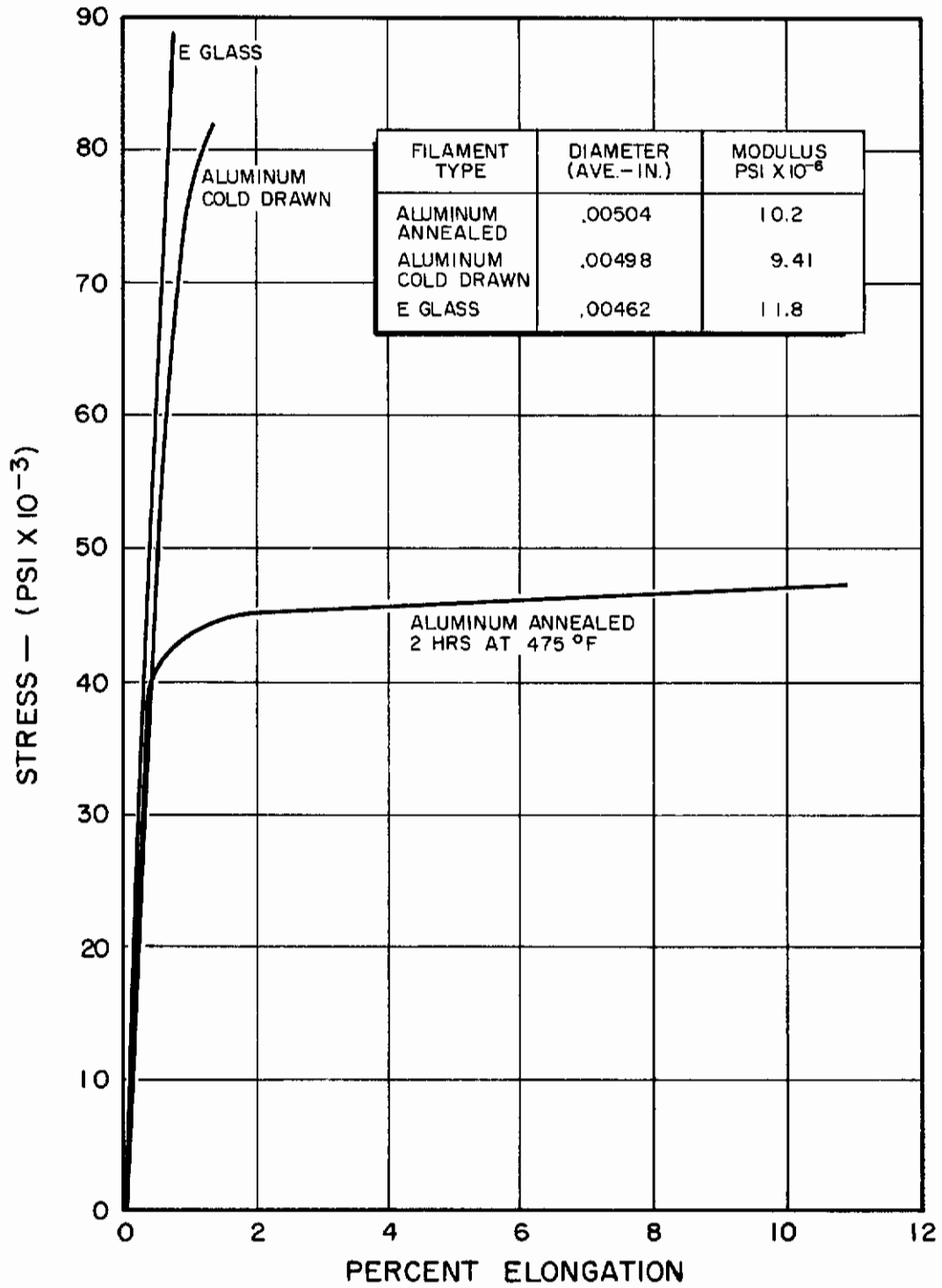
Figure 2.   Aluminum Reinforcement

16
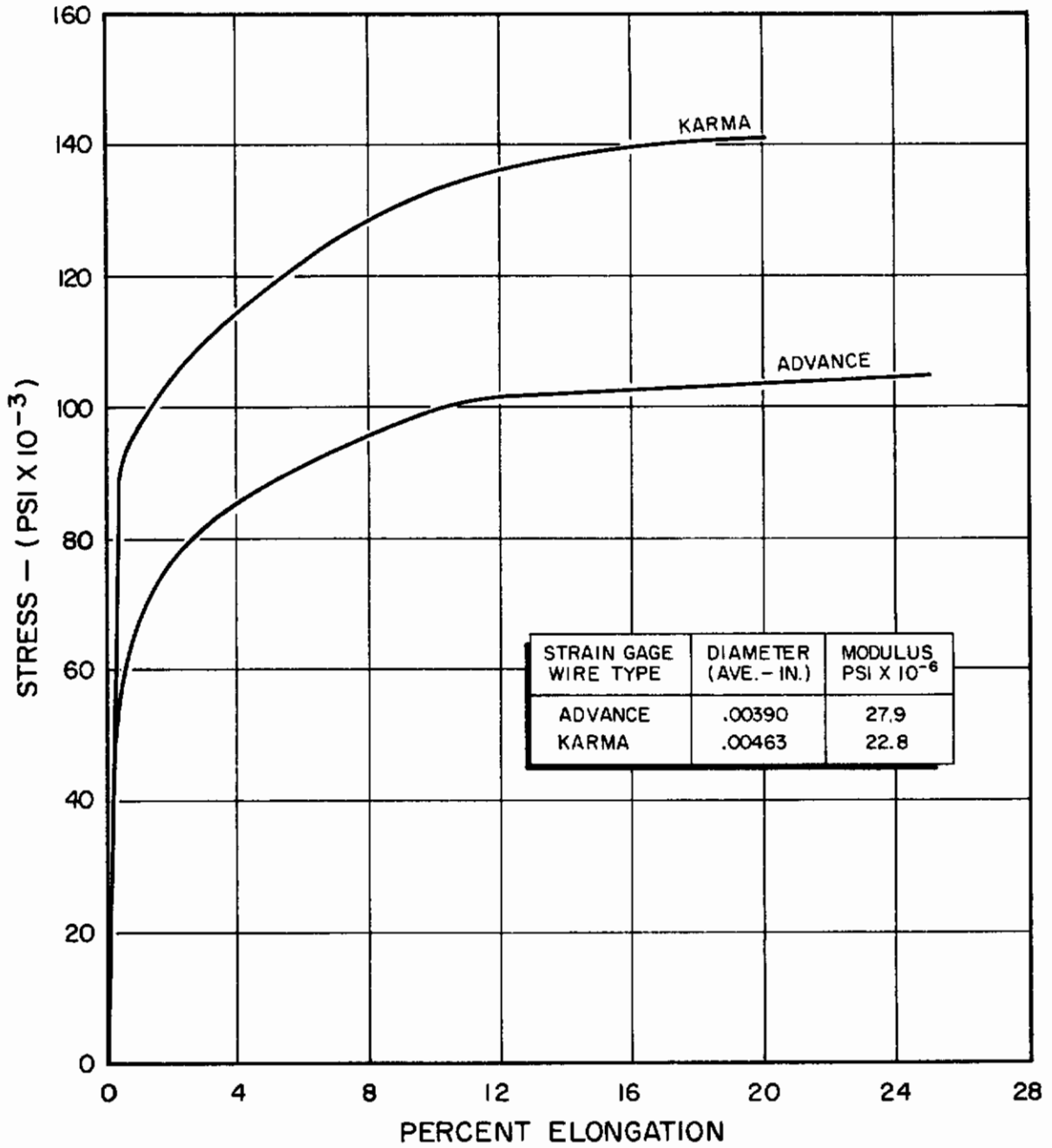
Figure 3.   Strain-Gage Elements

TABLE 1

FILAMENT MATERIAL PERFORMANCE

Filament Material	Mil[1] Diameter	Pounds Force	Stress,[2] psi x 10^{-3}	Elongation, percent	Effective Gage Length, inches	Initial Modulus, psi x 10^{-6}
High-Strength Steel	3.98	1	· 80	0.27	11.1	29.4
		2	161	0.55		
		3	241	0.82		
		4	322	1.10		
		5	402	1.40		
		7	563	2.44		
		7.03	565	2.50		
Rene' 41	3.98	1	80	0.25	10.9	31.8
		2	161	0.50		
		3	241	0.76		
		4	322	1.02		
		5	402	1.28		
		6	482	1.59		
		7	563	1.99		
		7.77	625	2.61		
Tungsten	5.08	1	49	0.09	11.3	54.7
		2	99	0.18		
		3	148	0.27		
		4	197	0.37		
		5	247	0.46		
		6	296	0.58		
		7	346	0.70		
		8	395	1.00		
		8.28	408	1.80		
Boron		1	51	--	11.3	56.7
		2	102	0.17		
		3	152	0.27		
		4.5	228	0.41		
		6	305	0.53		
		7	355	--		
		8	406	0.72		
		9[3]	457	0.82		
		9.21[3]	467	0.84		

[1] Average of 5 specimens

[2] Average of 4 or more tests unless otherwise noted; all tests performed at 70 ±5°F, 0.2-in./min crosshead travel, 10-inch apparent gage length.

[3] Maximum value, average force to break = 7.70 pounds

18

TABLE 1
(Continued)

Filament Material	Mil Diameter[1]	Pounds Force	Stress[2], psi x 10^{-3}	Elongation, percent	Effective Gage Length, inches	Initial Modulus, psi x 10^{-6}
Aluminum Cold Drawn	4.98	0.2	10.3	0.11	10.5	9.41
		0.4	20.5	0.22		
		0.6	30.8	0.32		
		0.8	41.1	0.44		
		1.0	51.4	0.55		
		1.2	61.6	0.70		
		1.4	71.9	0.88		
		1.59	81.7	1.34		
Aluminum Annealed	5.04	0.2	10.0	0.10	11.1	10.23
		0.4	20.0	0.19		
		0.6	30.1	0.30		
		0.8	40.1	0.43		
		0.88	44.1	1.09		
		0.94	47.0	10.9		
Advance (Strain-Gage Wire)	3.90	0.2	16.7	0.06	11.4	27.9
		0.4	33.5	0.12		
		0.6	50.2	0.20		
		0.8	67.0	0.90		
		1.0	83.7	3.70		
		1.2	100.3	10.3		
		1.26	105.5	24.9		
Karma (Strain-Gage Wire)	4.63	0.5	29.7	0.13	10.9	22.8
		1.0	59.5	0.26		
		1.5	89.0	0.39		
		2.0	119	5.10		
		2.3	137	12.7		
		2.37	141	19.8		
E-Glass	4.62	0.2	11.9	0.11	10.5	11.8
		0.4	23.9	0.20		
		0.6	35.8	0.29		
		0.8	47.8	0.40		
		1.0	59.8	0.50		
		1.2[4]	71.6	0.60		
		1.4[4]	83.5	0.70		
		1.48[4]	88.4	0.74		

[1] Average of 5 specimens

[2] Average of 4 or more tests unless otherwise noted; all tests performed at 70 ±5°F, 0.2-in./min crosshead travel, 10-inch apparent gage length.

[4] Maximum value average force to break = 1.12 pounds

TABLE 1

(Concluded)

Filament Material	Mil[1] Diameter	Pounds Force	Stress,[2] psi x 10^{-3}	Elongation, percent	Effective Gage Length, inches	Initial Modulus, psi x 10^{-6}
Beryllium	5.20	0.5	23.5	0.05	12.3	45.5
		1.0	47.1	0.10		
		1.5	70.6	0.16		
		2.0	94.0	0.22		
		2.5	118	0.30		
		3.0	141	0.41		
		3.5	165	0.56		
		3.96[5]	186.5	0.81		
		4.0	188	0.93		
		4.165[5]	196	1.72		
		4.185[5]	197	2.17		

[1] Average of 5 specimens

[2] Average of 4 or more tests unless otherwise noted; all tests performed at 70 ±5°F, 0.2-in./min crosshead travel, 10-inch apparent gage length

[5] Average of two tests, ±0.005-pound force to break.

and tungsten slightly weaker. Boron and E-glass have one common distinction when compared to the other filaments; both materials retain a fairly constant elastic modulus to failure, i.e., no significant yielding is noted. The behavior of annealed beryllium differs markedly; yielding occurs at comparatively low stress levels after an initial high elastic modulus.

The major portion of the reinforcing elements produced reliable and consistent data over a wide range of test conditions. Three materials, E-glass, boron, and beryllium exhibited anomalous behavior. Figures 4 through 6 depict these irregularities in conjunction with an example of one of the more typical consistent materials, tungsten.

E-glass, in addition to wide scattering in filament break forces, was the only material which proved susceptible to gage-length variations at the cross-head test speed of 0.2 in./min. The gross variation in tensile fracture forces is not unexpected. Considerable previous effort (Ref. 3 through 5) has been expended in testing, evaluating, and statistically analyzing failure distributions resulting from similar mixed-flaw populations.

Obviously, the accurate measurement of tensile properties for brittle filaments is difficult (Ref. 6). Boron, in addition to its inherent handling characteristics, is also unique in its fiber structure. The nonhomogeneous nature of the filaments used in this program certainly contributes to the scattering of tensile values. Although microscopic examination did not reveal any filament-surface irregularities which could be related to the scattered test results, the possibility of residual surface stresses, variation in core diameters, and irregular areas of tungsten-boron diffusion undoubtedly exert some influence on the measured performance.

21
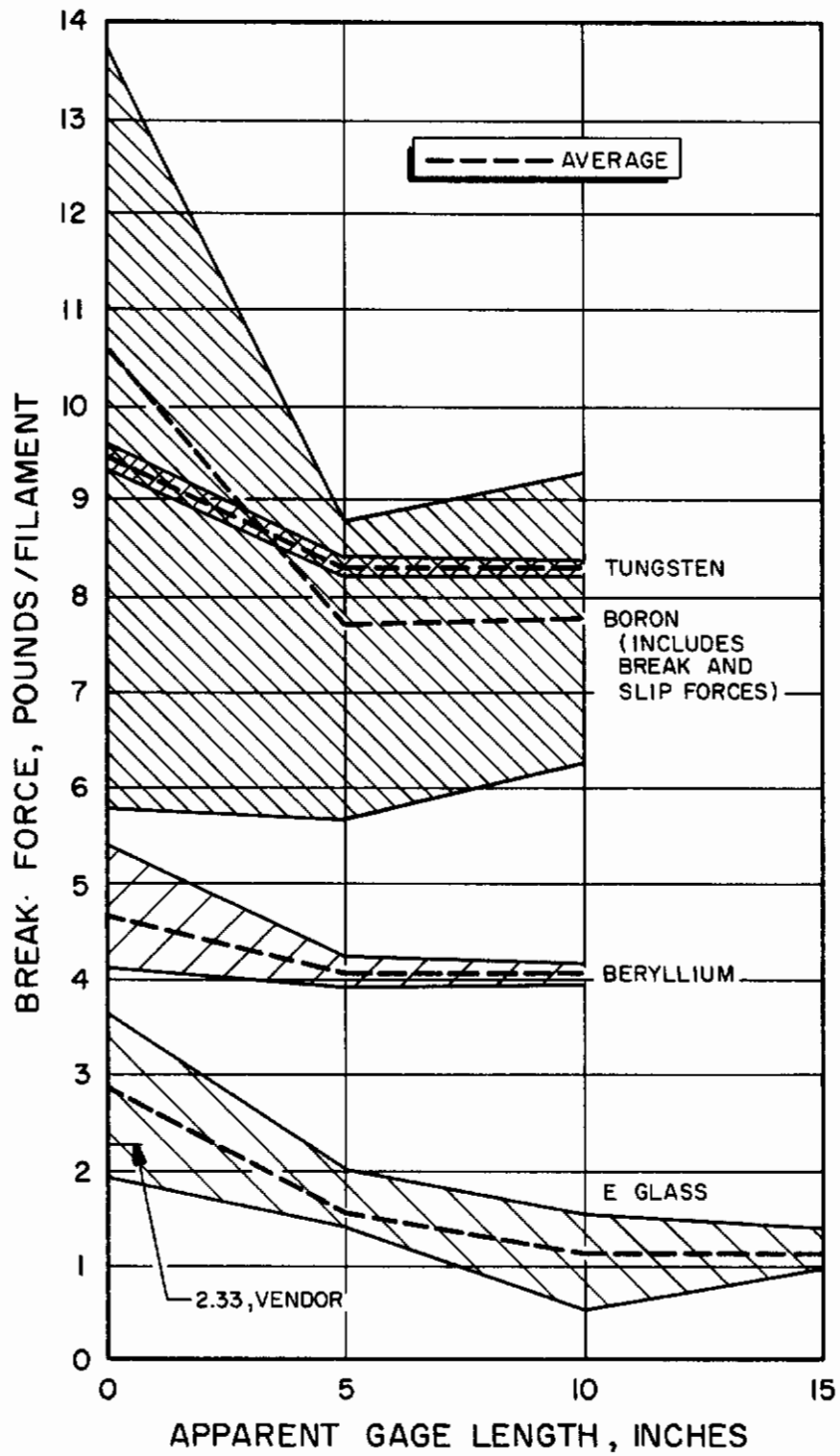
Figure 4. Variation in Wire Properties

22

LEGEND				
	APPARENT GAGE LENGTH – INCHES			
	0.1	5	10	15
BREAK	▲	⬟	●	■
SLIP (OR JAWBREAK)	△	⬡	○	☐
VENDOR TEST	◆			

E GLASS

BORON

FREQUENCY

BREAK FORCE,
POUNDS

BREAK & SLIP FORCE,
POUNDS
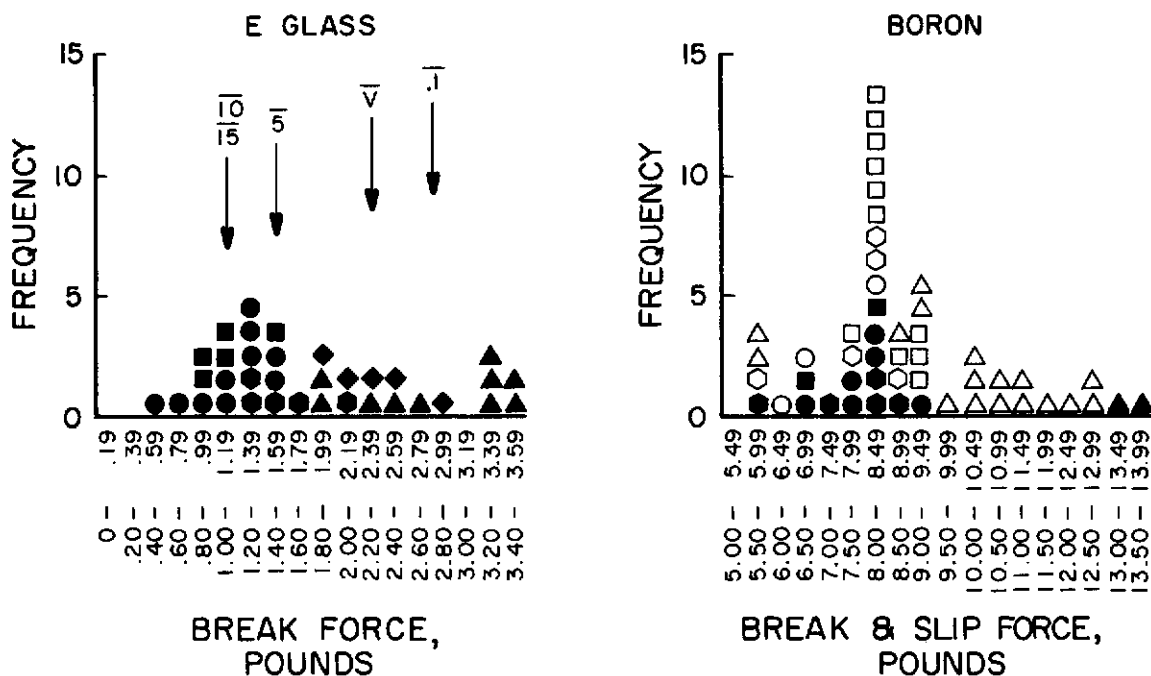
Figure 5. Frequency Distribution

23

BREAK FORCE LBS	GAGE LENGTH–IN. APPARENT	EFFECTIVE	ELONGATION %
3.96	10	12.3	0.85
3.96	10	12.3	0.80
4.16	100	12.3	1.72
4.17	10	12.3	1.71
4.16	5	6.5	2.18
4.19			2.15
4.03	.1	—	—
4.16	.1	—	—
4.63		—	—

BERYLLIUM

——— AVERAGE
——— RANGE

BREAK
△ 10" APPARENT GAGE LENGTH
○ 5" APPARENT GAGE LENGTH

PERCENT ELONGATION

BREAK FORCE, POUNDS/FILAMENT
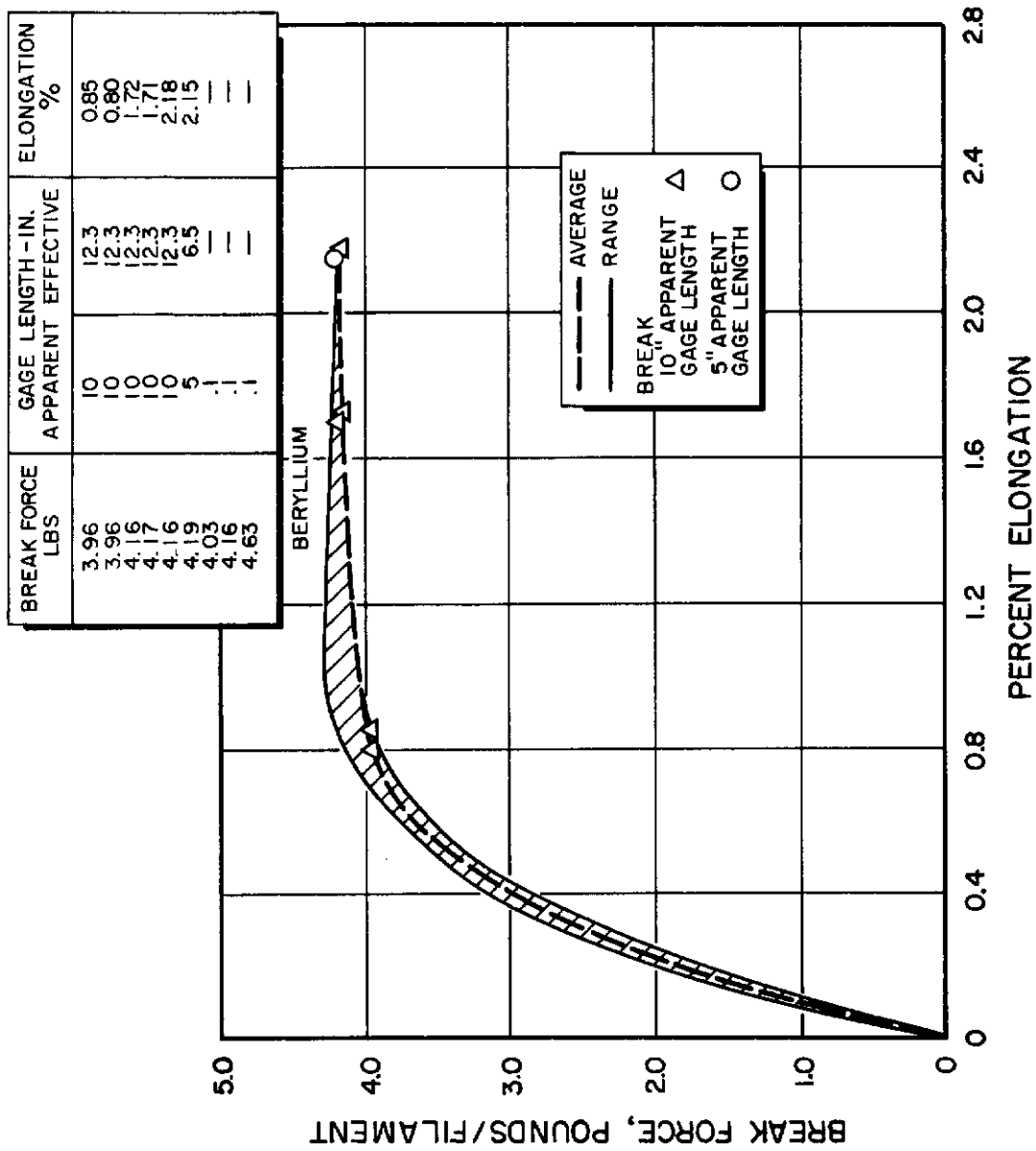
Figure 6.   Characterization of Beryllium Wire

Beryllium is the third material to exhibit irregular behavior, but differs from E-glass and boron in that its tensile strength is accompanied by ductility variations. This phenomenon was observed during a limited number of tests which ranged from a zero- to 10-inch apparent gage length. Figure 6 shows the conditions under which the strain measurements were obtained. Hughel (Ref. 7) discusses the studies of several investigators reporting on the beryllium crystal structure orientations and the modes of deformation which lead to fracture and limited ductility. The possibility also exists that impurities may cause similar occurrences.

PHOTOELASTIC RESIN CHARACTERIZATION

To determine the ability of anisotropic models to give reliable and reproducible measurements, a number of commercially available photoelastic systems were studied. Table 2 describes a typical series. Some of the factors considered in the initial evaluation were resin physical properties, molding procedures, cured resin characteristics, and stability.

Resin systems in the 1000- to 500,000-psi modulus range were evaluated as candidates for the choice of a basic resin system for this program. One high-modulus and one low-modulus system were ultimately chosen and characterized with respect to conditions of cure, stress-optical properties, relaxation, and general molding properties.

The photoelastic resin systems used in this program were selected on the basis of two different levels of Young's modulus and elongation properties. Table 2 summarizes vendor information on some of the mechanical and optical properties of these resins. These photoelastic resins can cover a wide range of properties going from a rubber-like material to a hard brittle structure. The k-factor given in Table 2 is known as the strain-optical coefficient. There is, however, another factor known as

25

TABLE 2

TYPICAL PHOTOELASTIC RESINS*

Type	k^1	Maximum Elongation, percent	Young's Modulus (1000 psi)	Nominal Thickness Available	Tolerances	Maximum Usable Temperature, °F
Sheet Materials						
PS-1	0.14	10	360	0.120 0.080 0.040 0.020 0.010	±0.002 ±0.001	300
PS-2	0.02	3	450	0.120 0.080 0.040	±0.003	500
PS-3	0.02	30	30	0.080	±0.003	400
PS-4	0.005	150	1	0.120	±0.003	350
PS-5	0.11	3	420	0.250	±0.005	Model Material

Type	k^1	Maximum Elongation, percent	Young's Modulus (1000 psi)	Sensitivity Constant To °F	Maximum Usable Temperature, °F
Casting Materials					
PL-1	0.10	3 to 5	420	180	450
PL-2	0.02	50	30	110	400
PL-4	0.10	3	420	250	–

*Photolastic, Inc., Malvern, Pennsylvania

[1] The sensitivity is expressed as fringes per unit of strain applied per unit thickness of plastic.

26

the stress-optical coefficient. These coefficients are used to determine the difference of principal strains or the difference in principal stresses. However, the strain-optical coefficient was not used in this program.

The k-factor, or stress-optical coefficient, is analogous to the gage factor of resistance strain gages and can be determined from:

$$k = \frac{\delta}{t(\sigma_1 - \sigma_2)}$$

where

t = thickness of the model

σ_1, σ_2 = principal stresses

δ = relative retardation of the polarized beams traveling through the model

All of the resin systems used were epoxy in structure. The differences between the resin systems were a result of the curing agent used and differences in polymer backbone. The stability of the resin system and its subsequent optical and mechanical properties are directly related to the curing agent, curing schedule performed on the system, and environmental conditions during the curing period. The principal parameters affecting the optical properties of photoelastic resins are: (1) environmental temperature at time of casting, and (2) amount of hardener added to the photoelastic resin. The environmental temperature at the time of casting affects the optical constant of the resin system only in the time required for the k-factor to reach its stabilized value. A specimen cast with PL-1 resin system at 70 to 90°F will attain 97 percent of the stabilized k-factor value in approximately 24 hours. If the environmental temperature is reduced to 60°F, the period necessary to obtain stable k-factor value will increase to a few weeks.

The stress-optical coefficient reaches a maximum value then decreases as the amount of curing agent or hardener is increased in the photoelastic resin formulation. It is desirable to achieve maximum photoelastic sensitivity (maximum value for k); therefore, an optimum concentration for the curing agent exists. However, formulations containing the amount of curing agent to obtain maximum optical sensitivity may lead to the following undesirable characteristics:

1. The polymerization becomes so rapid that insufficient time is available to process the specimens properly.

2. The cast material is optically nonhomogeneous.

3. Resin elongation decreases sharply.

4. Residual thermal stresses are induced by heat of the polymerization reaction.

For the above reasons, a curative level which yields less than the maximum k-value is frequently used. The resin manufacturer usually supplies information on optimum formulation for each resin system. In the case of PL-1, the manufacturer's recommendation of 18 to 24 parts of hardener per 100 parts of photoelastic resin was followed. In fabricating the specimens with PL-2 photoelastic resin system equal parts of hardener and resin were used.

MODEL PREPARATION

The two routes of model preparation pursued were laminating and casting.
It was expected that the laminating procedure would offer the possibility
of producing specimens with a complex geometry of reinforcing elements
accurately placed. It was also thought possible to produce complex two-
and three-dimensional models by constructing photoelastic laminate struc-
tures containing more than one layer of reinforcement with a minimum of
laboratory time. However, there were certain difficulties in the lami-
nating procedure, and undesirable optical and mechanical properties which
limit the use of this technique.

LAMINATING PROCEDURES

There were, in general, two routes taken in laminating photoelastic
models. The techniques used were: (1) using commercially available
photoelastic sheets, and (2) casting a photoelastic sheet for use in
laminates. Both techniques consist of placing the required reinforcing
elements in a predesignated configuration on a sheet or layer of photo-
elastic matrix.

The difference between the two laminating techniques is that for the
commercial photoelastic sheets, a film of cement is applied to the sheet
and reinforcing elements and a second photoelastic sheet placed on top.
The second technique required the casting of a photoelastic layer and
allowing partial cure of the resin system prior to placing the reinforc-
ing elements. After the reinforcing elements are in place, a second
layer of photoelastic resin is cast on top.

The accurate placement of the reinforcing elements in the laminating
process was not realized because the placing of the cement tended to
run underneath the first photoelastic sheet, changing the dimensions of
the model. Furthermore, the reinforcing elements were displaced from
their original position during the placing of the second sheet and curing
of the cement.

29

In the second laminating technique, the cross-sectional dimensions of the specimen were not changed by resin underrun, but the reinforcing elements were displaced from their original position during the casting and curing of the second layer.

The exclusive use of the casting technique for the production of the photoelastic models was incorporated into this program when preliminary tests on laminated models indicated anisotropic optical properties of the model. Furthermore, the interface present in the photoelastic models produced by the laminating technique prevented microstudies of stress phenomena.

CASTING PROCEDURE

Special casting molds were constructed for the fabrication of photoelastic specimens. One mold consisted of a pair of contoured silicone rubber side dams with split ends to allow for continuous adjustment of size and wire placement in the mold (Fig. 7). A second mold consisted of a special aluminum plate with a 1/2-inch depth and 16-inch span. This plate was used as a master mold from which molds made of silicone rubber were cast. The silicone rubber molds were then used to cast photoelastic reinforced beams. Other molds consisted of split-end dams with straight side dams. These molds were used for the fabrication of reinforced plates, and for specimens used in studies of micromechanics of stress transfer phenomena.

Silicone RTV rubber was selected on the basis of better performance after a number of materials were evaluated as possible molding surfaces. Among those materials considered were aluminum, glass, Mylar, Teflon, and polished brass. Some of these materials were used with various release agents while others such as Teflon and Mylar were used in the virgin state.

30
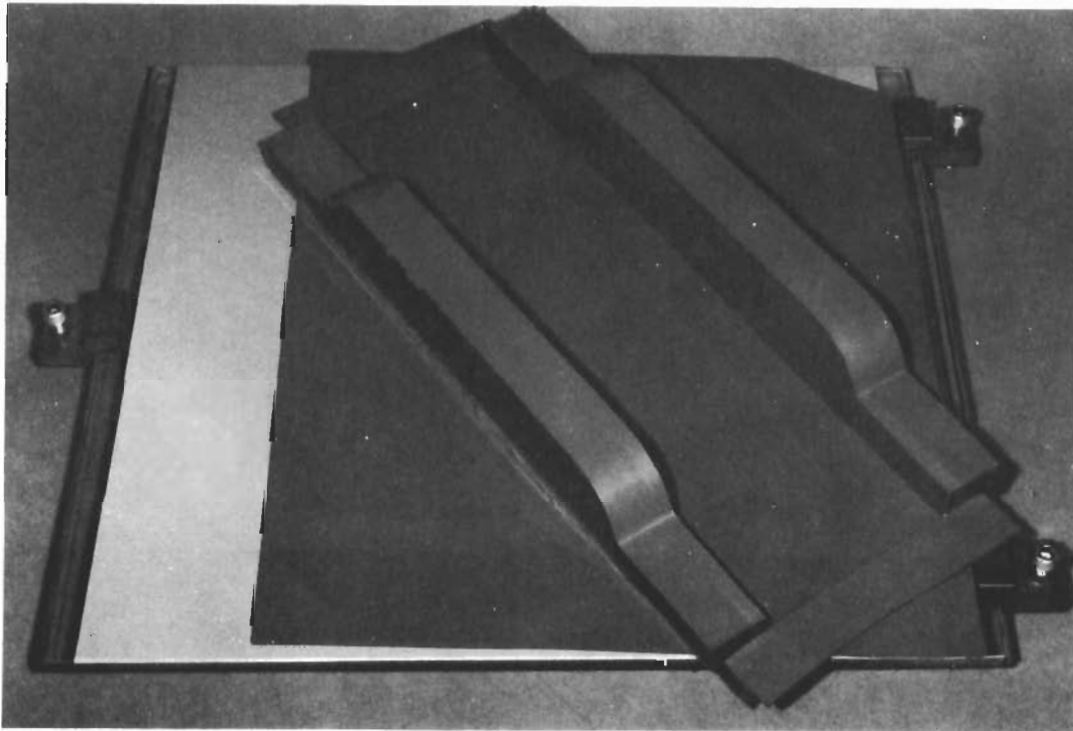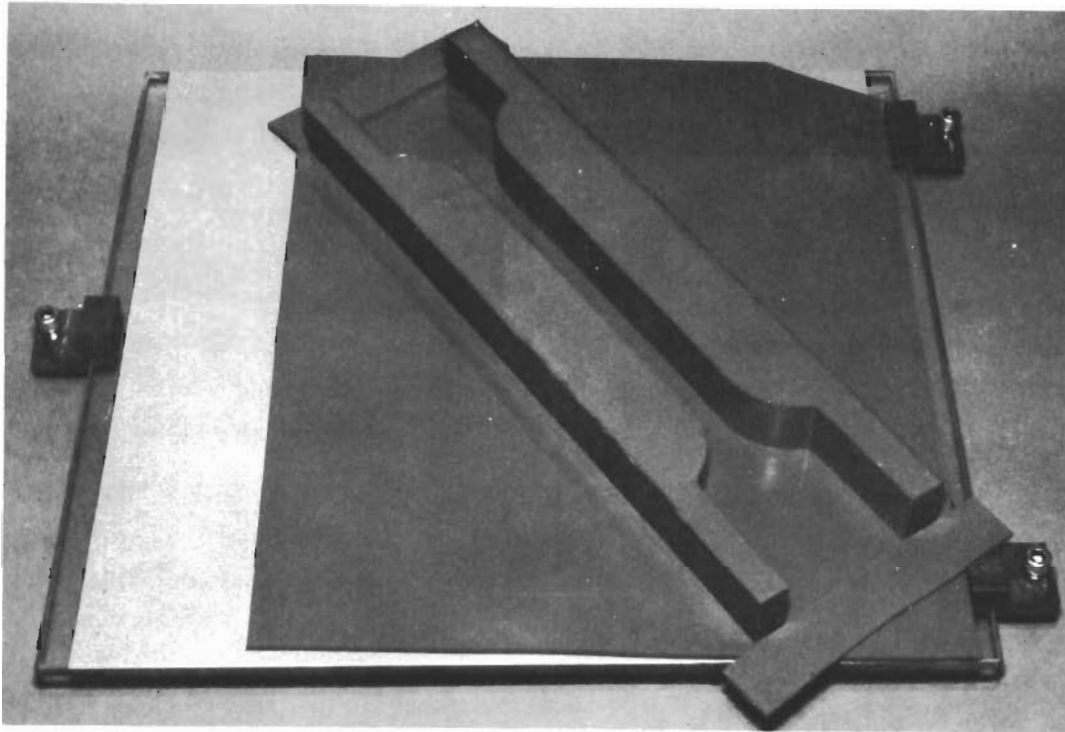
Figure 7. Casting Mold

31

The mold was cleaned with alcohol and placed on a massive granite surface plate. The parts of the silicone RTV rubber mold were supported in this way to minimize effects of vibration during cure, to ensure a high degree of dimensional stability (thermal expansion was negligible with the mold on the granite block), and to provide the required surface smoothness and level condition necessary for good castings. The proper amount of resin was weighed according to the manufacturer's instructions and heated to 150°F to drive off moisture and entrapped bubbles. After cooling the resin to 100°F, curing agent was added as suggested by the manufacturer's formulation instructions, and the mixture was thoroughly stirred. The beaker was then placed in a vacuum oven until a temperature of 120°F was attained. After the resin reached a 120°F casting temperature, it was immediately poured into the mold.

TEST FIXTURES

TENSION FIXTURE

A test fixture was designed and constructed for loading photoelastic
models in tension with the Instron testing machine. The fixture basically
consists of double adapter loading plates which transmit load to the
model through a clamp and pin arrangement. These plates are loaded
through the end-tab plate using a pin in a keyed slot to allow minor
adjustments of the sample for final alignment (Fig. 8).

The fixture design was intended to permit axial loads to be applied to
the model without any bending and to allow failure to occur within the
test section. However, problems which limit the use of the tension
fixture were discovered during the tensile testing by observing the
fringe pattern. The photoelastic fringe pattern indicated nonuniform
loading caused by the pins. Failure of the specimens occurred in the
tab regions rather than in the center section. Moreover, asymmetry of
the photoelastic pattern indicated poor alignment in the Instron tester.
Although the tension fixture fell short of its expected performance and
was not used for tensile tests which are reported, the photoelastic tech-
nique proved to be a powerful tool in detecting small alignment errors
which would escape detection in a standard tension test.

FLEXURE FIXTURE

Four-Point Loading

The four-point loading fixture (Fig. 9) was designed and constructed to
minimize small friction loads in the flexure tests by supporting the
1/4-inch loading shafts in bearings.

The loading heads are fixed to a 1/2-inch aluminum flat plate which is
attached to the Instron crosshead. The supporting heads are fixed to a
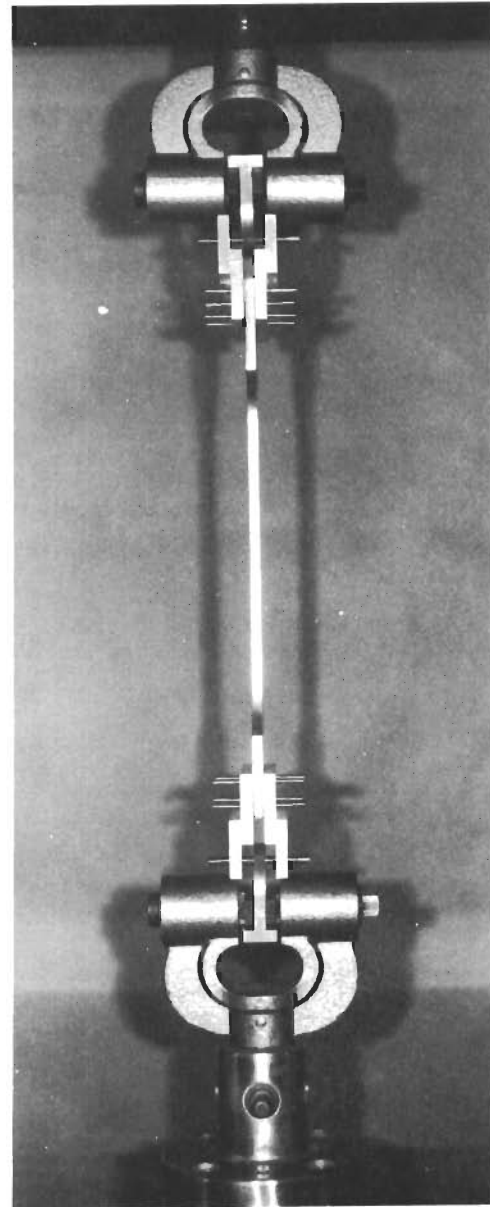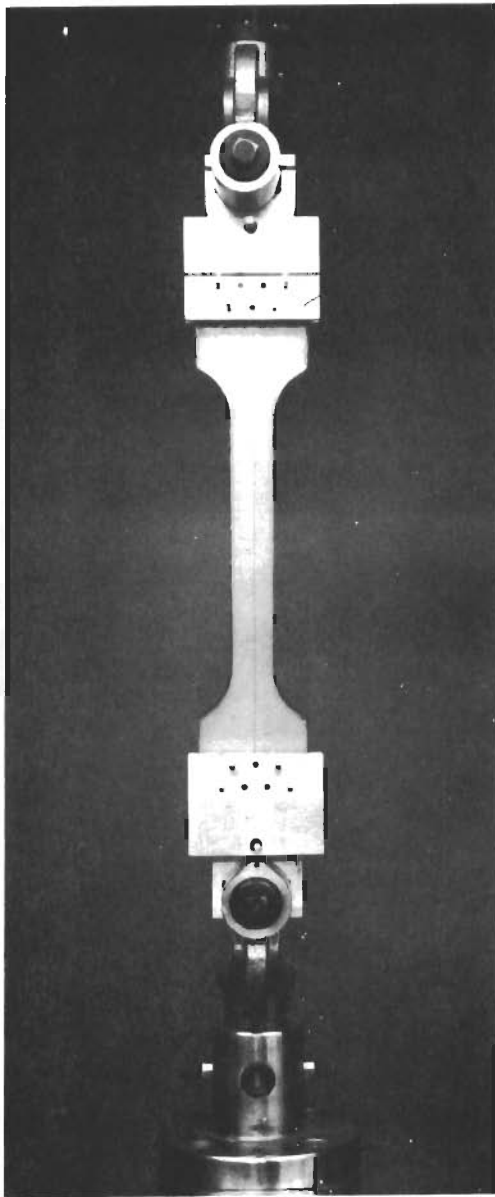
Figure 8. Tension Fixture
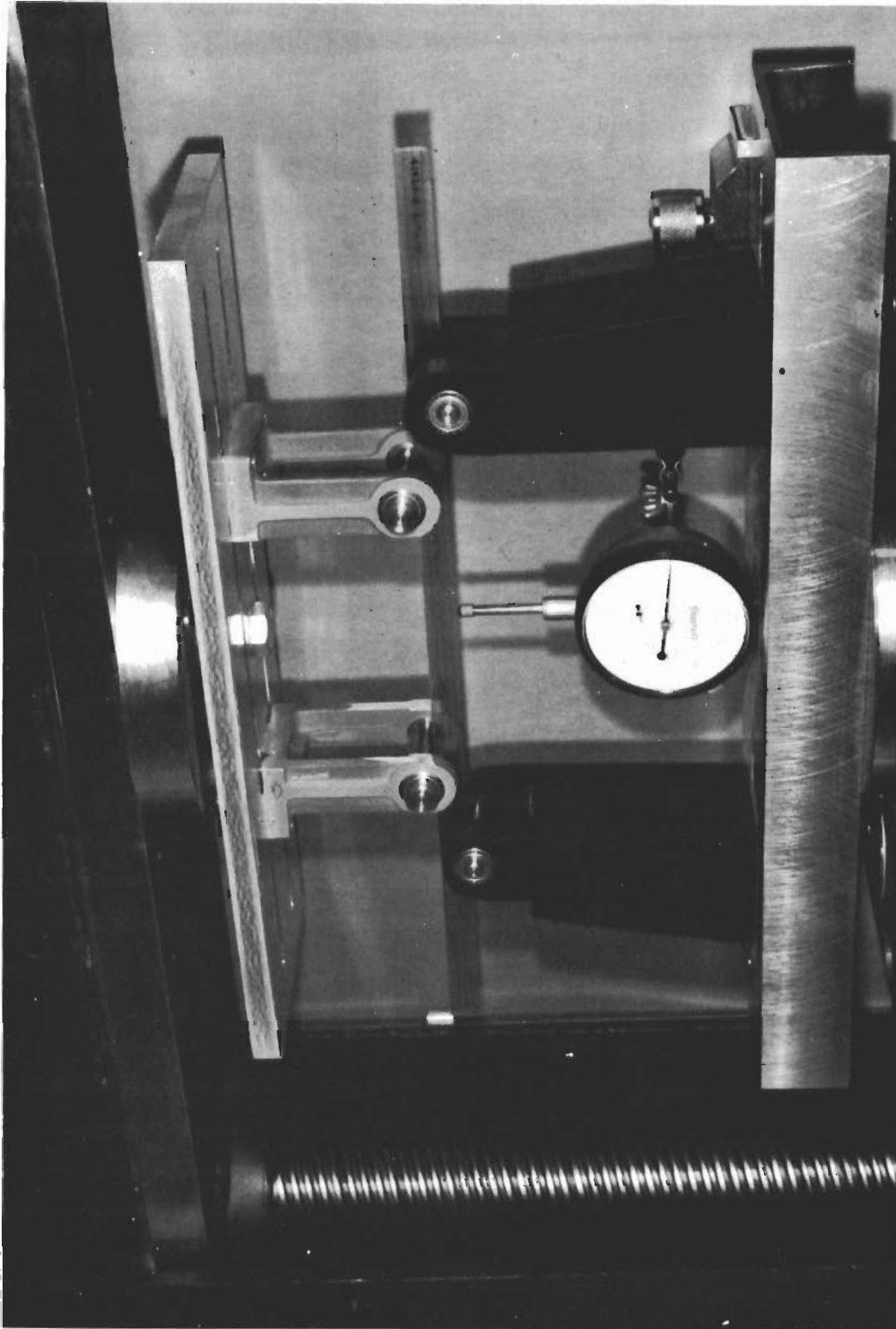
Figure 9. Flexure Fixture

machined channel section which is positioned on the compression cell of the Instron testing machine. The height of the supporting heads from the upper face of the base plate permits deflection measurements with a Starrett dial gage (Fig. 9).

Preliminary photoelastic analysis indicated that this arrangement gave excellent agreement between theoretical calculations and experimental data.

Mid-Point Flexure

The channel base plate and supporting heads of the four-point flexure fixture were used for mid-point loading. The load was applied by attaching the loading head to the crosshead of the Instron testing machine. The channel base was positioned on the compression cell of the Instron testing machine. The symmetry of the photoelastic patterns proved the above loading technique to be a good test method.

PHOTOELASTIC RESIN CALIBRATION

It is possible to obtain a representative sample for calibration from any given resin batch by concurrently producing reinforced and nonreinforced specimens from the same resin batch. In the earlier stages of this program it was only necessary to check the overall resin system variation in properties because the qualitative analysis did not require extensive calibration of specimen samples. In the later stages of the program, where a more quantitative analysis of the models was required, calibration specimens were made with each set of specimens cast.

EXPERIMENTAL PROCEDURE

Two types of tests were performed for the calibration of photoelastic specimens, flexure (four-point loading) and tension. The flexure tests were performed on an Instron testing machine equipped with a compression cell (Fig. 9). The load was applied with the crosshead moving 0.02 in./min. The beam supports were 7 inches apart with the load being applied 1-1/2 inches from each support. For the tension phase, the Instron testing machine was equipped with pneumatic grips. Flat steel jaws operating at 85 to 90 psi and faced with No. 600 sandpaper were found to be the most reliable (Fig. 10).

A dark-field polariscope was used for obtaining photoelastic data. Photographic techniques were used to record a fringe pattern at the points of interest.

DETERMINATION OF THE STRESS-OPTICAL COEFFICIENT

The calibration specimens were made with photoelastic resins (types PL-1 and PL-2) which have moduli of elasticity of 520,000 to 550,000 psi for the PL-1 and 30,000 psi for PL-2. The PL-1 specimens (approximately 1/8 by 1/2 inch) were equipped with SR-4 strain gages bonded to the center of the specimen. These specimens were tested in tension, using

37
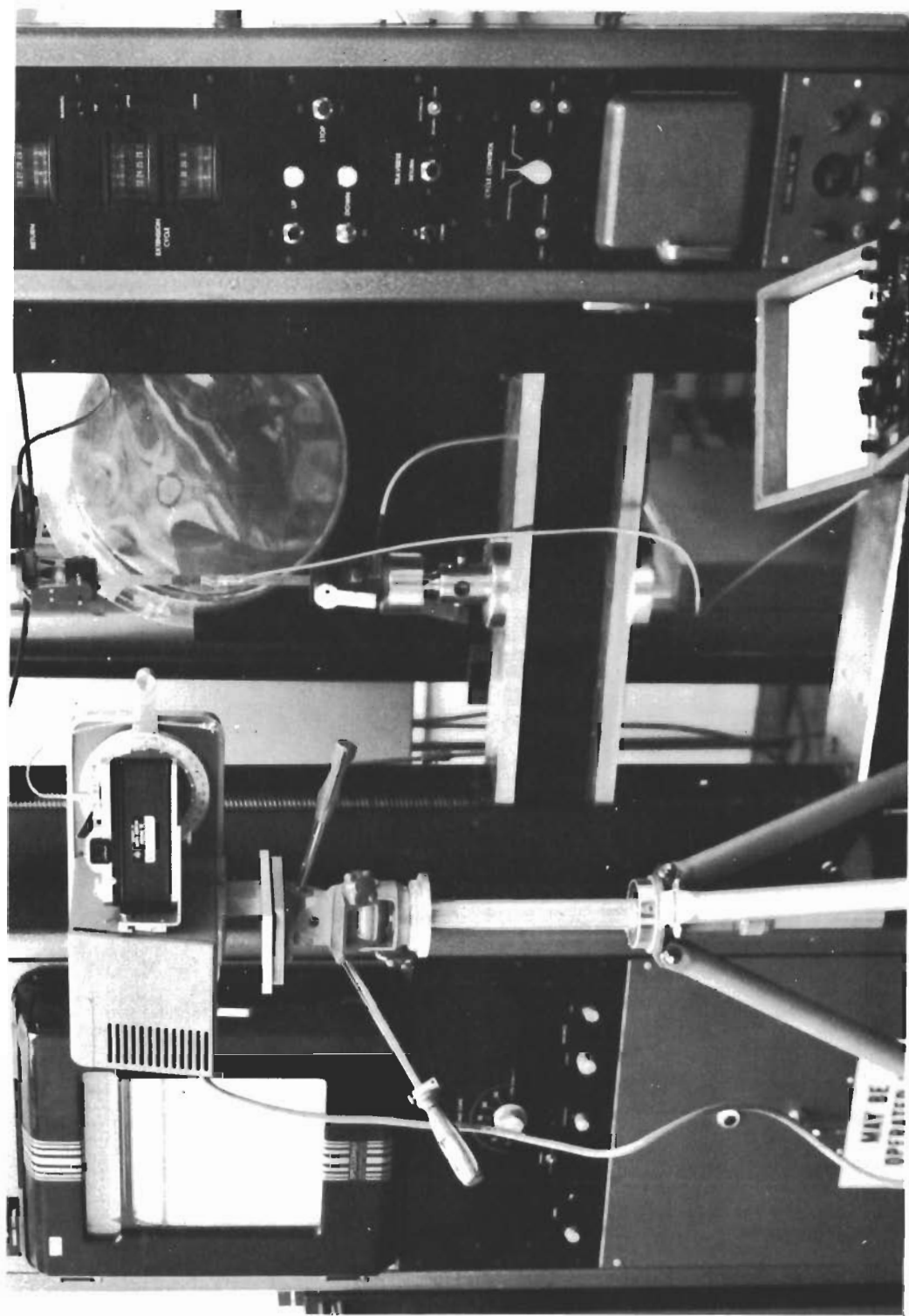
Figure 10.   Tension Test Setup for Calibrating Photoelastic Resins

38

the Instron testing machine equipped with pneumatic grips. A Wheatstone
bridge was used to determine the change of resistance in the strain gages
to facilitate computation of the strain. A transmission polariscope was
simultaneously used for photoelastic analysis.

The above arrangement gave excellent data on the optical and mechanical
properties of the photoelastic resin. In tests where the photoelastic
pattern exhibited asymmetry, indicating poor load distribution, results
of the test were rejected. The birefringent test specimens were quite
sensitive to nonaxial loading (bending superimposed on the tensile load).
This built-in control of the test procedure explains the high degree of
consistency that was obtained in these tests.

The data from the tensile tests are plotted in Fig. 11. The optical and
mechanical properties of the photoelastic resin show extremely good
linearity for the individual specimens. The deviations among Curves
1, 2, and 3 are primarily attributed to differences in the curing cycle
and temperature-time histories of the specimens. A small variation
may have occurred with respect to percent curing agent in formulating
the various series of specimens, and in the case of Curve 1, small bend-
ing stresses were observed in the specimen at higher loads. Replotting
the data from Fig. 11 to bring all the curves through the zero point
would be a valid procedure and would bring test results into closer
agreement. This is not necessary, however, because the only parameter
which is used in subsequent analysis is the slope of the stress vs fringe
order curve.

The modulus of elasticity for photoelastic resin type PL-1 is computed
to be 520,000 psi using Curve 2 and 3.

The stress-fringe curves (Fig. 11) are used to determine the stress-
optical coefficients. Curves 2 and 3 of the stress-fringe order plots
give a stress-optical coefficient of 0.240×10^{-6} fringes/psi, which is
in excellent agreement with the pure bending tests.

39
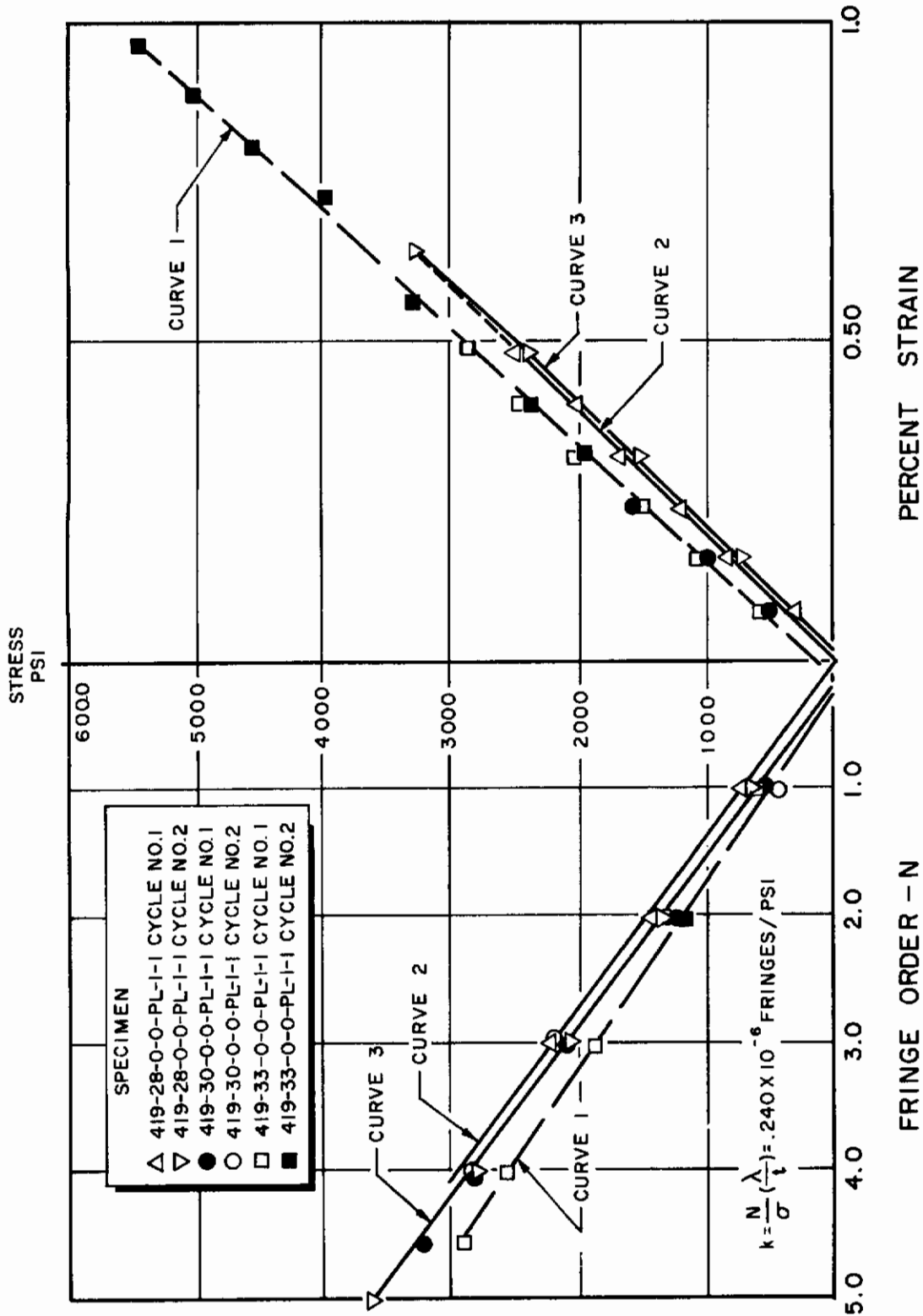
Figure 11. Calibration Curves and Stress-Strain Curves for Tension Testing

The presence of the SR-4 strain gages in the tension specimens did not appreciably reinforce the specimens. This conclusion was made after observation of the isochromatic fringes indicated that no discontinuities in the fringes existed in the area of the strain gage.

Figure 12 was also used to determine the stress-optical coefficient of the photoelastic resin. However, Fig. 13 represents calibration using flexure tests rather than tension where the stress distribution is for a bending moment of 23.25 in.-lb. The optical coefficient obtained from these tests is 0.230×10^{-6} fringes/psi.

Comparison of the stress-optical coefficient as obtained from the tension tests (0.240×10^{-6} fringes/psi) with the optical coefficient obtained from the pure bending tests (0.230×10^{-6} fringes/psi) indicates excellent agreement. The small variation (approximately 4 percent) may be partially a result of specimen aging. The specimens that were calibrated in pure bending were only a few weeks old while the tension specimens had been prepared 3 to 4 months prior to calibration. Also, it is more difficult to obtain pure bending stresses because of machining and edge effects. However, in view of the small variation between optical coefficients, the flexure tests of the beam composites have an added margin of confidence.

A lower-modulus higher-elongation resin (PL-2) was used for reinforced-plate specimens and for microspecimens to emphasize interactions between matrix and filaments. These specimens are described in detail under separate subject headings.

The information required to compute the stress-optical coefficient for the PL-2 resin system is shown in Fig. 14. Tests were conducted at two crosshead speeds (0.02 and 0.2 in./min), and two curves of stress vs fringe order were obtained. As would be expected for low-modulus plastic materials, the mechanical properties and the optical properties are strain-rate sensitive.

41
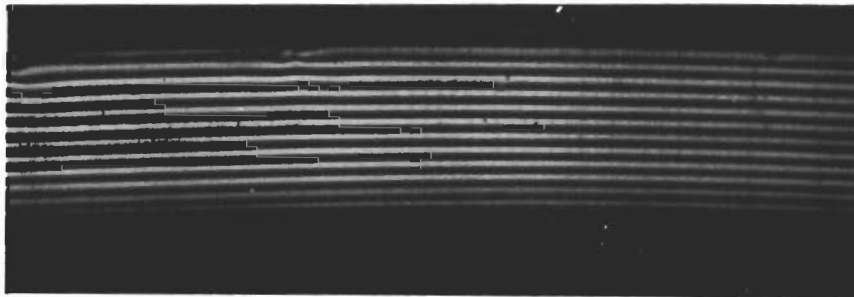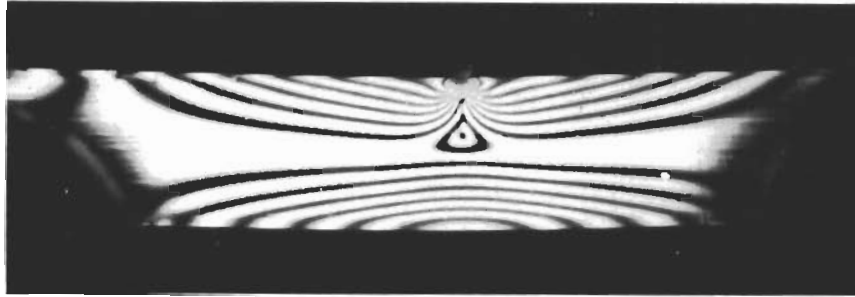
Figure 12. Stress Patterns for Mid- and Four-Point Loading
of Unreinforced Beams Tested in Flexure

The graph shows stress (PSI) versus fringe order N, with the following annotations:

$k = (\frac{N}{\sigma})\frac{\lambda}{t} = 0.226 \times 10^{-6}$ FRINGES/PSI

FRINGE ORDER - N

$k = (\frac{N}{\sigma})\frac{\lambda}{t} = 0.234 \times 10^{-6}$ FRINGES/PSI

$k_{AVRG.} = 0.230 \times 10^{-6}$ FRINGES/PSI

SPECIMEN 419-41-0-0-PL-H
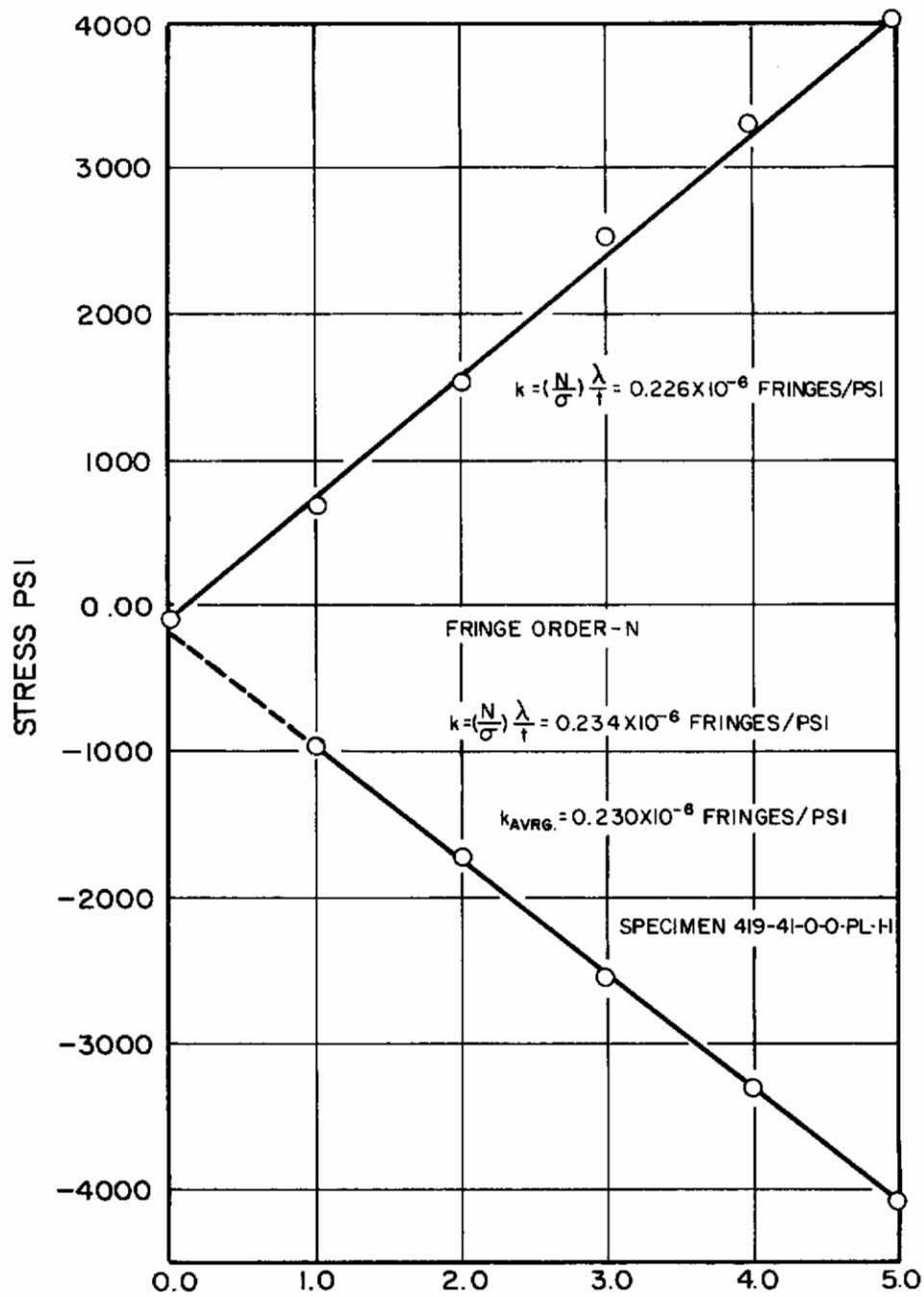
Figure 13. Calibration Curves, Pure Flexure
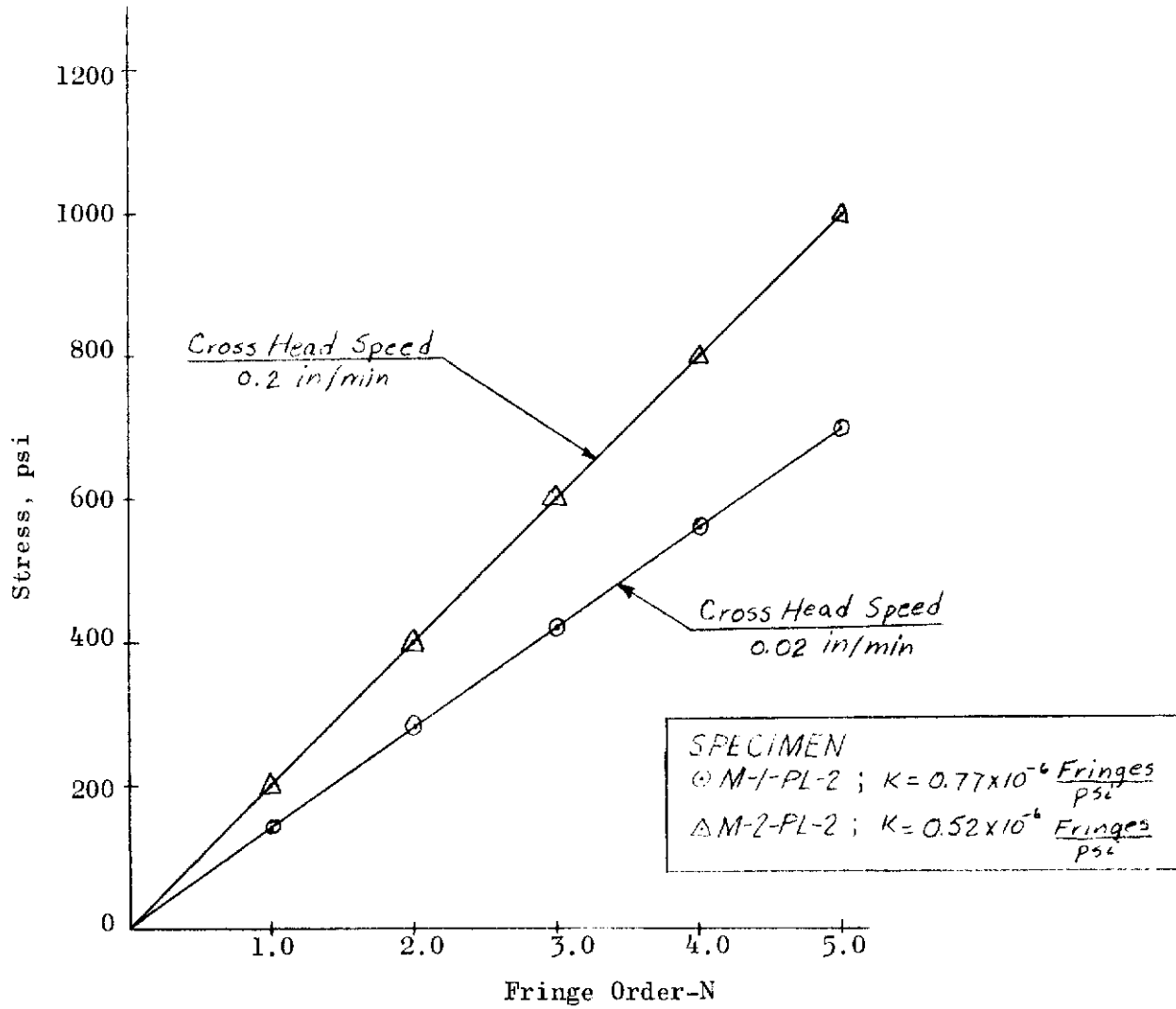
Figure 14. Calibration Curves, Tension Tests

44

The stress-optical coefficient k is calculated from the relation:

$$k = \frac{N\lambda}{\sigma t}$$

where

λ = wavelength at the tint of passage

t = distance traversed by the polarized light beam, inches

N = fringe order

The value of k in the above equation is time dependent. This would be important in dynamic analysis. However, the experimental definition of the complete functional relation involving effects of time, resin formulation, and temperature on k lies beyond the scope of this program.

REINFORCED BEAM ANALYSIS

The objective of reinforced beam analysis was to observe the effects of fiber modulus and low-density configurations on the behavior of fiber-reinforced beams. The approach taken consisted of a combination of load-deflection and photoelastic observations of reinforced beams. Mid- and four-point flexure test configurations were selected for this series of tests.

SPECIMEN PREPARATION

The beams were constructed of various types of fibers in a matrix of commercial photoelastic resin (PL-1). The fibers used were boron, beryllium, tungsten, René 41, high-strength steel, E-glass, and aluminum. The pertinent properties of the filaments, as determined in the Rocketdyne laboratory, are presented in a previous section of this report.

Particular care was exercised in positioning the reinforcing elements accurately and uniformly in each beam specimen. Filament ends were spaced accurately by positioning them over machine screw threads at each end of the mold or by threading the filaments through a precise hole pattern in two metal plates.

A predetermined load, which ranged up to 54 grams depending on the reinforcing element, was used to hold the elements in place during casting and curing of the resin. In addition, silicone RTV rubber split-end dams were used to retain the cast plastic and to position all of the reinforcing filaments at the midplane of the beam. Despite these measures to position the reinforcing filaments accurately, slight displacements near the center of the beam were sometimes produced when pouring and curing the resin.

The exotherm temperature of the PL-1 resin system was carefully controlled when using the resin in large concentrated volumes because temperatures as high as 500°F can be obtained by exothermic reaction.

However, the exotherm temperature of this resin system was not a problem in preparing these particular specimens. The beams were so thin that heat was readily dissipated. The temperature recorded during beam molding was constant at 100°F throughout the cure cycle.

SPECIMEN CONFIGURATION

The volume loading of filaments in the beams was extremely low in all cases. A small number of reinforcing elements was used to observe details of behavior which might otherwise be obscured by the presence of many filaments in the beams. Considerable photoelastic difficulties were also present; a larger number of wires requires a closer spacing of the wires with subsequent interactions of the stress fields. The photoelastic analysis of such a beam while under load was an extremely difficult matter.

Each batch of resin was used to prepare a nonreinforced control beam and a number of reinforced beams. Reinforced beams were made with three, four, and five fibers at the middle vertical plane. After curing of the resin and removal of the beams from the mold, the positions of the wires relative to an edge of the beam were determined with an optical comparator (Table 3).

Examination of fiber spacing in Table 3 reveals one of the major difficulties encountered in the model fabrication. More variation was present than desired in replicate specimens. This made interpretation of the test results more difficult. Fiber-misalignment difficulties of a similar nature have been previously noted by Islinger, et al. (Ref. 8).

FOUR-POINT FLEXURE

The testing was performed on an Instron testing machine equipped with a compression cell (Fig. 15). The load was applied with the cross head moving at a rate of 0.02 in./min, and midspan deflection readings were taken at approximately 0.03-inch intervals up to a maximum deflection of

48

TABLE 3

BEAM DIMENSIONS
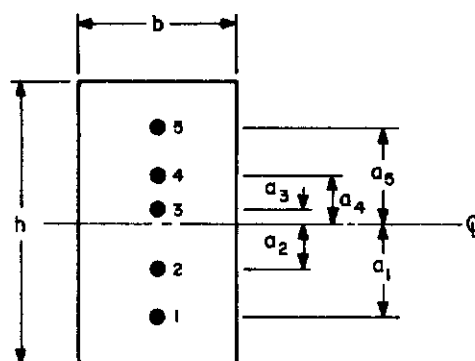
Wire Position Relative to Beam Centerline, inches

Specimen	a_1	a_2	a_3	a_4	a_5	b	h
419-30-2G-PL-1-1	0.1324	--	--	--	0.1175	0.085	0.501
419-30-2G-PL-1-2	0.1290	--	--	--	0.1261	0.103	0.501
419-27-3HSS-PL-1	0.0933	--	0.0274	--	0.1560	0.131	0.490
419-28-3R-PL-1	0.1277	--	0.0049	--	0.1032	0.144	0.487
419-28-3W-PL-1	0.0908	--	0.0243	--	0.1388	0.129	0.505
419-27-3B-PL-1	0.1155	--	0.0080	--	0.1190	0.126	0.497
419-27-4HSS-PL-1-1	0.1398	0.0758	--	0.0460	0.1291	0.1349	0.473
419-27-4HSS-PL-1-2	0.1017	0.0422	--	0.0830	0.1457	0.1360	0.507
419-28-4R-PL-1	0.1410	0.0765	--	0.0408	0.1112	0.149	0.493
419-28-4W-PL-1-2	0.1020	0.0402	--	0.0892	0.1445	0.115	0.509
419-27-4B-PL-1-1	0.1445	0.0645	--	0.0668	0.1393	0.114	0.499
419-27-4B-PL-1-2	0.1350	0.0570	--	0.0995	0.1240	0.128	0.474
419-27-5HSS-PL-1	0.1233	0.0610	0.0308	0.0516	0.1150	0.132	0.487
419-28-5R-PL-1	0.0943	0.0299	0.0208	0.0846	0.1351	0.160	0.507
419-28-5W-PL-1	0.1006	0.0364	0.0219	0.0839	0.1370	0.130	0.476
419-27-5B-PL-1	0.1399	0.0682	0.0116	0.0402	0.0940	0.135	0.485
419-27-0-PL-1	--	--	--	--	--	0.112	0.439
419-25-0-PL-1	--	--	--	--	--	0.123	0.517
419-28-0-PL-1	--	--	--	--	--	0.124	0.502
419-30-0-PL-1	--	--	--	--	--	0.124	0.488

49

TABLE 3

(Concluded)

Specimen	a_1	a_2	a_3	a_4	a_5	b	h
41925-2B-PL1	0.1168	-----	-----	-----	0.1066	0.124	0.503
41925-5B-PL1	0.1477	0.0844	-0.0236	0.0391	0.0966	0.121	0.514
41927-0-PL1	-----	-----	-----	-----	-----	0.111	0.436
41927-3B-PL1	0.1120	-----	0.0109	-----	0.1222	0.127	0.497
41927-4B-PL1-1	0.1446	0.526	-----	0.0675	0.1406	0.115	0.500
41927-4B-PL1-2	0.1359	0.0579	-----	0.0462	0.1197	0.128	0.475
41927-3 HSS-PL1	0.0914	-----	0.0309	-----	0.1508	0.132	0.501
41928-4W-PL1-2	0.1501	0.1218	-----	0.0338	0.994	0.115	0.510
41928-5W-PL1	0.1387	0.0377	0.0199	0.0816	0.1335	0.129	0.472
41928-3R-PL1	0.0930	-----	0.0081	-----	0.1277	0.144	0.499
41928-5R-PL1-2	0.1252	0.0621	-0.0129	0.0582	0.1210	0.165	0.483
41930-0-PL1-1	-----	-----	-----	-----	-----	0.123	0.497
41931-0-PL1-1	-----	-----	-----	-----	-----	0.121	0.506
41931-3A22-PL1-2	0.1498	-----	0.0144	-----	0.1291	0.116	0.499
41931-AL2-PL1-2	0.1510	0.0567	-----	0.0376	0.1294	0.118	0.501
41933-3BE-PL1	0.0990	-----	0.0024	-----	0.1025	0.125	0.495
41933-4BE-PL1	0.0776	0.0267	-----	0.0537	0.1116	0.123	0.498
41933-5BE-PL1	0.0645	0.0140	0.0327	0.0796	0.1330	0.127	0.496
41940-3K-PL1-5	0.1648	-----	0.0067	-----	0.1871	0.156	0.500
41940-3K-PL1-6	0.1782	-----	0.0018	-----	0.1758	0.128	0.509
41941-0-PL1-1	-----	-----	-----	-----	-----	0.119	0.503

(-) indicates wire below center line of cross section.
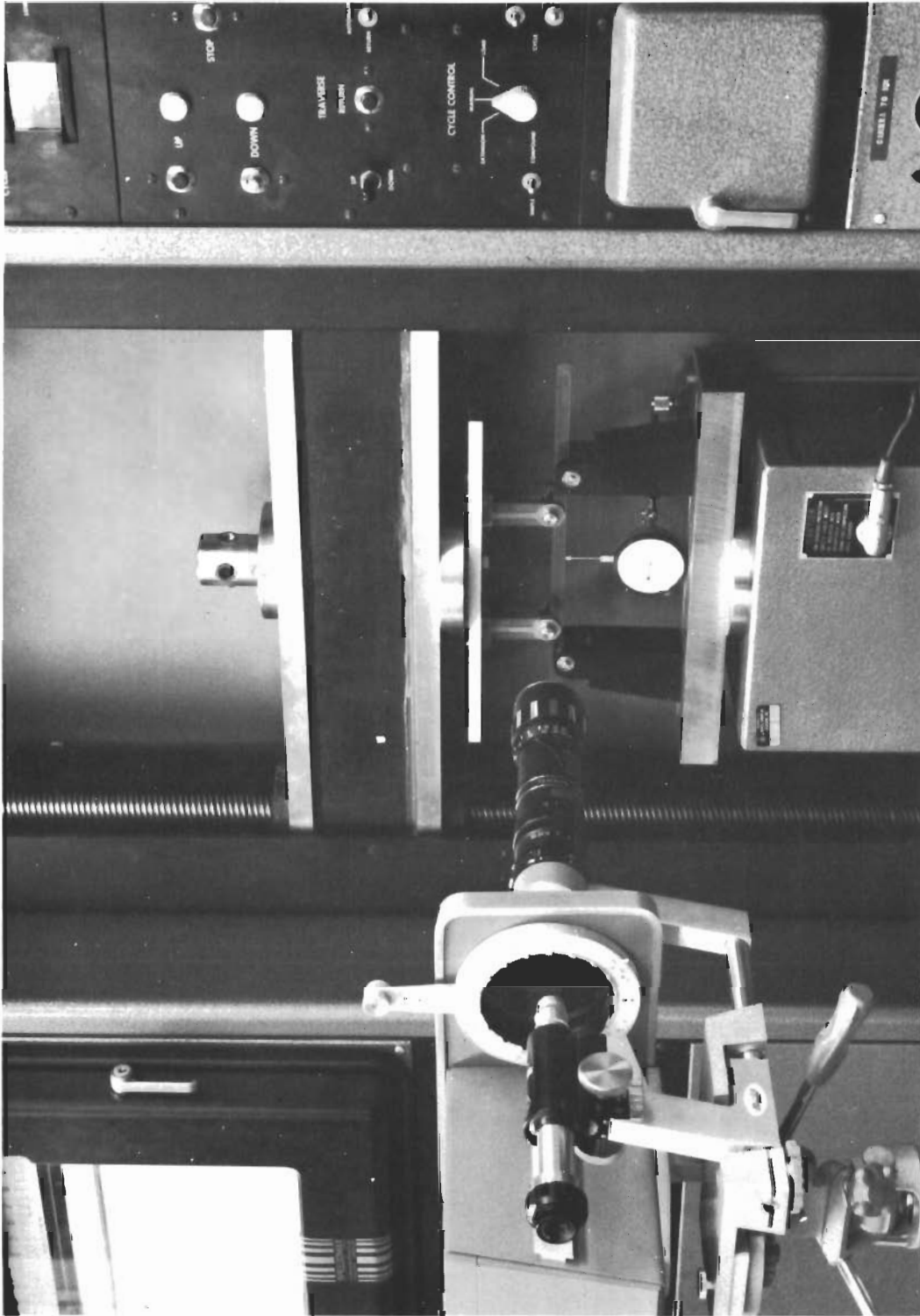
Figure 15. Reinforced Beam Investigation

51

0.18 inch. Deflection measurements were obtained with a Starrett dial gage which reads to 0.001 inch. The beam supports were 8 inches apart with the load being applied 1-1/2 inch from each support. The Instron chart was marked each time a deflection reading was taken. The beam was observed photoelastically throughout the load cycle by a circular polariscope arrangement. Observations were made with a telemicroscope (Fig. 15). A white light source was used, and by the use of quarter-wave plates in the circular polariscope, only the isochromatics were visible. In the portion of the beam where there was a constant bending moment, the fringes were parallel to the edge of the beam, and the zero-order fringe appeared to be at the center of the beam. Near the ends of the beam, in the regions where shear was present, there was a ten-dency for the fringes to contour along the reinforcing elements. This phenomenon of the affinity of the fringes for the reinforcing elements was later observed on studies of beams in mid-point flexure, where the shear gradient is higher, and on microstudies of stress transfer.

The data obtained from the reinforced-beam measurements are tabulated in Appendix B. Reduction of these data is shown in the table headings where the resultant load has been corrected for the moment of inertia and matrix properties of the beam. Figures 16 and 17 summarize the data obtained.

It is significant that despite variations in beam geometry and the low density of reinforcement, the effect of the modulus of the reinforcing elements is evident. It is also significant that independent of the variation in number of reinforcing elements, boron consistently con-tributes the maximum stiffness to beams with low-volume high-modulus elements. Figures 16 and 17 show the effect of the various moduli of the reinforcing elements on the stiffness parameter.
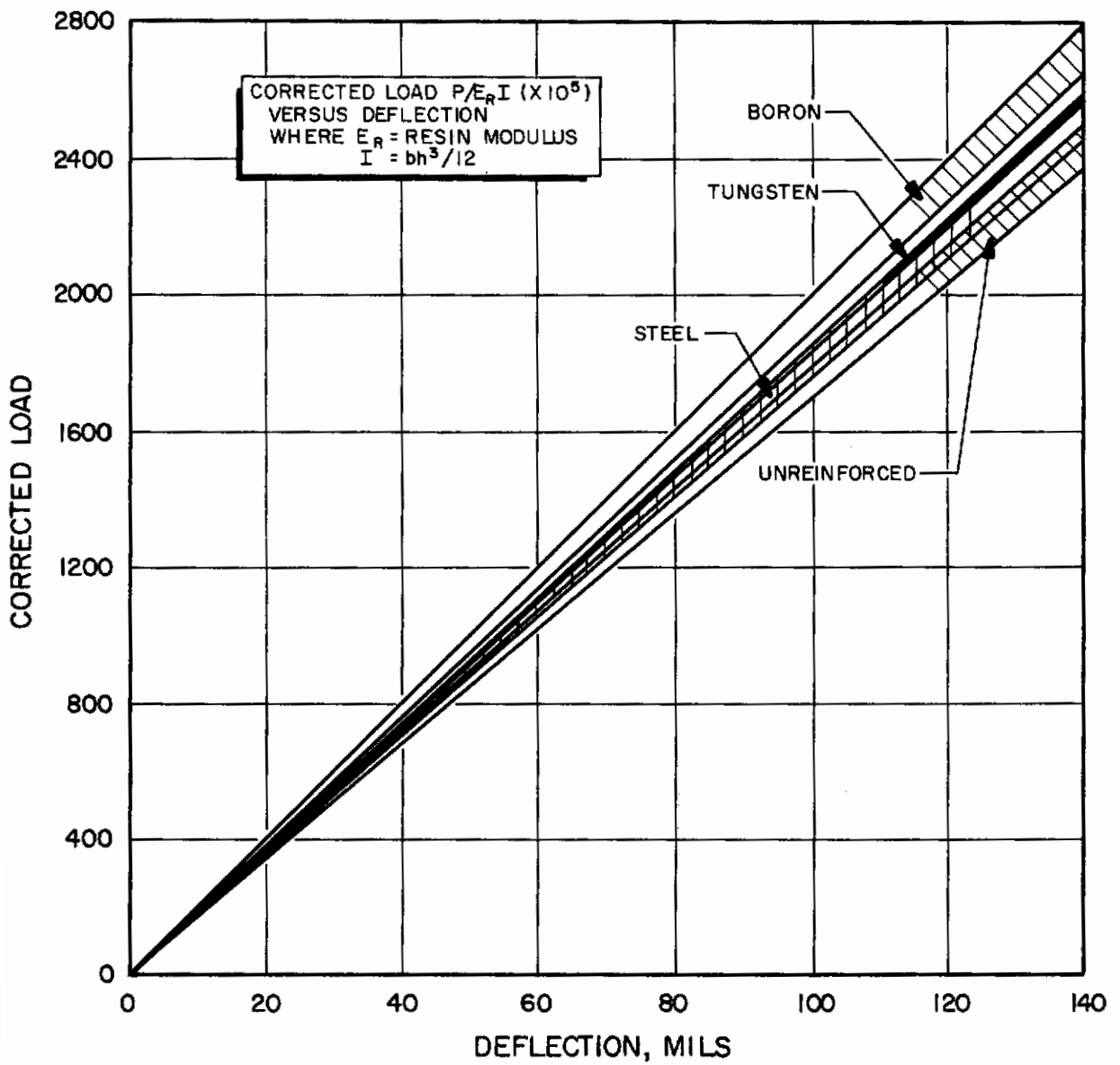
Figure 16. Reinforced Beam Analysis

The chart shows CORRECTED LOAD (y-axis, 0 to 2800) versus DEFLECTION, MILS (x-axis, 0 to 140).

Legend box:
CORRECTED LOAD $P/E_R I$ $(\times 10^5)$
VERSUS DEFLECTION
WHERE E_R = RESIN MODULUS
$I = bh^3/12$

Curve labels: BORON, TUNGSTEN, STEEL, UNREINFORCED

53
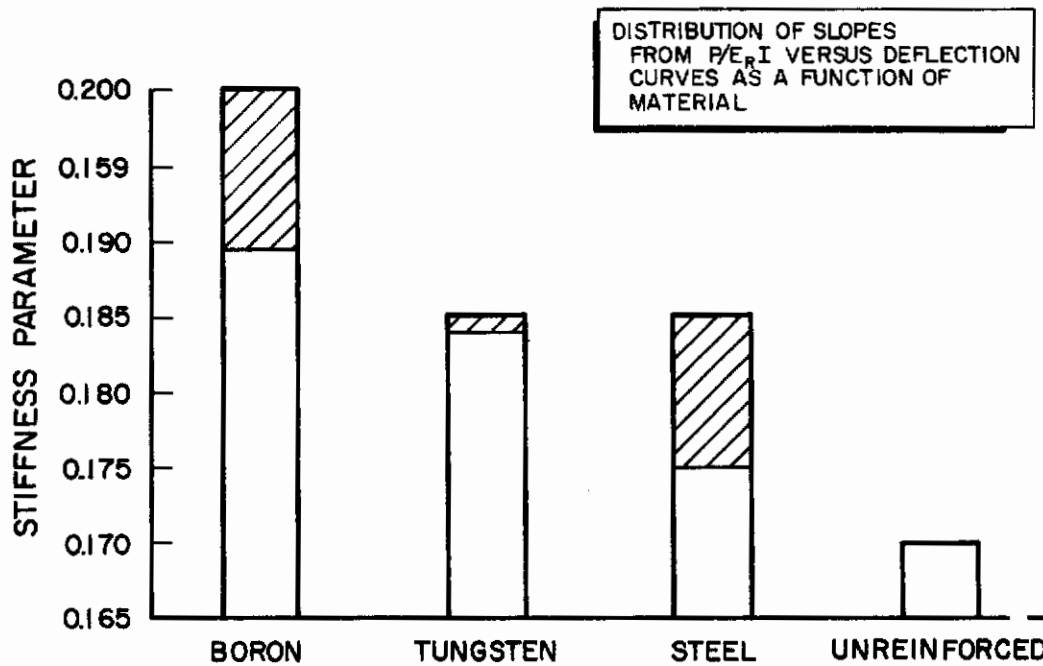
Figure 17. Flexural Test Measurements

MID-POINT FLEXURE

The purpose of testing the wire-reinforced composite beams in three-point loading was to investigate wire-loading phenomena and stress transfer mechanisms. It was believed that if the shear gradient was sufficiently high, the shear stress redistribution could be detected as discontinuities in the isochromatic fringes. The three-point loading arrangement and the use of a shorter span accentuated the stress transfer effects which the experiments were intended to reveal. The testing procedure for the beams was set up so that comparison between beams of different reinforcing elements could be made at the same load level. The beams were loaded to destruction, and photographs were taken at 20-, 40-, and 60-pound loadings. Some beams were photographed at loads higher than 60 pounds in an attempt to obtain data as close to the failure point as possible.

Quantitative data were obtained from the photographs. However, because of the volume of data which can be obtained from these photographs, only a representative set of tests has been reduced and presented. It was decided to analyze maximum shear stress in a vertical section of the beam specimens at an applied load of 60 pounds and at two vertical sections of the beam. The first section was taken at 0.04 inch to the left of the center of the span. These data are plotted in Fig. 56 through 66 (Appendix C).

A two-dimensional quantitative analysis of shear stress can be constructed by replotting the two section traverses across the beams. Examining Fig. 56 through 66 (Appendix C) for (1) maximum shear stress along a vertical plane vs percent elongation or modulus of wire, and (2) maximum shear stress along a vertical plane vs the density of reinforcing indicates that no general correlations with respect to the effect of these parameters on the maximum shear stress distribution can be made on the basis of these tests. However, it is of interest to point out that the boron-reinforced specimens exhibited higher maximum shear stress distribution for the same load level than any of the other reinforced specimens regardless of volume density of reinforcement in

55

the composite. It is believed that the higher maximum shear stress distribution of boron-reinforced specimens is a result of the elongation properties of the boron wire.

DISCONTINUITIES OF ISOCHROMATIC FRINGES

Fringe discontinuities were observed at high loading in beams subjected to mid-point flexure. These discontinuities, which occurred as the isochromatic fringe crosses the wire-reinforced element, were observed in every test at higher loads. The degree of discontinuity depends on the applied load, the filament used, and the geometrical distribution of the filaments. Figures 18 through 24 show the discontinuity of the fringes as they crossed the reinforcing element.

The isochromatic fringe discontinuities arise from a redistribution of shear in the vicinity of the reinforcing element. This redistribution of shear stress, which the isochromatic fringes represent, indicates that a longitudinal stress transfer phenomenon is taking place and that the embedded element accepts a portion of the load at one point and imparts it to the matrix at some distance down the wire.

A somewhat more dramatic form of shear stress redistribution can be observed in Fig. 25. This figure represents a boron-reinforced specimen under a 70-pound load. The area between points A and B indicate high fringe discontinuities and represents unbonding phenomena. By examining point A and point B, it can be seen that at point A fringe orders 8 and 9 come together and at point B fringe orders 7 and 8 meet. It can also be seen that from point A to approximately three quarters of the distance between point A and B, the ninth fringe order is constant.

It is not yet clear why unbonding in this area took place because tests on other boron specimens did not exhibit this phenomenon. However, it is encouraging to know that any discontinuities between the photoelastic matrix and the reinforcing elements will be manifested by discontinuities

56
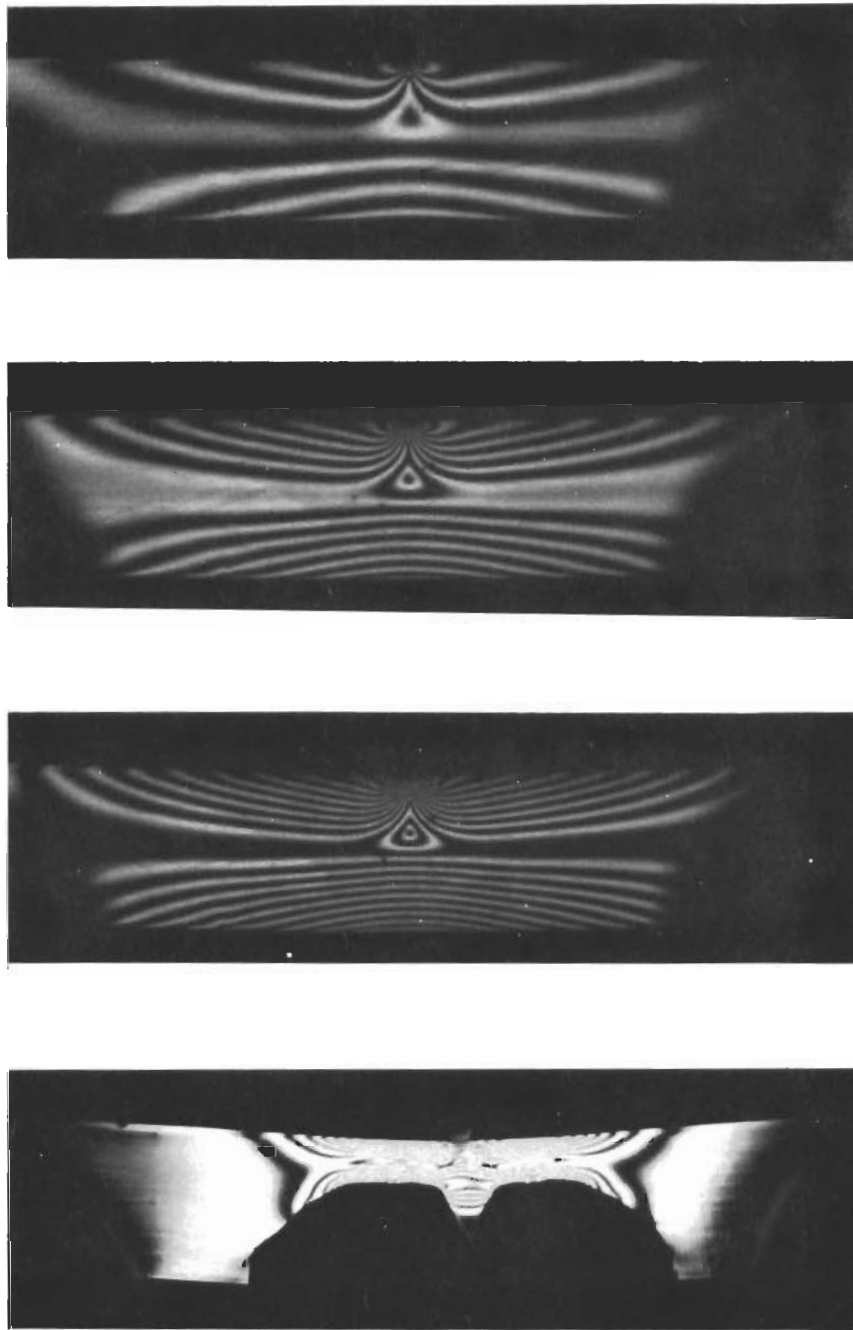
Figure 18.   Stress Pattern for a Mid-Point Loading of a
Nonreinforced Beam Tested in Flexure
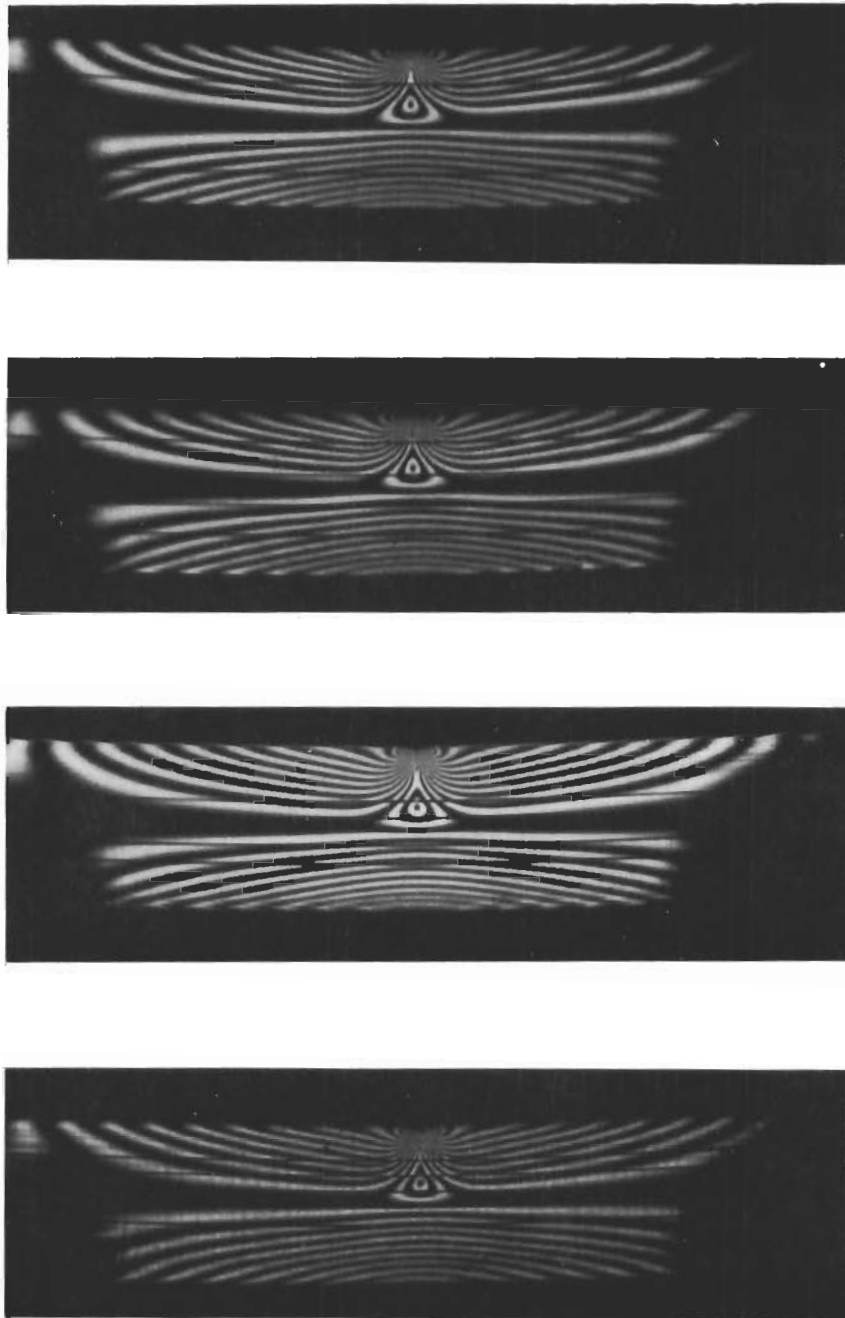
Figure 19. Stress Patterns for Mid-Point Loading for
Reinforced Beams Tested in Flexure
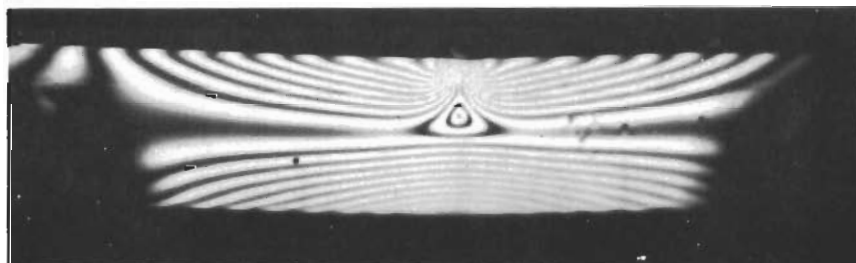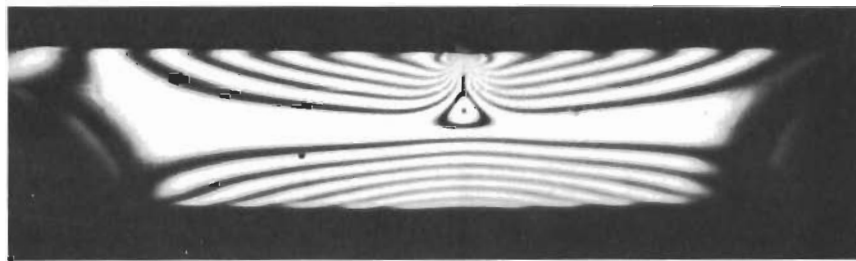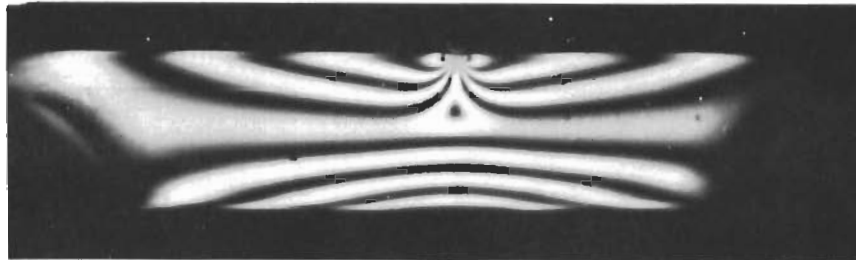
Figure 20. Stress Patterns for Mid-Point Loading for
E-Glass-Reinforced Beams Tested in Flexure
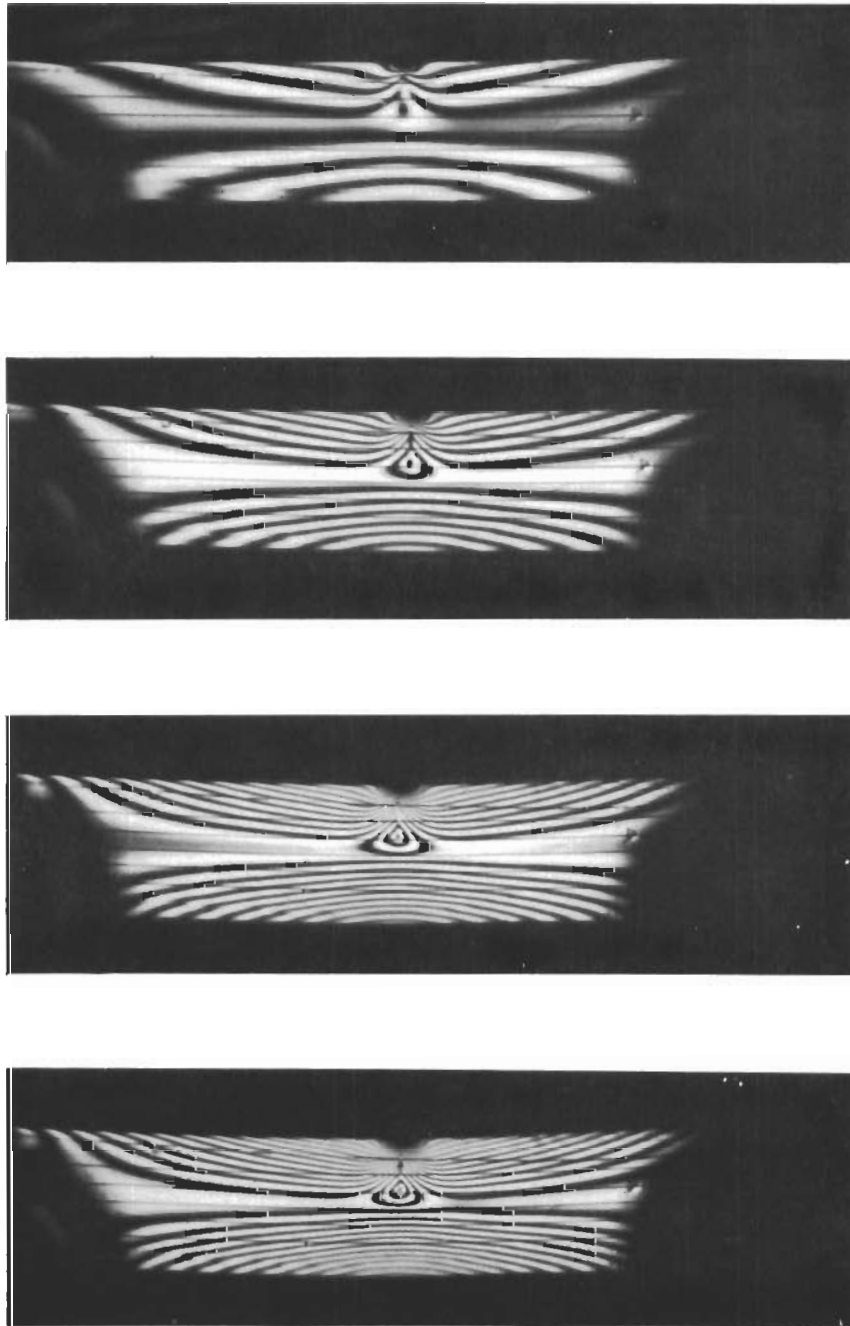
Figure 21. Stress Patterns for Mid-Point Loading for High-Strength
Steel-Wire-Reinforced Beams Tested in Flexure
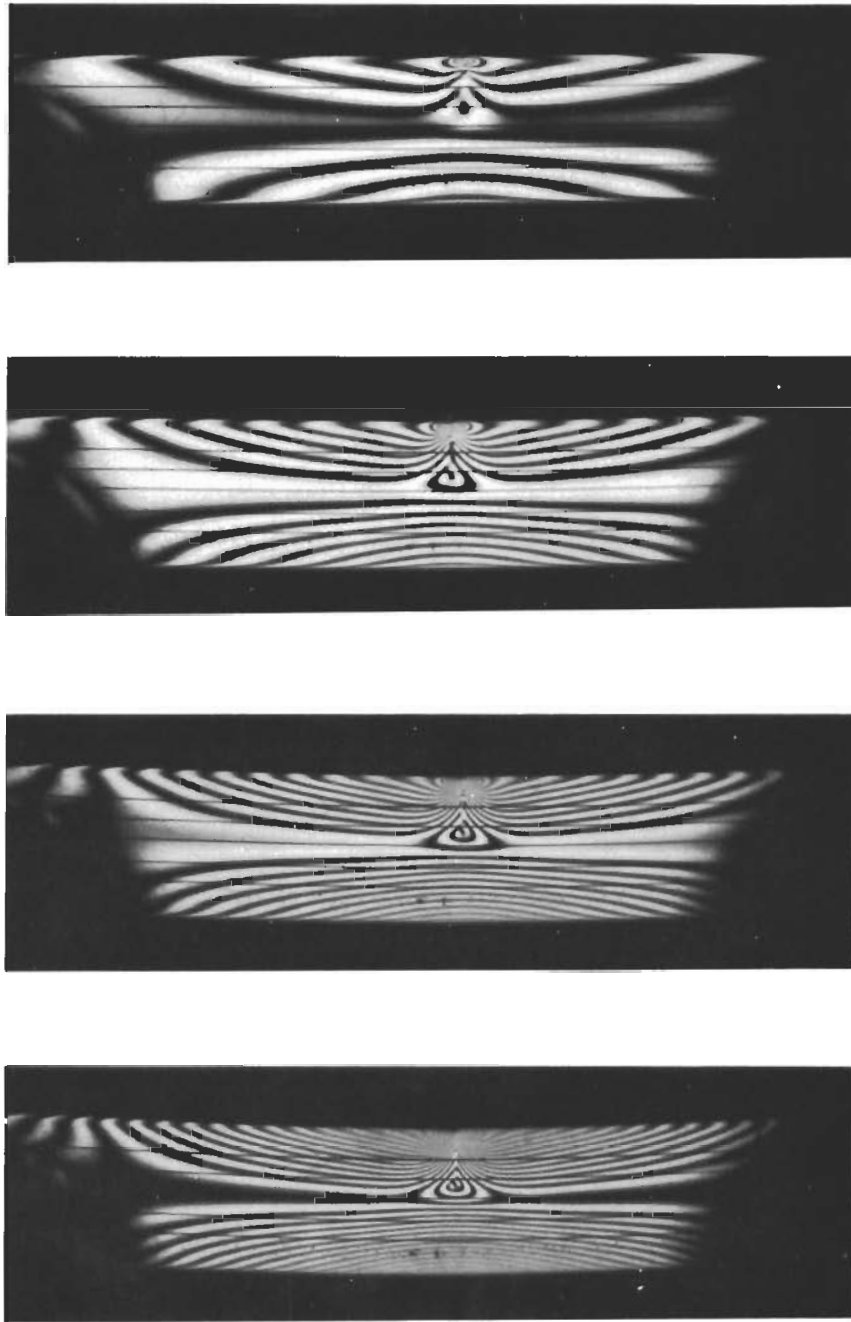
Figure 22. Stress Patterns for Mid-Point Loading for René
41-Reinforced Beams Tested in Flexure
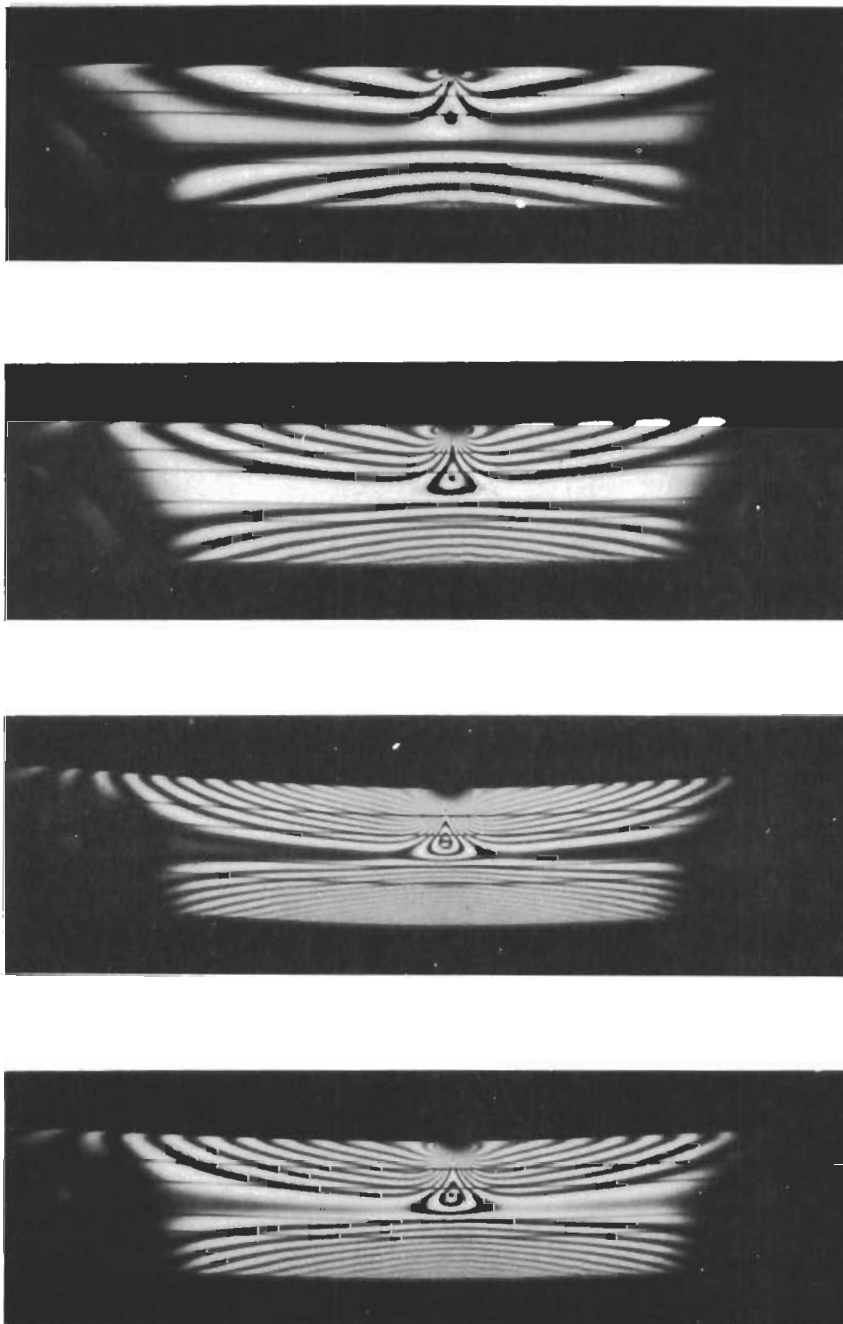
Figure 23. Stress Patterns for Mid-Point Loading for
Tungsten-Reinforced Beams Tested in Flexure
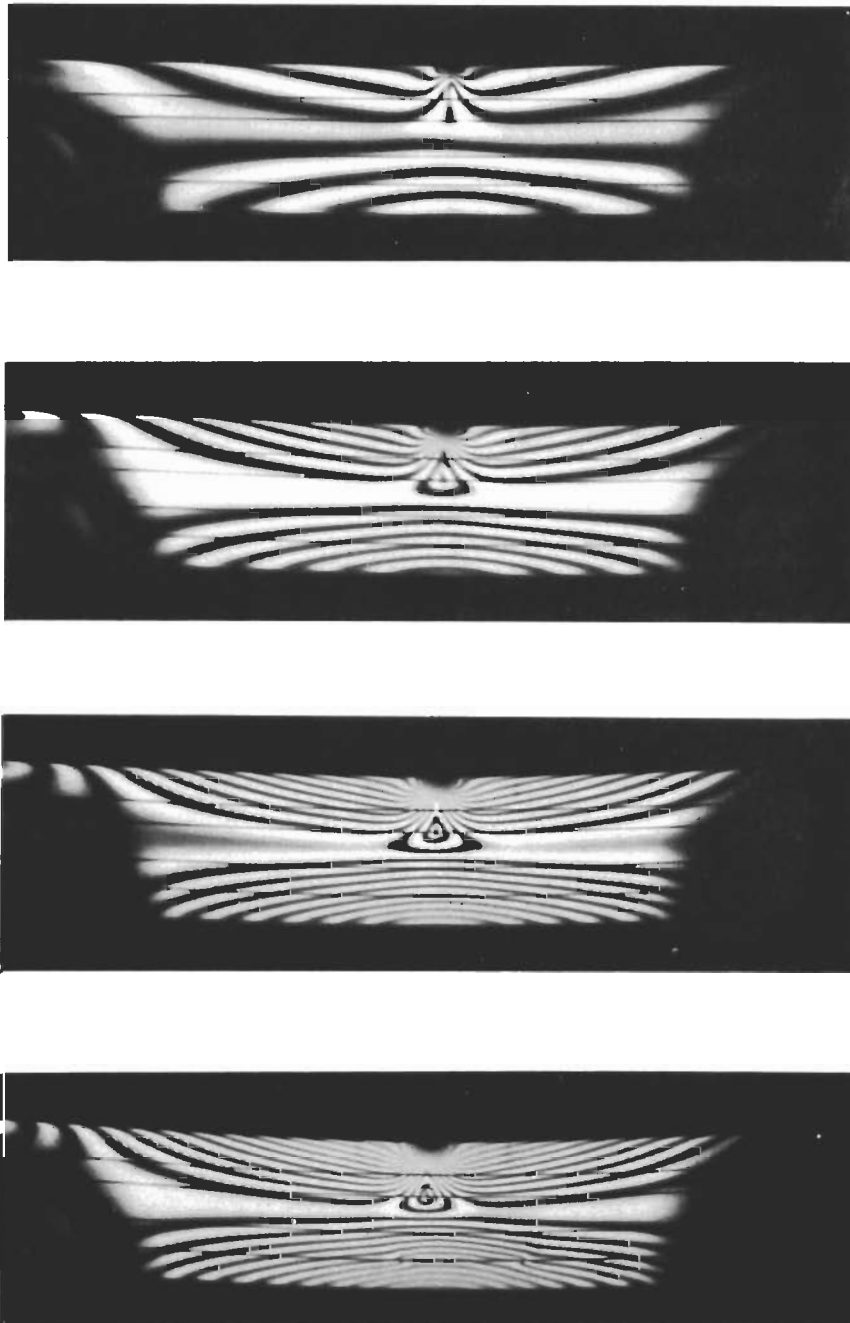
Figure 24.   Stress Patterns for Mid-Point Loading for
             Boron-Reinforced Beams Tested in Flexure
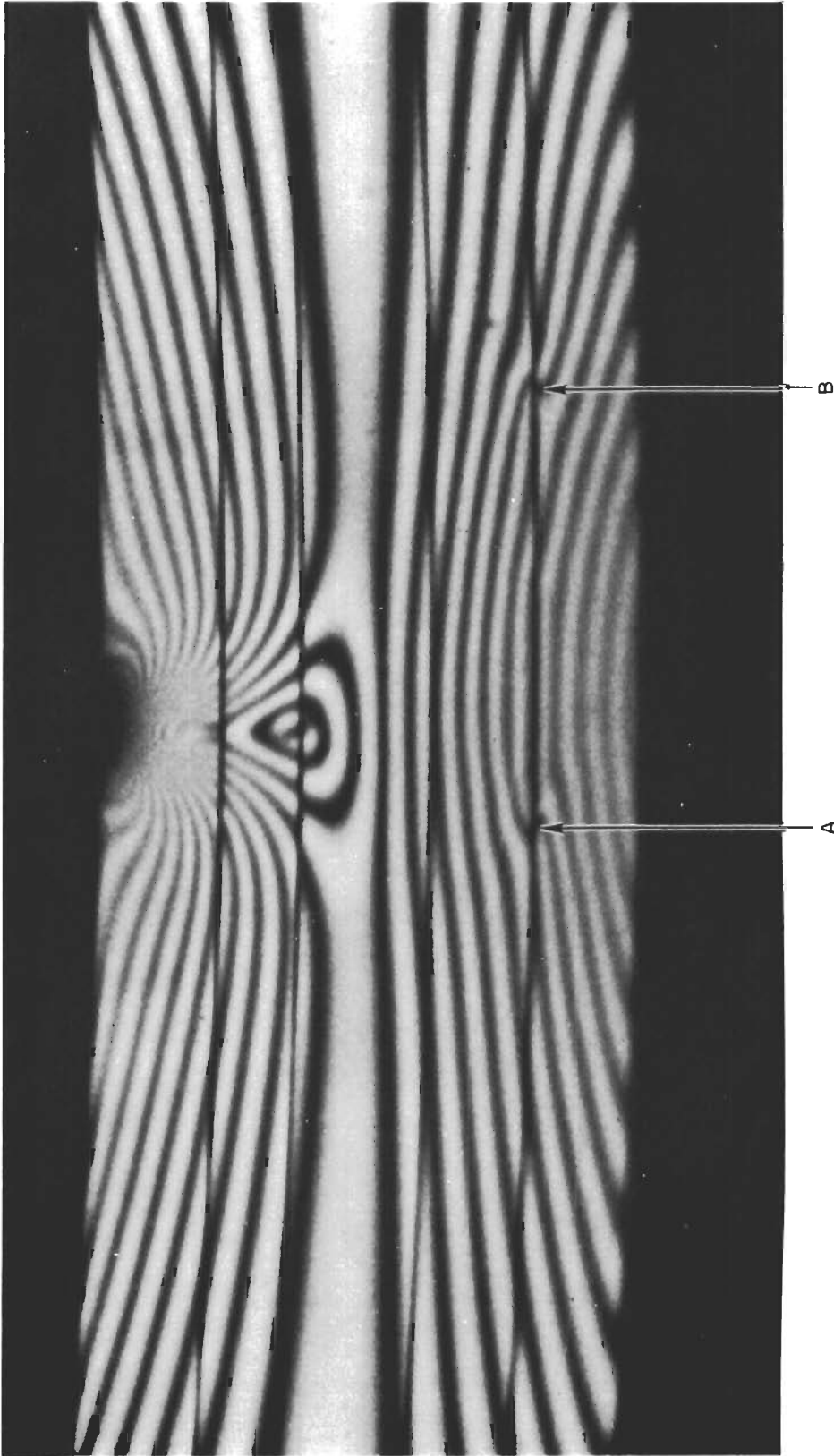
•Figure 25. Stress Patterns for Mid-Point Flexural Loading of Boron-Reinforced Beam Illustrating Unbonding Phenomena

64

in the shear stress distribution of the beam. This provides experimental verification of the use of photoelastic techniques to detect unbonding and to study filament-matrix stress transfer phenomena.

MID-POINT FLEXURAL LOADING FAILURE ANALYSIS

The mode of failure as affected by the modulus of elasticity, elongation, and volume density of the reinforcing elements was studied. All of the beams being considered here were tested in three-point loading. A non-reinforced beam was also tested under the same conditions as the reinforced beams, and is used to compare failure mechanisms.

First, the difference in failure characteristics as affected by the mechanical behavior of the filaments used in the composite will be considered. Figure 26 shows failure characteristics of beams reinforced with boron, tungsten, beryllium, and René 41. Each of the specimens has five reinforcing elements.

The effects of modulus of elasticity and elongation on the failure mechanism are evident in Fig. 26. However, it is apparent that modulus of elasticity of the reinforcing elements is not a primary factor in the failure mechanism. This conclusion can be extended by categorizing the beams according to the elongation properties of the reinforcing elements in two separate and distinct groups. These groups are:

1. High-elongation group $\delta > 1.5$ percent (tungsten and steel)

2. Low-elongation group $\delta < 1.0$ percent (boron and glass)

For the high-elongation group, the mechanism of failure is similar among elements whose modulus of elasticity range from $29.4 (10^6)$ psi to $54.7 (10^6)$ psi. From Fig. 26, it can be seen that for the nonreinforced specimen, the failure pattern is that of two half circles. For the René-and beryllium-reinforced specimens, failure patterns change to one

65

BORON   E = 56.7 X 10^{+6} PSI $\delta = <1$

TUNGSTEN   E = 54.7 X 10^{+6} PSI $\delta = >1.5$

BERYLLIUM   E = 45.5 X 10^{+6} PSI $\delta = >1.5$

RENE '41   E = 31.8 X 10^{+6} PSI $\delta = >1.5$
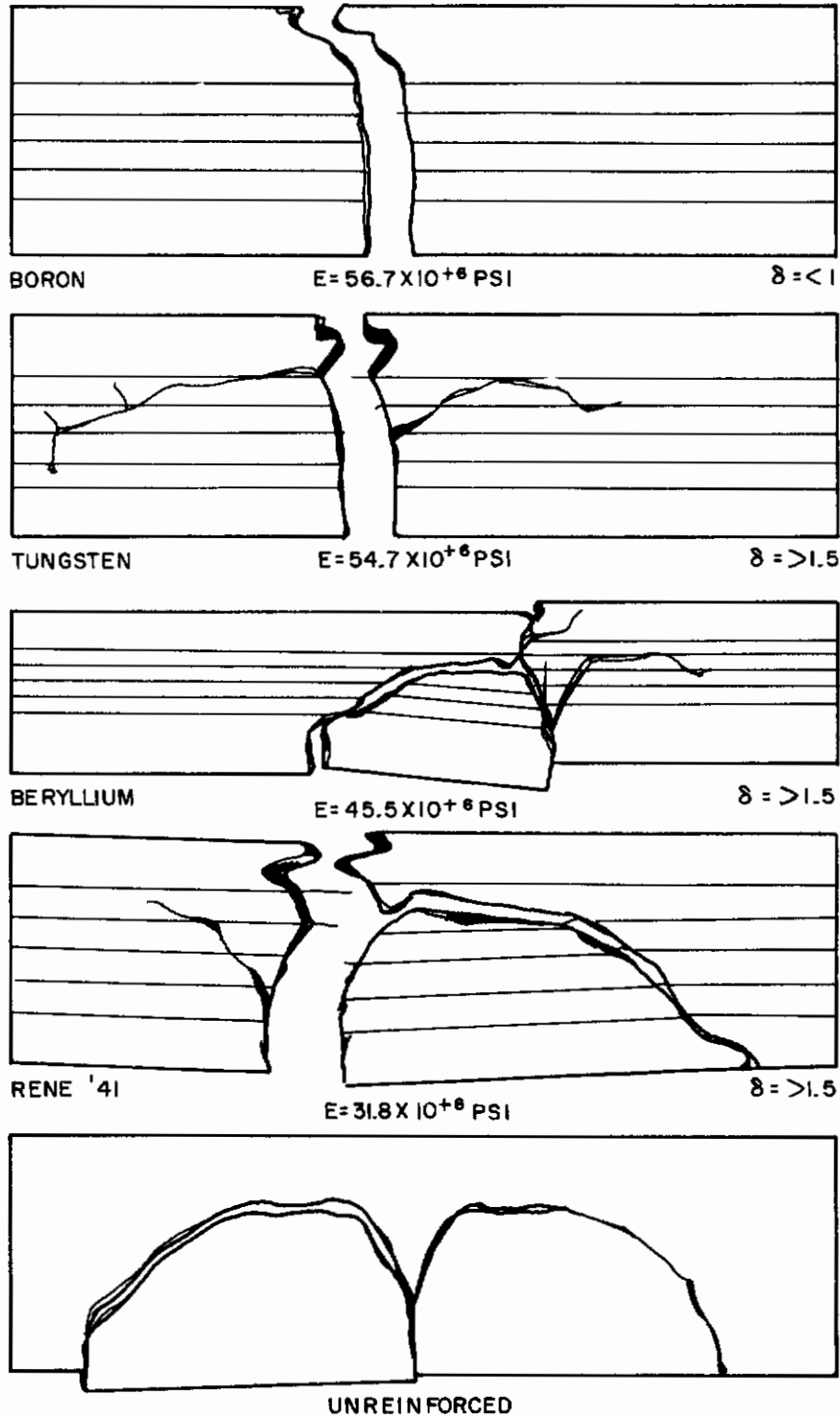
UNREINFORCED

Figure 26. Failure Characteristics for Beam Composites

66

half circle and a crack which resembles the outline of a partial half circle. For the tungsten-reinforced specimen, the half-circle failure is no longer present. However, cracks resembling half circles on either side of the plane of fracture are present.

The low-elongation group of beams which contained three or more boron fibers exhibited failure in a vertical plane with no crack propagation on either side of the plane of fracture. This type of failure is shown in Fig. 27.

The volume density of the reinforcing elements in composite beams also affects the failure characteristics of the beam. In the boron-reinforced composites (Fig. 27), it can be seen that the character of failure changes from two half circles for the unreinforced case to one half circle for the beam with two elements, and finally to a vertical plane fracture for three-, four-, and five-element beams. Figure 28 indicates the same trend showing that the fracture of a three-element René 41 composite beam and the nonreinforced beam are similar. The four-element René 41-reinforced beam character of failure changes as compared to a three-element René 41-reinforced beam.

CONCLUSIONS ON BEAM FAILURE MODES

Generally, experimental data to date indicate that the character of beam failure for a given matrix depends on:

1. Elongation characteristics of the reinforcing elements

2. Modulus of the reinforcing elements

3. Volume density of reinforcing elements in the matrix

Pronounced differences were observed in the modes of beam failure. The above three factors all influenced the type of failure in the direction which would be expected, with high modulus and a high density of reinforcing filaments tending to produce a brittle fracture straight across the beams.
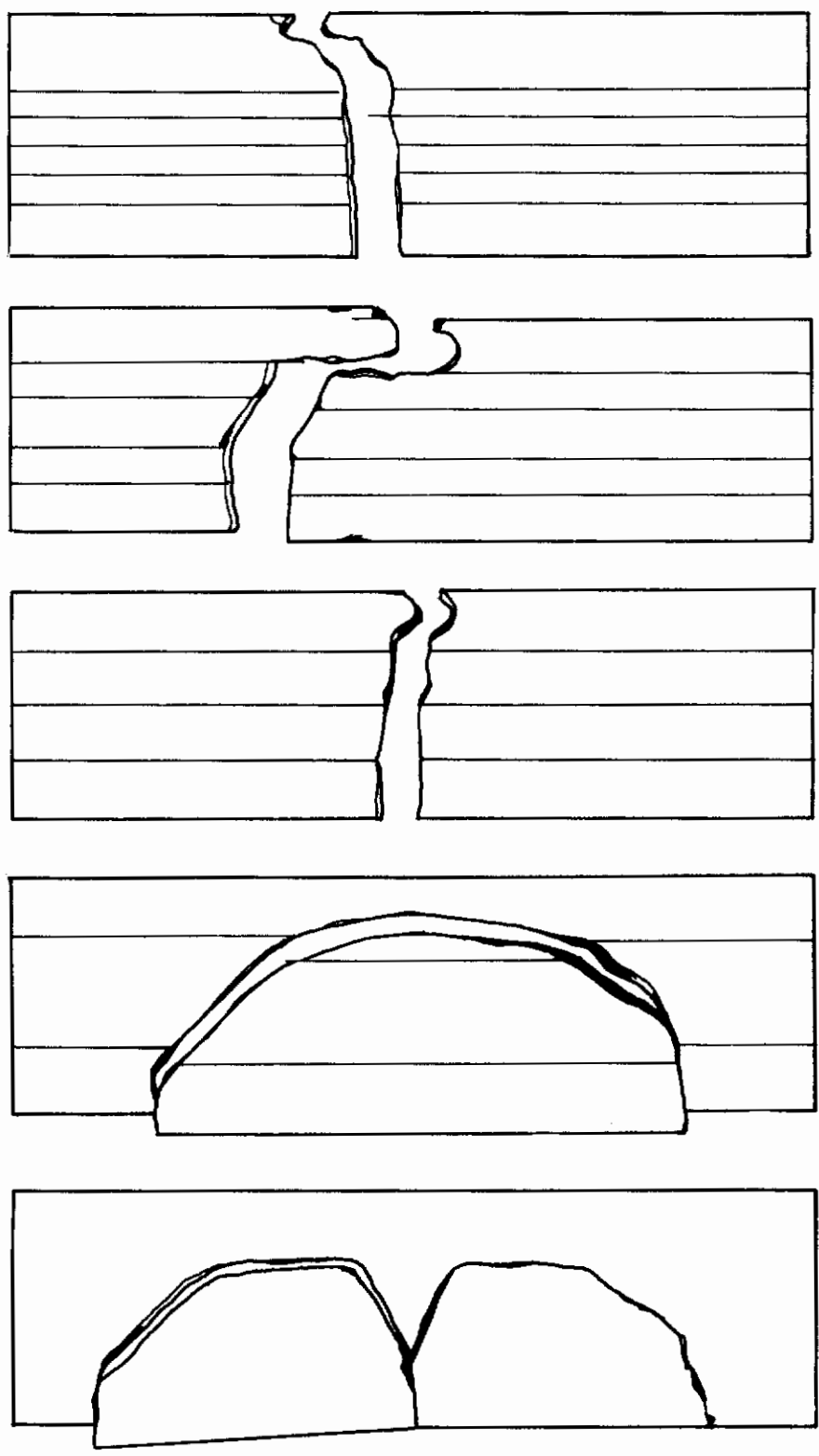
Figure 27. Boron-Reinforced Beams Failure Mechanism
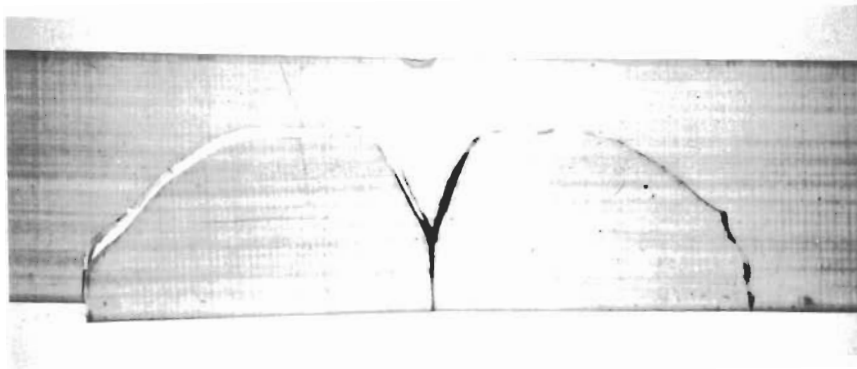
UNREINFORCED
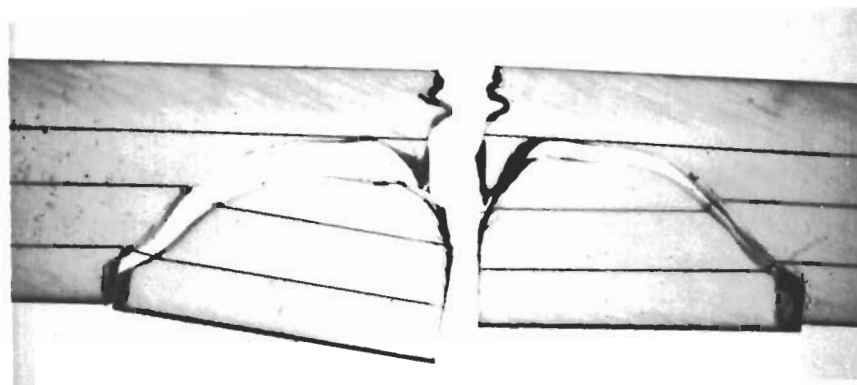
3-ELEMENT RENE REINFORCEMENT
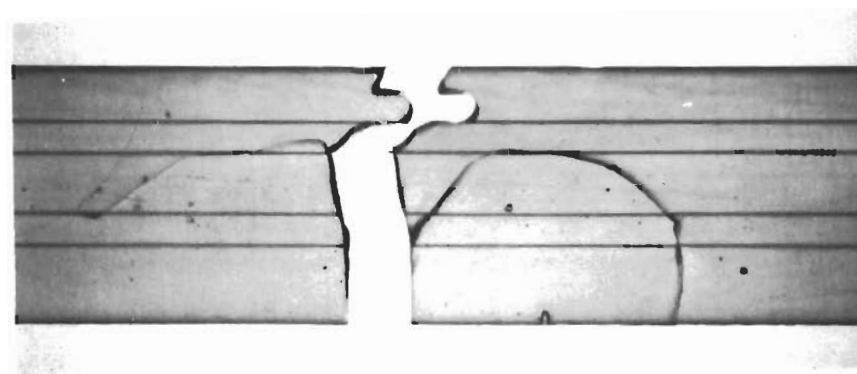
4-ELEMENT RENE REINFORCEMENT

Figure 28. René 41-Reinforced Beams Failure Mechanism

69

INTERNAL STRAIN-GAGE TECHNIQUE

The technique of obtaining internal strain measurements with embedded
gage wires was developed under another contract (Ref. 9) in a study of
the structural response of fiber-reinforced cylinders. Results obtained
from these tests were very useful in gaining an insight into the phenome-
nological behavior of reinforced cylinders. In the current contract, the
embedded-gage technique was used to observe the behavior of reinforced
beams.

The internal strain-gage technique involves the embedding of strain-gage
wires in the matrix of a reinforced composite during fabrication, and
subsequently monitoring resistance changes when the cured specimens are
loaded. Two aspects of this technique have been investigated under this
contract. One approach consisted of using strain-gage wires simultaneously
as reinforcing elements and as strain-indicating devices. The other
approach used extremely fine strain-gage wires, with resulting negligible
reinforcing effect as strain-indicating devices. Applications for these
two techniques will be discussed later.

Specimen Description

Beam specimens were fabricated with PL-1 photoelastic resin as matrix
materials and Karma strain-gage wires as reinforcing elements and strain-
indicating devices.

Karma (76 Ni, 20 Cr + Fe + Al, manufactured by Driver-Harris) strain-
gage wires of two different diameters were used; 5-mil wire having a
resistance of 32 ohms per foot and 1.2-mil wire having a resistance of
555 ohms per foot. There has been little information reported on the
gage factors of these wires, even from the manufacturer, and a detailed
study of this point was beyond the scope of this program. However, based
on previous work conducted at Rocketdyne, a gage factor of approximately
2 was calculated for the 5-mil wire. Furthermore, a linear relation
between resistance change and change in length was observed up to the

70

yield point. Therefore, it is quite reasonable to report results in terms of resistance change.

Three gage wires were used in each of the beams, one approximately at the center and one on each side of center. The beam dimensions were approximately 1/2 by 1/8 by 12 inches. Exact dimensions and wire locations are given in Table 3 . A nonreinforced control beam was also prepared. The casting technique used was described previously.

Test Setup

The embedded gage wires extended beyond the ends of the beam and were soldered to electrical posts attached to the flexure fixture (Fig. 29). The gages were connected in parallel to a Leeds and Northrup 5-decade Wheatstone Bridge with a multichannel switch in the circuit. The circuit held switching errors below one-half of 0.001 of an ohm.

The beams were subjected to mid- and four-point flexure in an Instron test machine. The span for the three-point tests was chosen to be 3 inches to preserve similarity with the other fracture tests. In four-point loading, the span was 10-1/16 inch and load points were 3-1/2 inches on each side of midspan.

The transmission polariscope was set up so that the test beam was approximately in the center of the field of polarized light. A dark field (Fig. 29) was used. For the three-point load tests, a mercury green monochromatic filter was used.

The test procedure consisted of gradually loading the beams and simultaneously measuring center deflection (with a dial gage) and gage resistance changes. Photoelastic fringe patterns were photographically recorded.

71

TRANSMISSION
POLARISCOPE

PHOTOELASTIC
BEAM
SPECIMEN

DEFLECTION
READOUT

MULTI-
CHANNEL
SWITCH

STRAIN
GAGE
READOUT
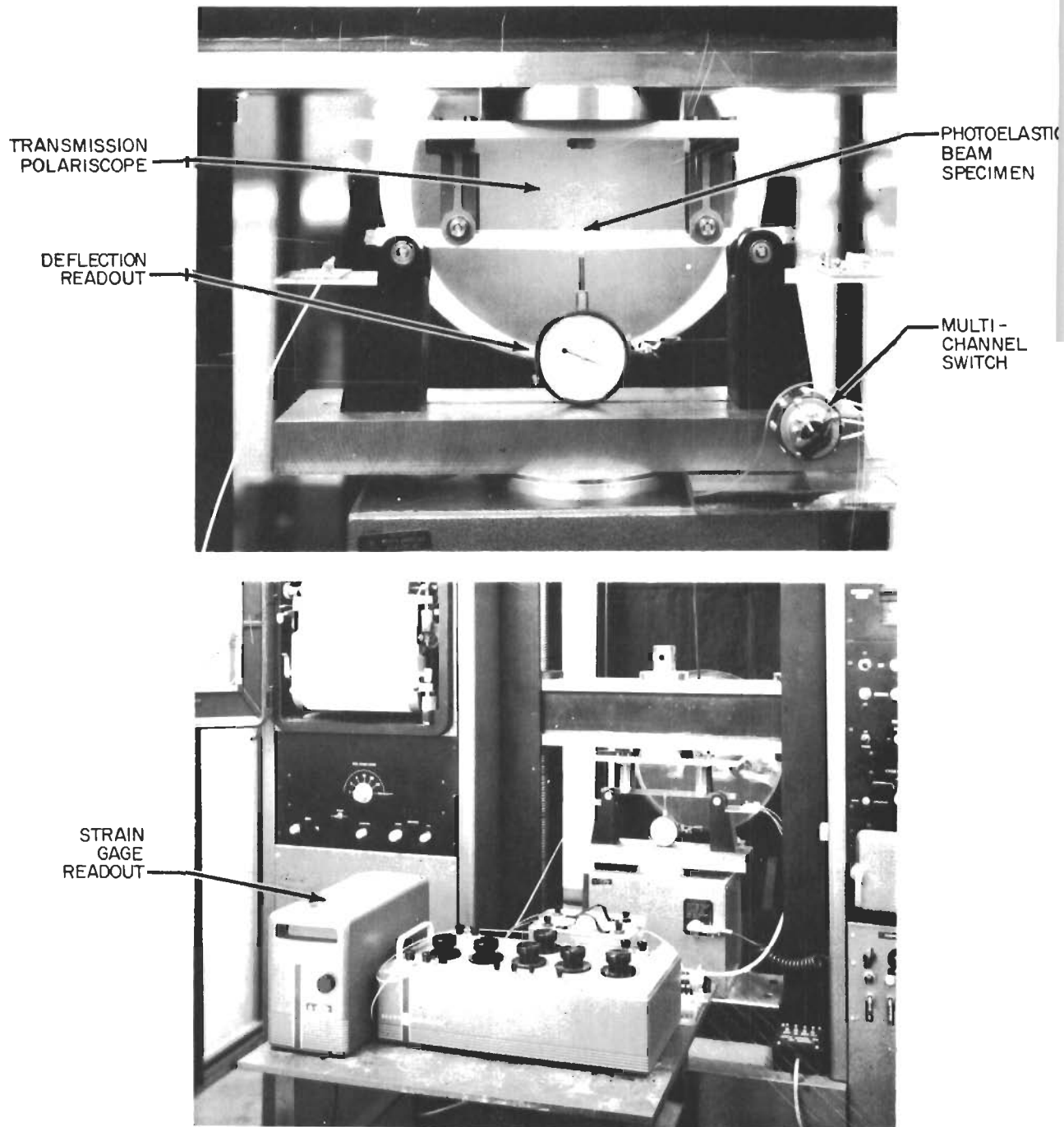
Figure 29. Combined Photoelastic and Strain-Gage Measurement

Results and Discussion

Four reinforced beams and one nonreinforced beam were tested in four-point loading. Specimens 41940-3-K-PL1-2 and 3 contained 1.2-mil gage wires and specimens -5 and -6 contained 5-mil gage wires. These two groups of specimens represented the two embedded strain-gage approaches. A comparison of the load-deflection curves for the nonreinforced beam and the beam containing 1.2-mil gage wire confirmed the hypothesis that a negligible reinforcing effect was provided by the wires, and that they were, therefore, only strain-indicating devices. However, the 5-mil wires were reinforcing elements and strain-indicating devices. Curves of gage resistance change vs center beam deflection for beams -2 and -5 are presented in Fig. 30 . These curves are representative of the behavior of all the specimens subject to four-point loading. Reproducibility between test runs is also apparent from these curves.

In all of the specimens tested, the center gage displayed almost no resistance change. This indicates a strain-free region (neutral axis) close to the centerline of the reinforced beams. The comparison of the ratio of wire distances from the center of the beam with the ratio of the corresponding plus or minus gage resistance changes shows good agreement. This implies a straight-line strain distribution across the beam cross section. It can further be concluded that the reinforced resin was behaving in substantially the same manner in tension and compression (at least for the reinforcing configurations and stress levels considered). The small differences between the two ratios may be a result of the fact that the active gage passes through regions (between the load points and the supports) where a state of pure flexure does not exist.

Two of the beams with 5-mil gage wire (specimens 41940-3-K-PL1-5 and -6) were subsequently tested to failure in mid-point flexure. The curves of gage resistance change vs center beam deflection for specimen -6 is presented in Fig. 31. Similar curves were obtained for specimen -5. As could be expected, the ratio of the resistance changes is not as close to the ratio of the distances of the gages from the beam centerline

73
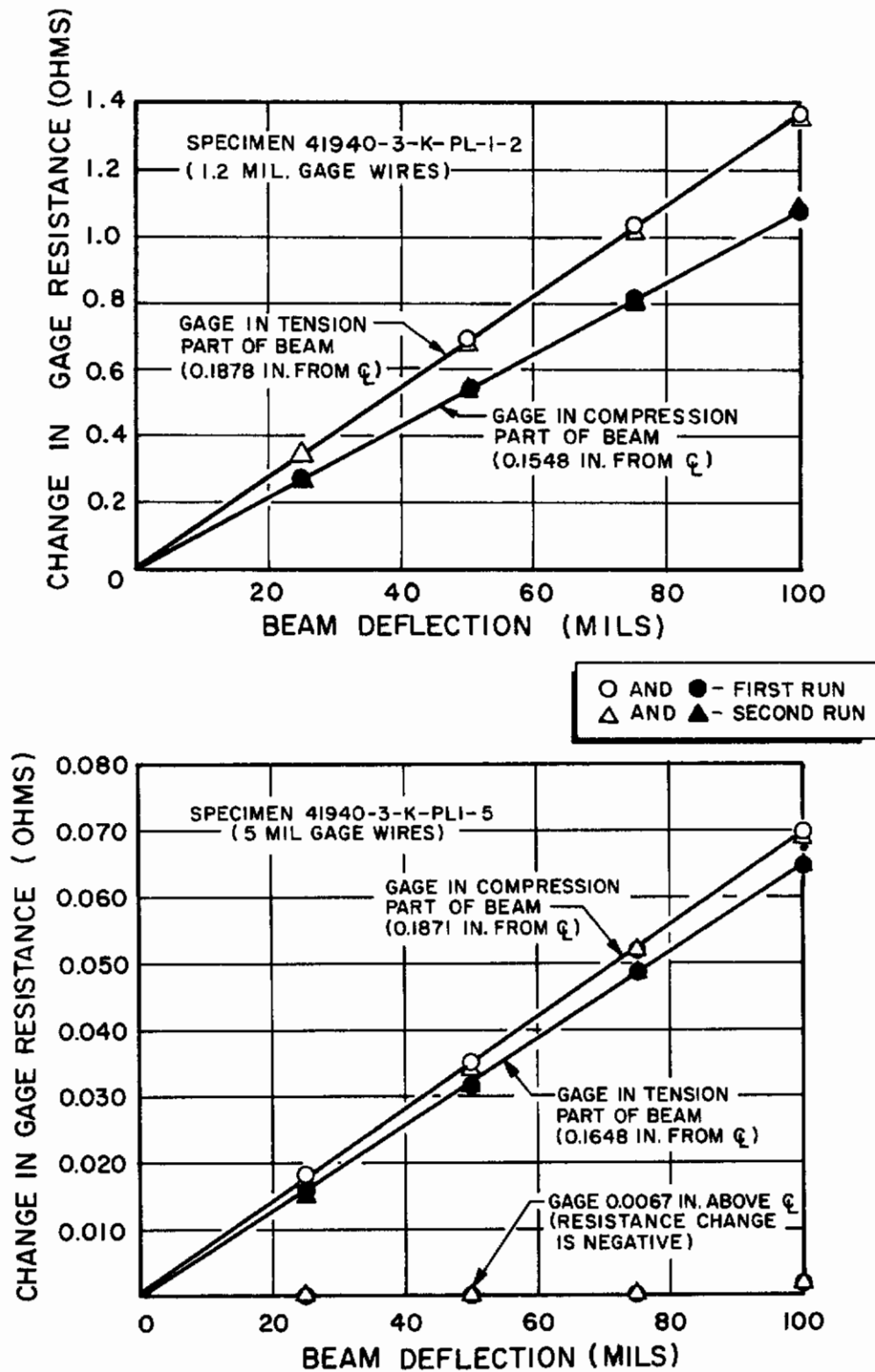
Figure 30.   Internal Strain-Gage Measurements in Beams Under
Four-Point Loading in Flexure

74
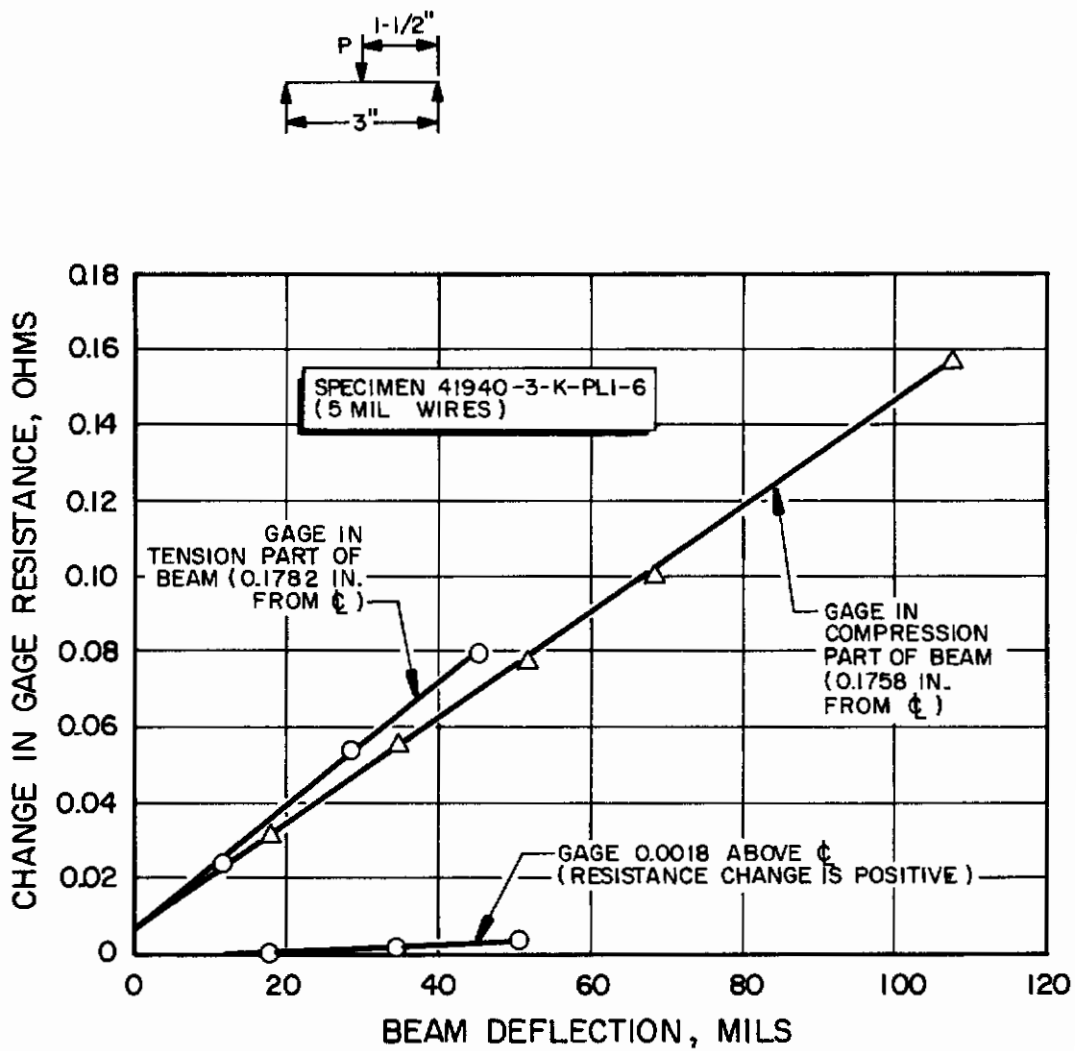
Figure 31. Internal Strain-Gage Measurements in Beams Under
Mid-Point Loading in Flexure

as was the case in four-point loading. This is a result of the nature
of the stress field which is not uniform in any region as was noted in
the photoelastic observations.

Photographs of the monochromatic fringe patterns of the loaded beams were
similar to those shown in the section on beam analysis. An attempt
to correlate the photoelastic and strain gage observations in the mid-
point loading configuration was not carried very far because the strain
wire, which passes through a complicated stress field, has an output
which is averaged over its entire length, whereas photoelastic observa-
tions are point measurements.

The internal strain-gage technique has been demonstrated to be a poten-
tially powerful tool for investigating the behavior of reinforced com-
posites. The two approaches investigated permit internal strain measure-
ment in photoelastic and opaque matrix materials. A major improvement
in the technique can be accomplished by butt welding copper lead wires
to the strain gage wires. This would have the effect of providing a
well-defined gage length in the region which is to be investigated. The
copper lead wires would go through the surrounding extraneous stress
fields, and these effects would be eliminated from the strain gage reading.

It occurred to the investigators that it would be possible to use the
1.2-mil gage wire in determining the neutral axis of nonsymmetrically
reinforced beams and plates and also in strain rosette configurations
for observations between plys of laminates. The 5-mil gage wires can
be used as reinforcement and strain-indicating devices in reinforced com-
posites. It is important to note that this technique need not be
restricted to composites with low fiber loadings.

76

MULTIAXIAL TESTING OF REINFORCED PLATES

The primary objective of this series of tests was to observe stress transfer and failure mechanisms of reinforced plates subjected to multi-axial stress fields. Thin reinforced plates were constructed and tested. The test is the familiar strip biaxial tensile test where a biaxial tensile field develops near the center of the plate. The ratio of the tensile stresses is approximately 2:1 in a nonreinforced plate.

SPECIMEN DESCRIPTION

One nonreinforced and two reinforced plates, with approximate dimensions of 7 by 9-1/2 by 1/8 inches were cast in a manner similar to that previously described. The photoelastic resin used as matrix material was PL-2/PH-3, which has a nominal modulus of 30,000 psi and elongation to break of 50 percent. One of the reinforced plates contained 5-mil steel wire and the other contained 5-mil boron fibers. The wire pattern consisted of 20 crossed wires making an acute angle with the horizontal of approximately 60 degrees (Fig. 32). Photoelastic observation of cured plates after removal from the mold revealed no appreciable residual stress field.

TEST SETUP

As shown in Fig. 32 the plate was clamped between aluminum bars along its longer edge. The assembly was then set into an Instron test machine. A transmission polariscope with crossed quarter-wave plates was set up so that the plate was in the center of the polarized light field. A tensile load was gradually applied, and the ensuing fringe patterns photographically recorded. Color photographs of isochromatics using white light, as well as black and white photographs using a mercury green filter, were taken. Two test runs were performed on the plate containing steel reinforcement. In the first run, the plate was subjected to low load levels. In the second run, an attempt was made to take the plate to

77
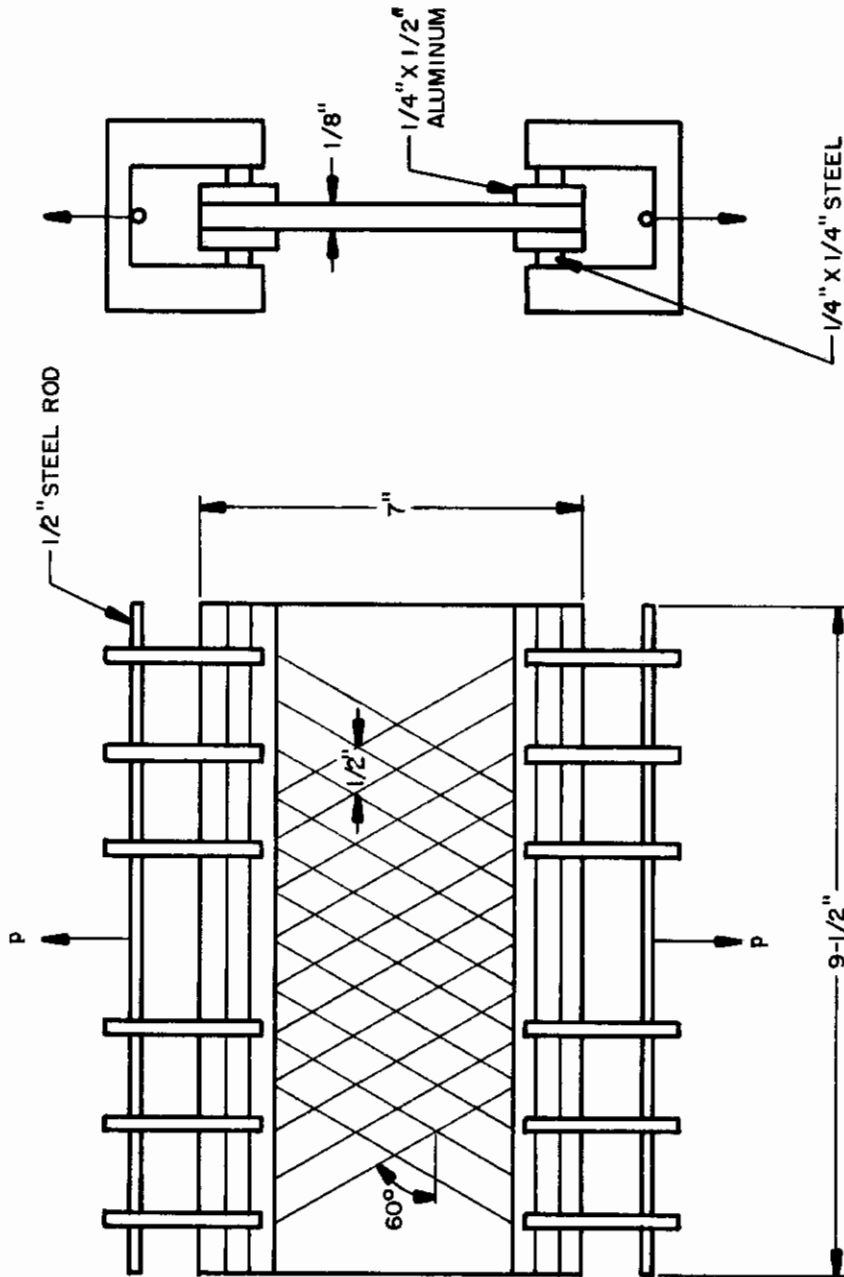
Figure 32. Configuration of Reinforced Plate and Loading Fixture

78

failure. Failure was not achieved because of slippage in the clamping device. The boron-reinforced plate was taken continuously to failure, as was the nonreinforced plate. In all three cases, the Instron crosshead motion was stopped where photographic recording was desired. There was considerable relaxation each time the crosshead was stopped.

RESULTS AND DISCUSSION

Figures 33 and 34 were taken during the first test on the steel-wire-reinforced plate. These photographs indicate that there was a reasonably uniform biaxial field near the center of the plate. In the center region, there is no abrupt color or shade change which implies that the stress transfer between the matrix and wires is occurring uniformly.

In the second run, the specimen shifted slightly upon application of load, resulting in a higher stress level on one side of the plate (Fig. 35 through 38). This is quite evident in Fig. 35 through 38 from the discrete shade change across the wires in the regions where the stress is not uniform. With further increase of load, the fringe pattern shown in Fig. 36 began to appear. At this point, the Instron crosshead motion was stopped, and an extremely interesting phenomenon was observed. The process of stress transfer was observed to be taking place in incremental fashion accompanied by a distinct high-frequency crackling sound.

The unusual fringe pattern started at the wire in the upper left of the plate, and with the crosshead stopped, the pattern was seen to move to the wires immediately to the right. This was observed to occur in discrete steps. When a new state of equilibrium was achieved, no further fringe change was observed. This process was repeated several times with increasing load and the pattern progressed as shown in Fig. 36 through 38. The reinforcing wires distributed the imposed stress in a way that enabled the central portion of the plate to maintain a very uniform stress field. The residual stress field is shown in Fig. 38 after load was removed. Post-test examination revealed waviness of the wires in the regions of extremely convoluted fringe pattern as well as portions of

79

O LOAD
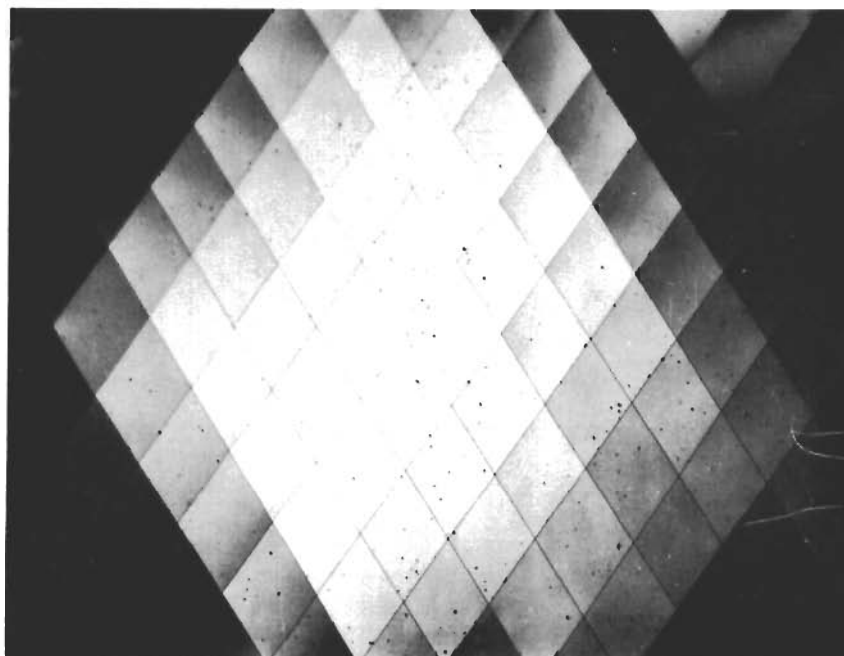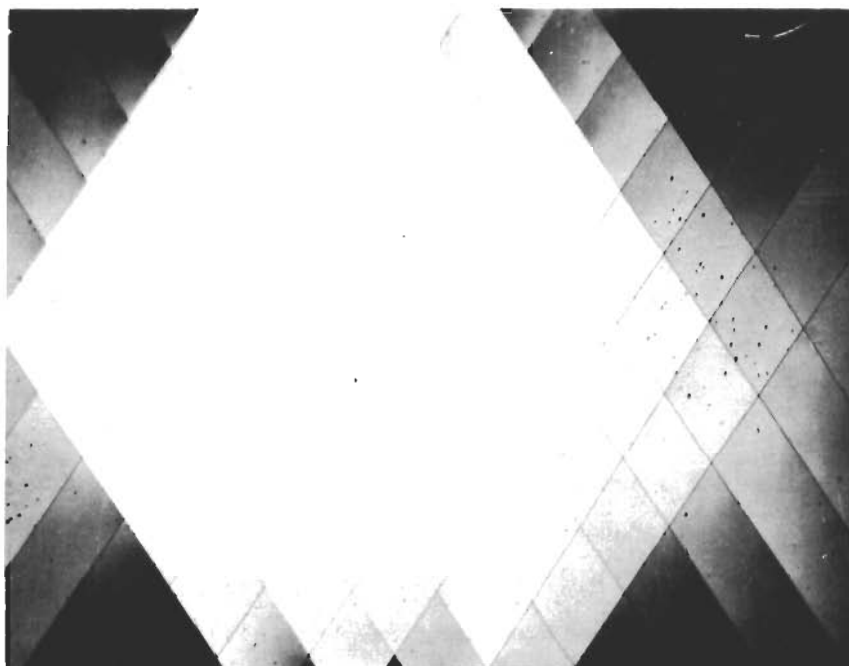
IO LB LOAD

Figure 33. Stress Patterns for a Tension Loading of a
High-Strength Steel-Wire-Reinforced
Plate
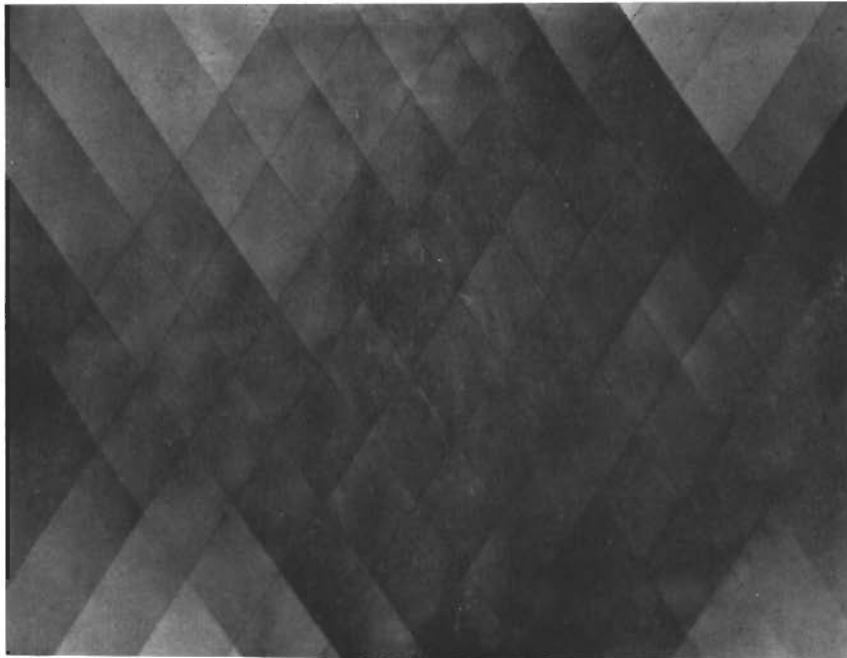
38 LB LOAD
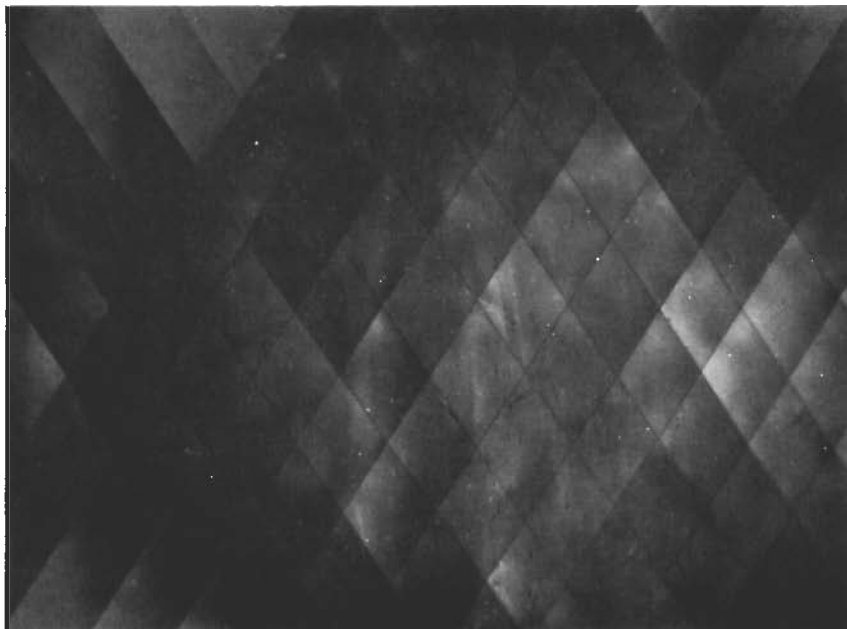
47 LB LOAD

Figure 34. Stress Patterns for a Tension Loading of a
High–Strength Steel–Wire–Reinforced
Plate

81
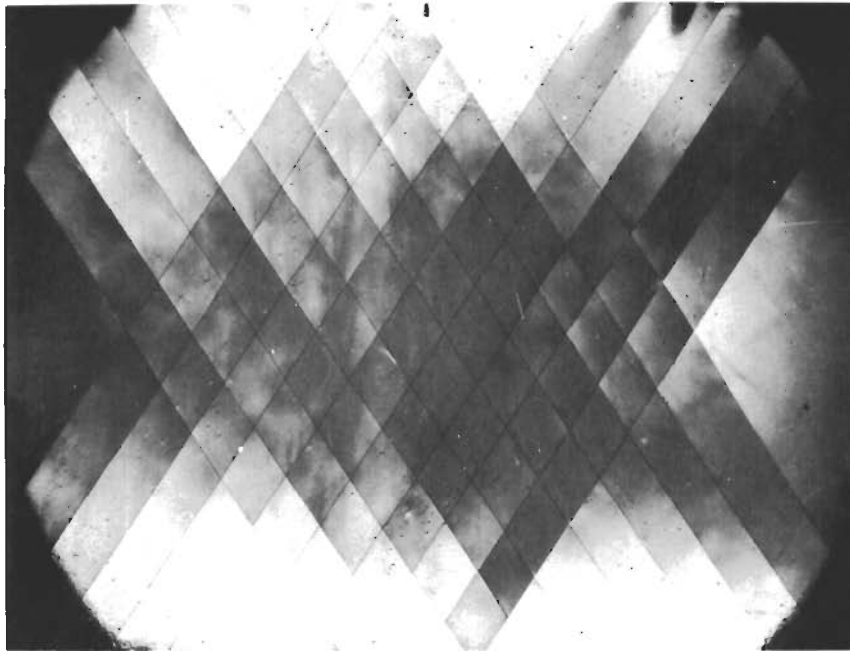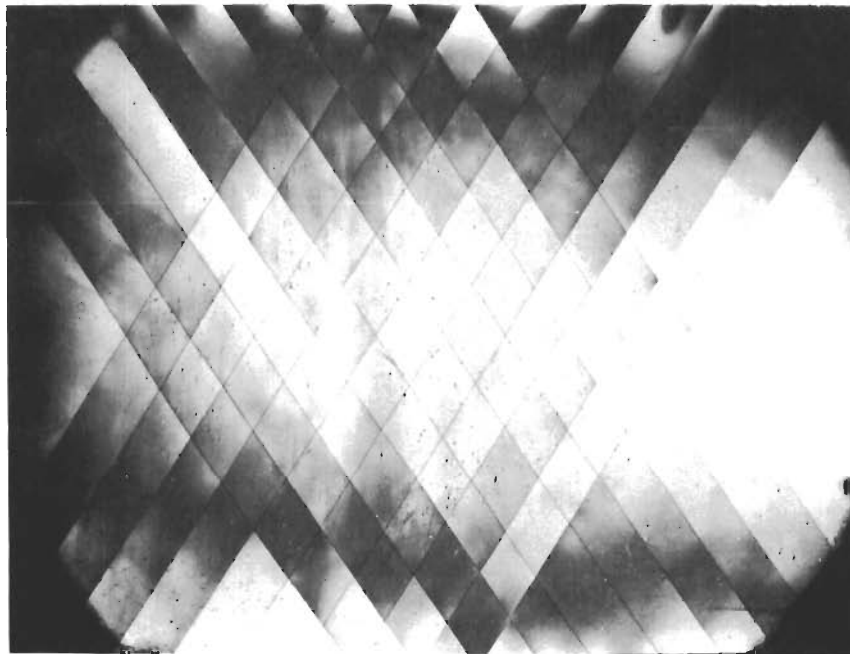
90 LB LOAD

110 LB LOAD

Figure 35. Stress Patterns for a Tension Loading of a
High-Strength Steel-Wire-Reinforced
Plate.

82

136 LB LOAD
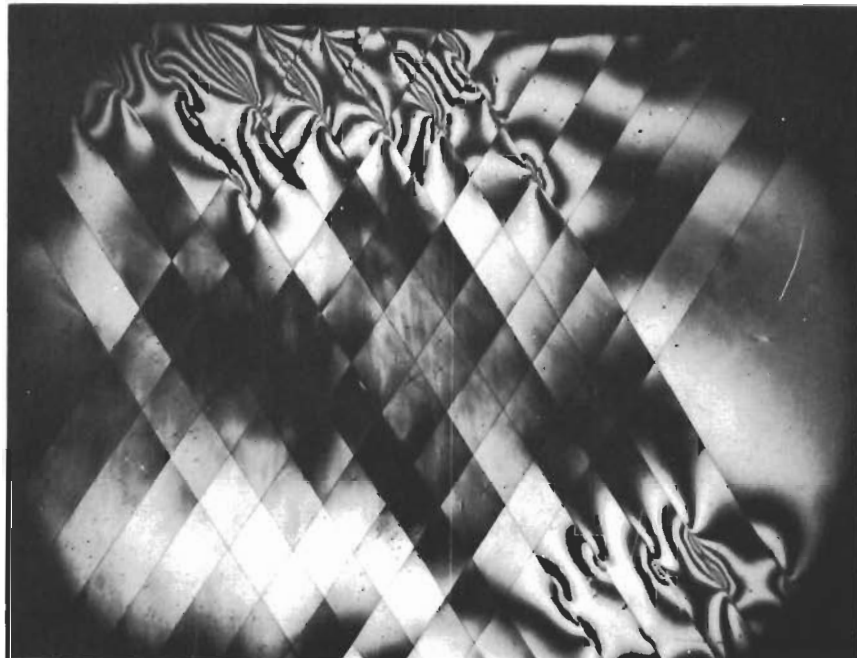
137 LB LOAD

Figure 36. Stress Patterns for a Tension Loading of a
High-Strength Steel-Wire-Reinforced
Plate

83
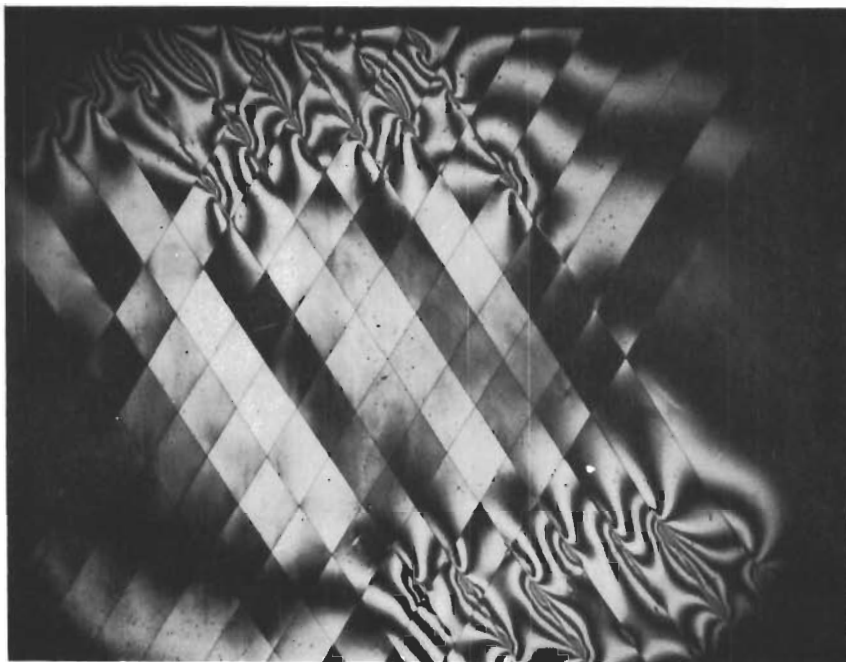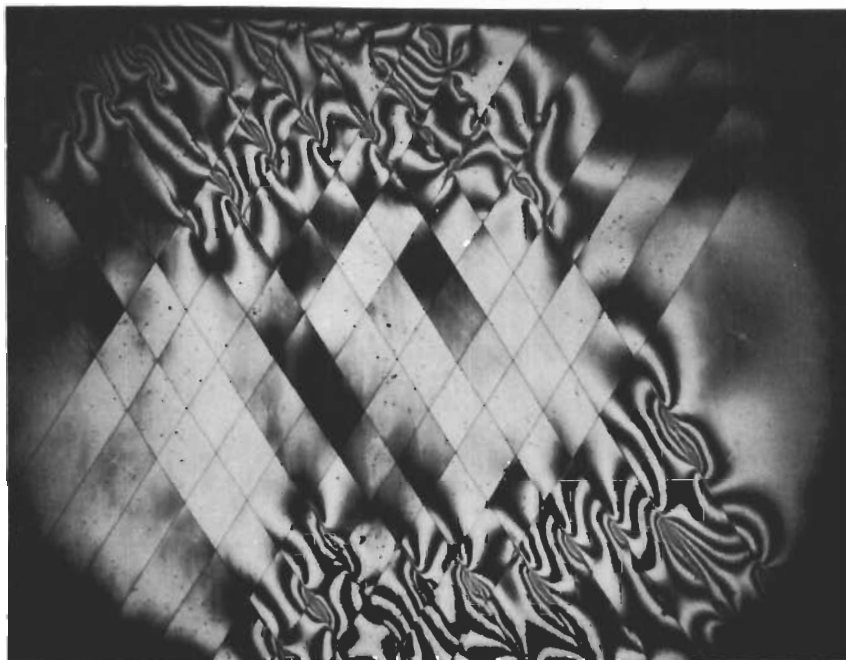
144 LB LOAD

144 LB LOAD

Figure 37. Stress Patterns for a Tension Loading of a
High-Strength Steel-Wire-Reinforced
Plate

84
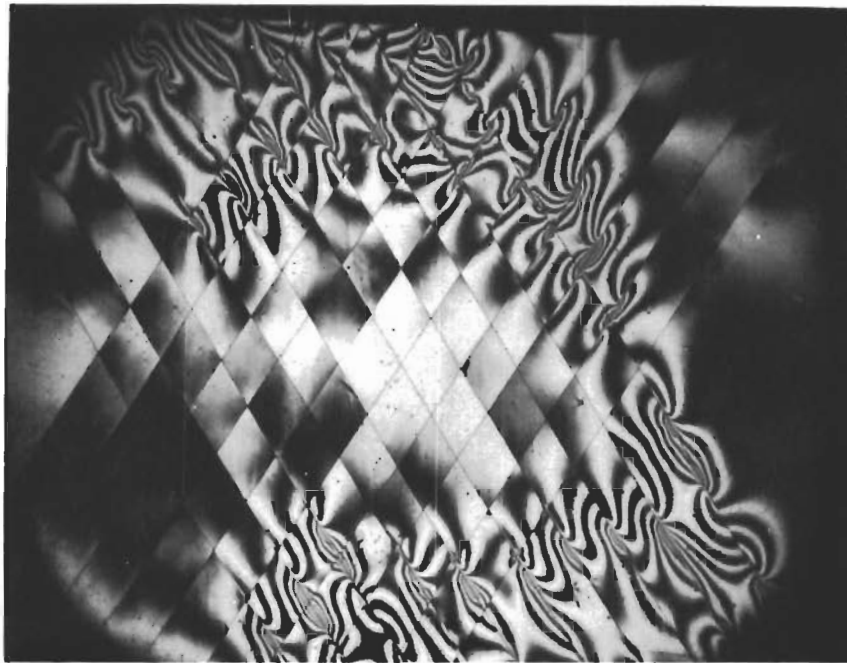
143 LB LOAD
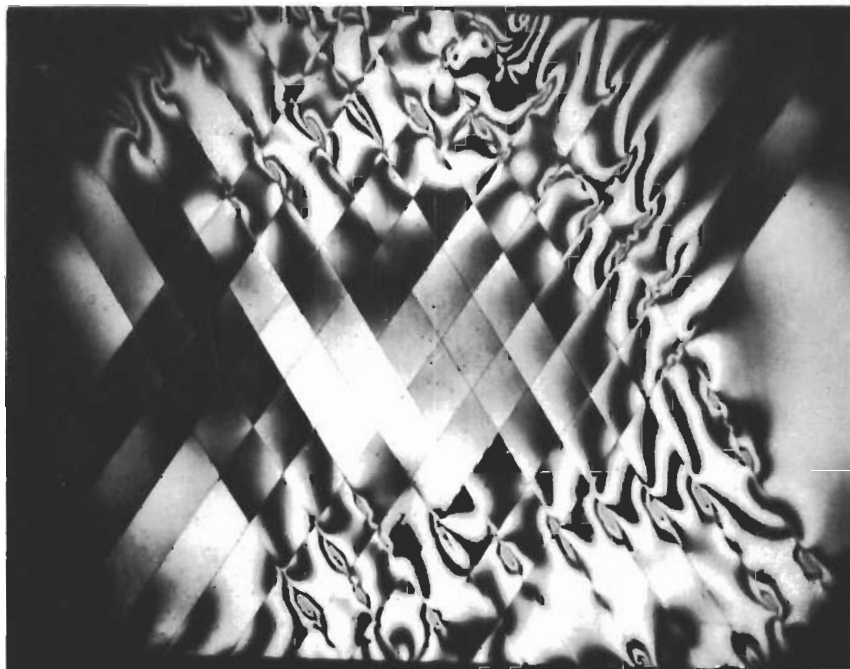
NO LOAD

Figure 38.   Stress Patterns for a Tension Loading of a
             High-Strength Steel-Wire-Reinforced
             Plate

85

unbonding of the wires. It is important to note that in some places where there was waviness, the wires had moved from their original position into the wave configuration. Careful study of the photographs shows a definite bending of the initially straight wires. This is probably a result of the fact that the wires were forced to change angle (increase from original 60 degrees) to accommodate the increasing loads. This bending is generally observed to occur at a node (intersection of two wires).

To ensure more uniform distribution of the applied loads on the boron-reinforced and nonreinforced plates, an improved device to couple the plates into the Instron tester was devised. The application of the load to the boron-reinforced plate was considerably more uniform than the loading imposed on the steel-reinforced plate (Fig. 39). The differences in the uniformity in loading and load levels makes a quantitative comparison of the boron- and steel-reinforced plates difficult. However, certain qualitative comparisons are possible.

At low load levels up to about 600 pounds, the stress transfer between the matrix and boron fibers was taking place smoothly. This was demonstrated by no abrupt fringe or shade changes. However, when the load level reached 650 pounds, a higher-order fringe pattern developed along part of one of the fibers. This can be seen at the lower left portion of Fig. 39. The appearance of this fringe pattern was accompanied by a sound similar to that which was observed in the steel-reinforced plate. With further increase in load, a similar pattern appeared near the center of the plate, and subsequently the pattern covered almost the entire plate. As with the steel-reinforced plate, this stress transfer usually occurred in discrete steps, always accompanied by the characteristic sound. Failure occurred at a load of 2650 pounds. Figure 40 shows the plate prior to failure and Fig. 41 immediately after failure. Post-failure examination revealed that the high-order fringe patterns were associated with unbonded regions of filaments. However, unlike the steel-reinforced plate, there was no buckling or bending of fibers.

The nonreinforced plate failed in the grips at a relatively low load, thereby making comparisons impossible.

86
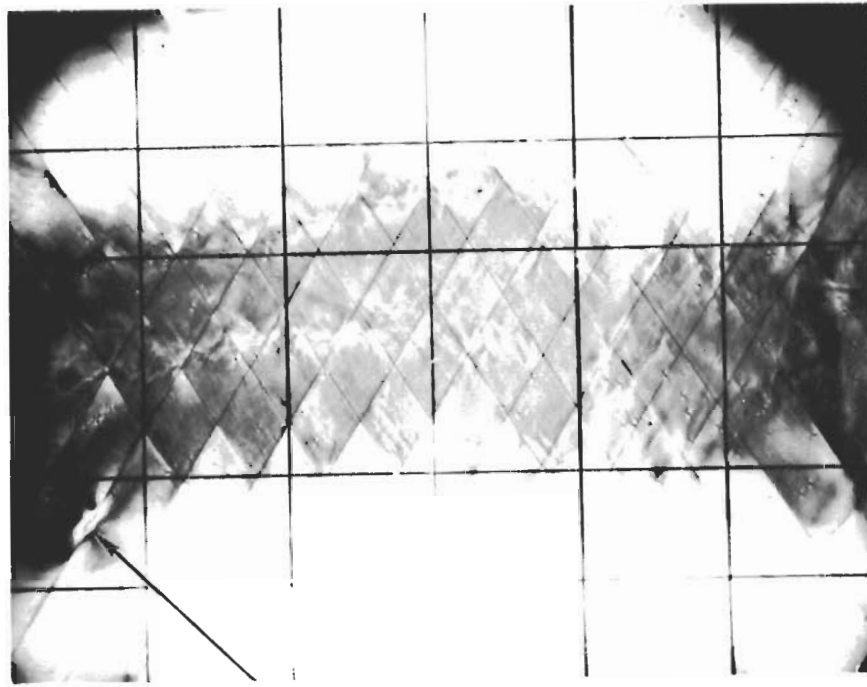
Figure 39. Stress Patterns for a Tension Loading of a
Boron Filament-Reinforced Plate

87
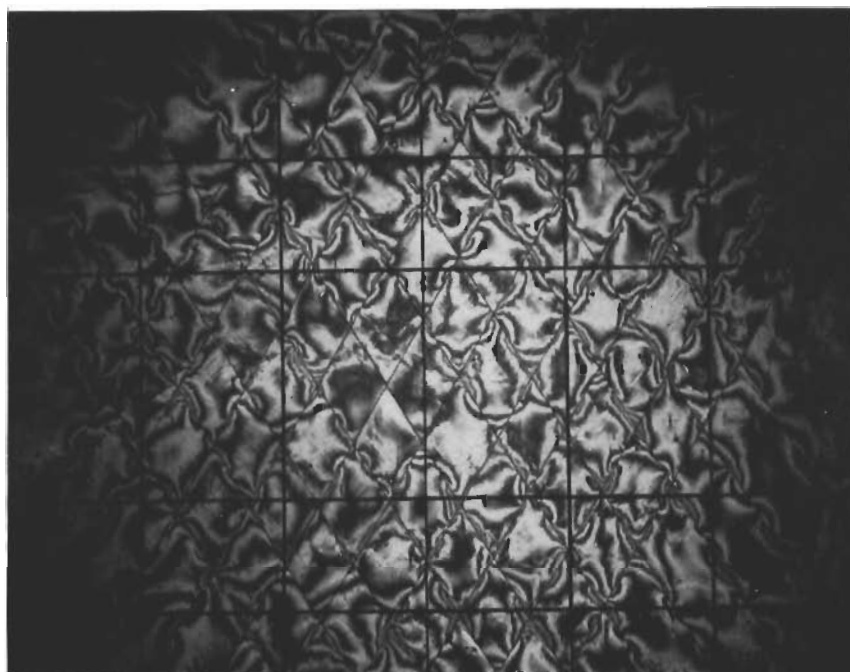
Figure 40. Stress Patterns for a Tension Loading of a
Boron Filament-Reinforced Plate

Figure 41 . Stress Patterns for a Tension Loading of a
Boron Filament-Reinforced Plate, Post
Failure

88

These qualitative observations of the stress transfer between matrix and wires could have far-reaching implications in the applications of filament-reinforced composites. It is believed that the photoelastic technique may be the most effective tool for gaining insight to the answers to such questions as:

1. What is the mechanism of the bond failures and subsequent redistribution of the stresses which were observed in the tests reported?

2. What was the effect of wire migration (as observed in the steel-reinforced plate) on the stress transfer mechanism?

3. What is the role of fiber and matrix elongation properties in the observed discrete stress transfer process?

The answers to such questions may better allow the composite designer to use the properties of reinforced composites more efficiently. However, much more work is needed along these lines.

MICROPHOTOELASTIC ANALYSIS OF
THREE-DIMENSIONAL SPECIMENS

To obtain more efficient and versatile reinforced composite structures, a better understanding of the mechanism by which stress is transferred between matrix and filaments is required. The techniques of microphotoelastic analysis were developed toward this end. As will be shown below, microphotoelasticity may provide insight into the complex interactions which occur and hopefully serve as a guide to the applied mathematicians who are currently concerned with the problem.

SPECIMEN DESCRIPTION

To obtain microspecimens representing the variety of geometric arrangements found in reinforced-laminate structures, a twofold procedure was followed. First, the photoelastic matrix was cast about a three-dimensional fiber configuration. The next step involved cutting the requisite thin sections to be used for microphotoelastic analysis from the cured resin-fiber composite.

Sectioning of these three-dimensional specimens proved to be a difficult process. After investigating a number of possible cutting techniques, a diamond-edged lapidary saw was chosen. It was found that this technique reduced extraneous effects in the neighborhood of the wires. This method of cutting sections worked best with boron-reinforcing filaments.

Experience gained from this program has shown that loading and observing micromodels present many problems which are not encountered with macromodels. Extremely sharply resolved fringe patterns are essential for obtaining meaningful photoelastic information under high magnification. It was found that excellent optical systems and highly polished specimen surfaces are required to achieve satisfactory fringe resolution.

91

A number of micromodels, reflecting a variety of filament configurations and volume percents of reinforcement, were fabricated and tested. With one exception, all of these microspecimens were designed to show the interacting stress fields which develop around the filaments when the specimens are loaded.

The three-dimensional microspecimens included the following filament configurations:

1. A row of filament ends between two parallel filaments

2. A row of filament ends

3. Four filament ends in an approximate rectangular array

4. Two filament ends on each side of single long filament

5. A disk with a filament along a diameter

The reinforcing elements in specimens 1 through 4 were boron fibers while in specimen 5 a high-strength steel wire was used. Photoelastic resin (PL-2) was the matrix material in all of the above specimens.

TEST SETUP

The polished specimens were bonded to the faces of the microstraining frame by an epoxy adhesive. Loads were applied to the specimens while they were on the stage of a Leitz Ortholux microscope, or on the stage of the Rocketdyne microstraining instrument (Fig. 42). Specimens 1 through 4 were subjected to tensile and compressive loads. The disk was subjected to diametral compression with the filament along the axis of the compressive force.

The microphotoelastic observations were made with white light and mercury green monochromatic light. Photographs were taken of the isochromatics, and the isoclinic lines were traced or photographed.

92

— LIGHT SOURCE

— COLLIMATOR

— POLARIZER

— STRAINING FRAME

— STAGE

— ANALYZER

CAMERA
LENS

CAMERA
BACK

VIEWING
SCREEN

FRONT
SURFACE
MIRROR —
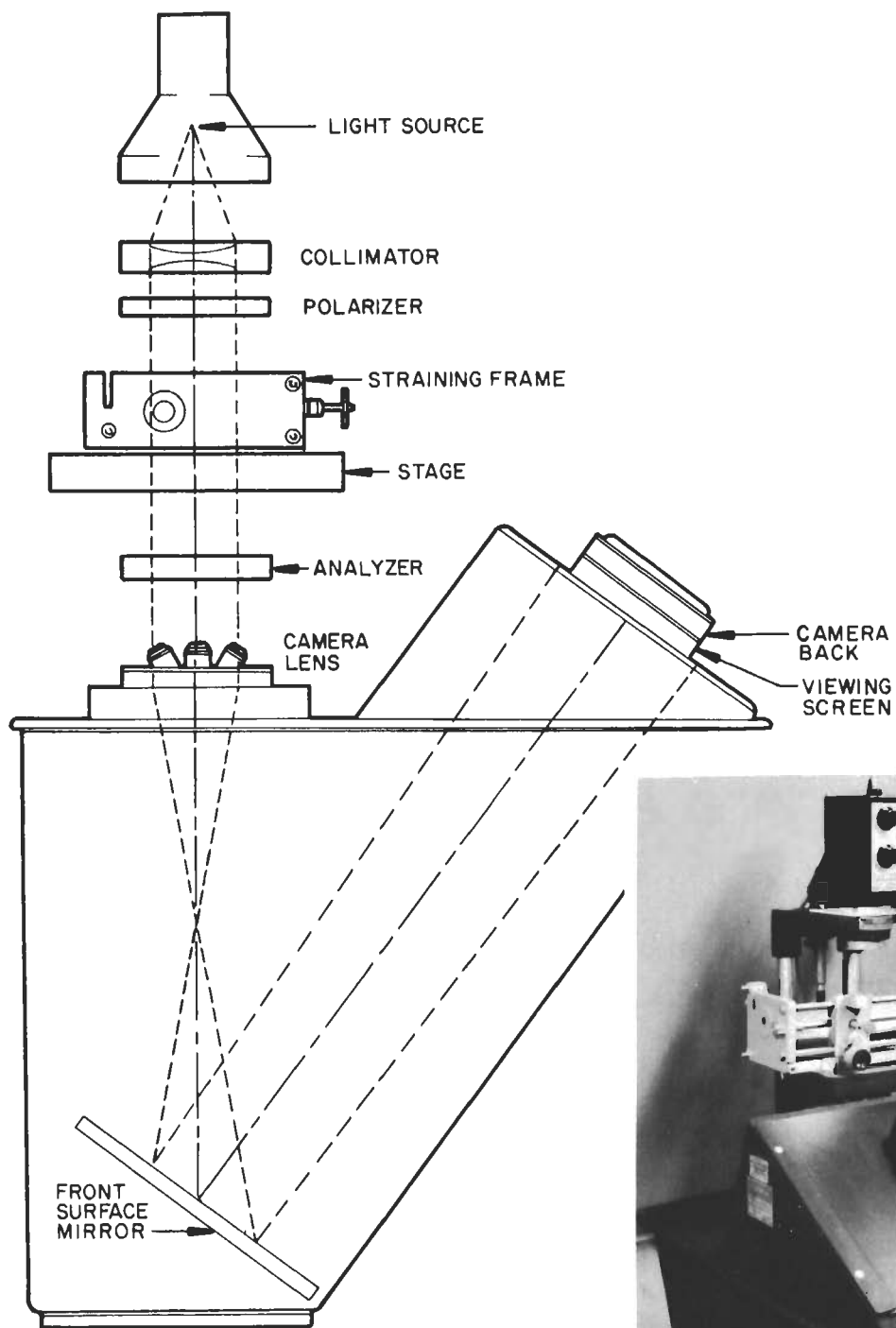
Figure 42. Microstraining Instrument

93

RESULTS AND DISCUSSION

Fabrication, loading, and photoelastic analysis of microspecimens proved
to be a difficult and exacting task. However, the techniques developed
enabled attainment of excellent resolution of the intricate patterns
which developed in the immediate vicinity of the fibers.

Four specimen geometries which have been subjected to compressive loads
are shown in Fig. 43 through 46. In Fig. 43 and 45 a swirl-like forma-
tion is observable which has not appeared in macrospecimens of PL-2
photoelastic resin. In checking on possible causes of the swirls, it was
found that the manufacturer was not aware of the problem. The swirls may
be due to insufficient mixing of the resin and hardener. Since they are
discernible only in thin specimens under magnification and with good
optical resolution, it is not surprising that the resin manufacturer
was unaware of the existence of this problem. However, this factor
should be further investigated if still better resolution is desired.

Figures 44 and 46 are examples of the excellent resolution which was
attained. The sharp fringe lines facilitate observation under much
higher magnification and permit quantitative observations to be made
with greater accuracy. Examples of the resolution obtainable at high
mangification are shown in Fig. 47 through 49.

The outstanding perturbations which flaws induce on otherwise very
symmetrical stress patterns are shown in Fig. 44 and 46. In both of
these cases, the effect of the flaws is felt by filaments which are
many wire diameters away from the flaw. The flaws were not apparent in
the unloaded specimens, but manifested themselves under load. Figure 48
is a higher mangification of the flaw region shown in Fig. 46. Since
the filament diameter is approximately 5 mils, it is apparent from the
photograph that the fringe gradient near the flaw is extremely high.
The flaw observed in Fig. 48 is a crack formation in the matrix. A
question which presents itself relates to what part this observable very
high fringe gradient plays in the propagation of such flaws.
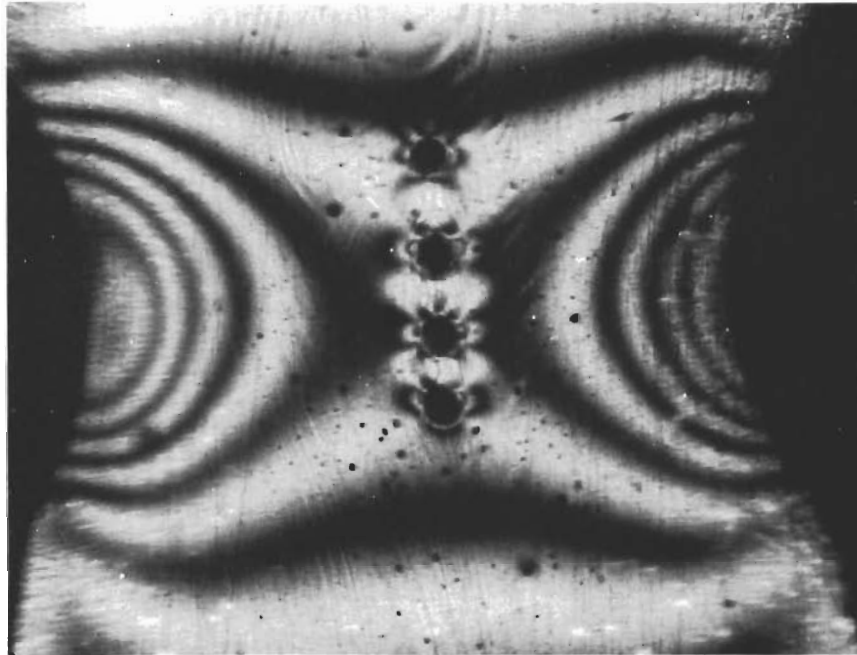
Figure 43. Microspecimen Subjected to Compression
(Mercury Green Monochromatic Light
With Crossed Quarter-Wave Plates)
25X
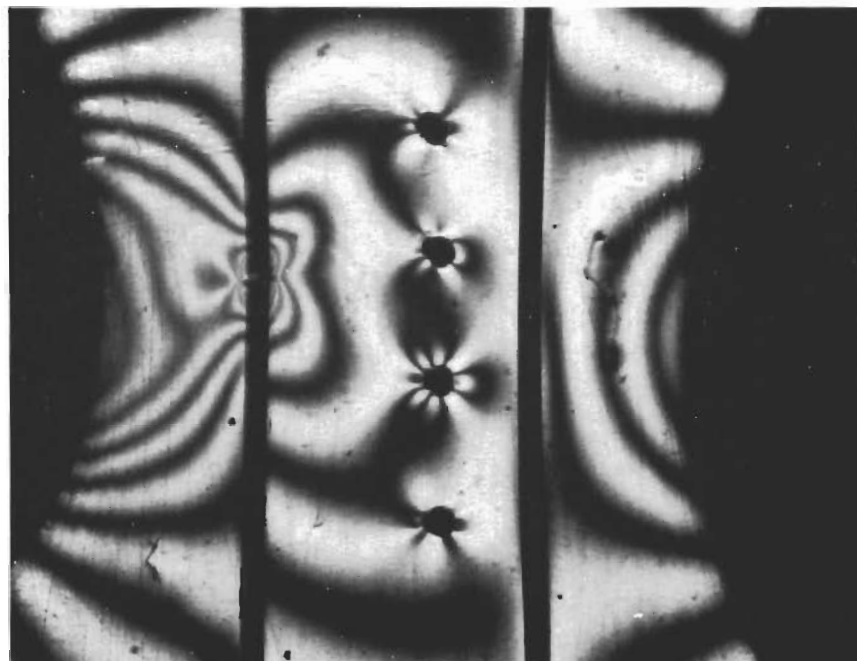
Figure 44. Microspecimen Subjected to Compression
(Mercury Green Monochromatic Light
With Crossed Quarter-Wave Plates)
25X
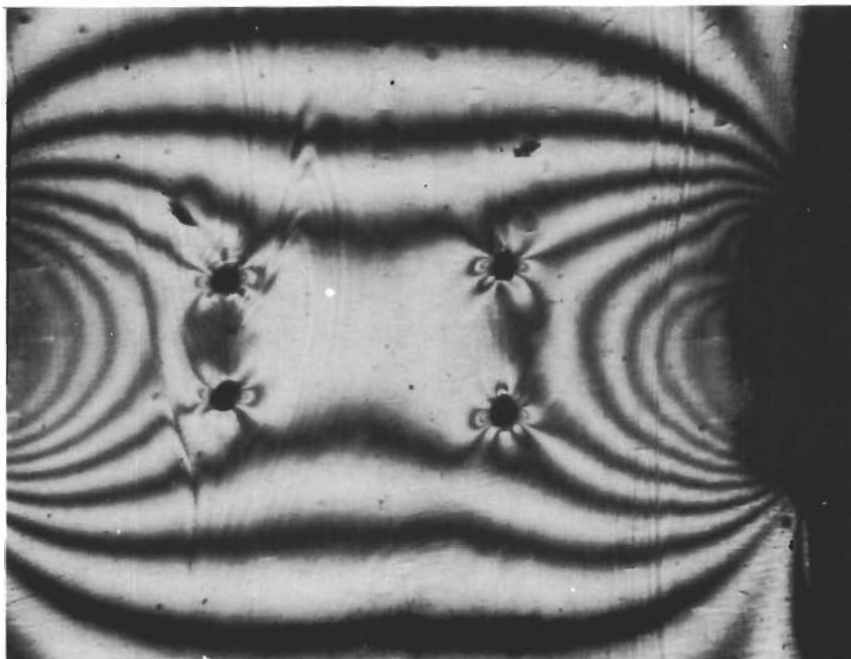
Figure 45. Microspecimen Subjected to Compression
(Mercury Green Monochromatic Light
With Crossed Quarter-Wave Plates)
25X
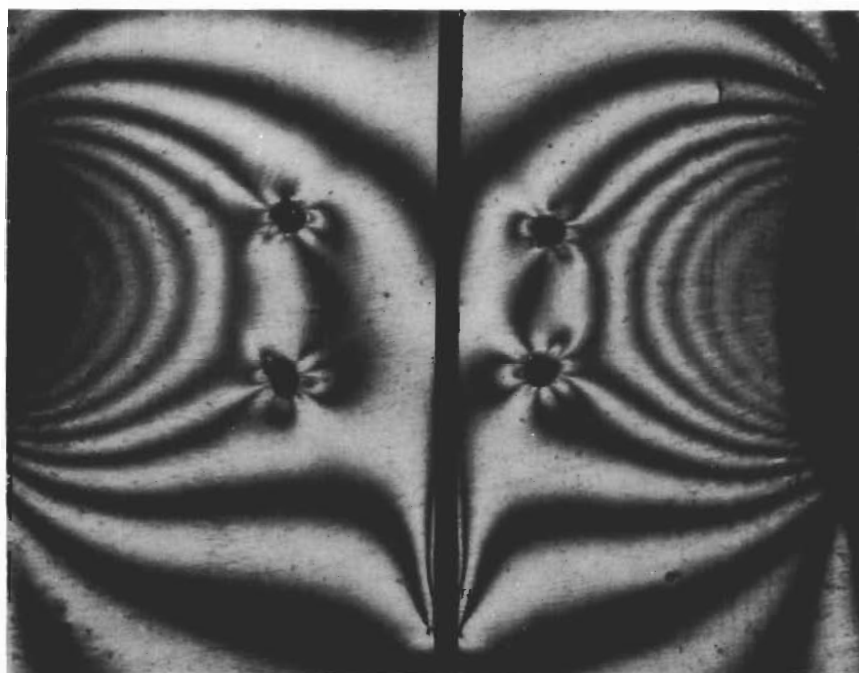
Figure 46. Microspecimen Subjected to Compression
(Mercury Green Monochromatic Light
With Crossed Quarter-Wave Plates)
25X
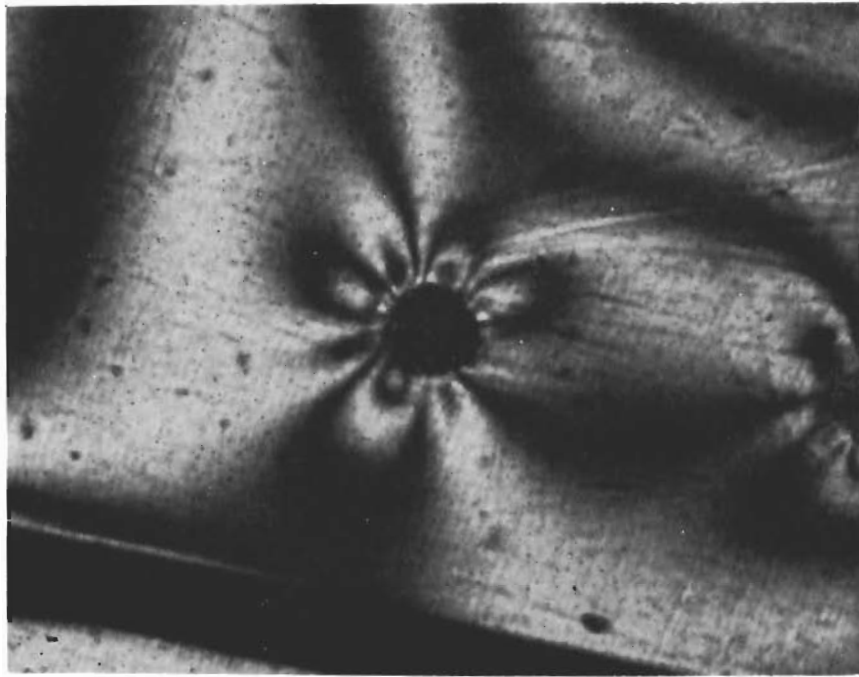
Figure 47. Detail of Microspecimen Subjected to
Compression (Mercury Green Mono-
chromatic Light With Crossed
Quarter-Wave Plates) 100X
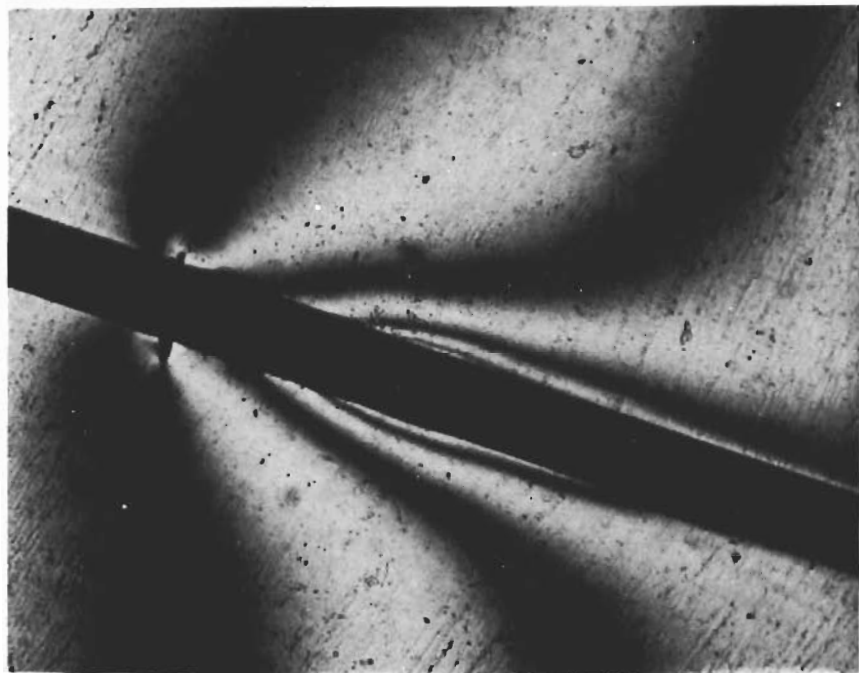
Figure 48. Detail of Flaw in Microspecimen Subjected
to Compression (Mercury Green Mono-
chromatic Light With Crossed Quarter-
Wave Plates) 100X

97

Figure 49 is an exceptionally illuminating photograph, at very high magnification (320X) of the flaw observable in Fig. 44. At first it was believed that this flaw represented a matrix crack similar to that shown in Fig. 48. However, under more detailed microscopic examination, a wire fracture was confirmed, as well as separation of the matrix in the fracture region (the dark triangular regions in Fig. 49). Again, extremely high fringe gradients are present.

As a consequence of the resolution attainable illustrated in Fig. 47, it is apparent that the techniques of microphotoelasticity could be instrumental in establishing the causes and mechanism of propagation of flaws in reinforced composite specimens. Continuous photographic recording would be used to advantage in such studies.

Figure 50 shows the complex interactions between the fiber ends in a tensile specimen. A similar specimen, with two parallel fibers on the side of the filament ends, was also subjected to tension for comparison with Fig. 51. Upon application of the tensile load to this specimen, unbonding occurred along portions of the longitudinal fibers. The unbonding initiated near the faces of the microstraining frame and propagated toward the center of the specimen. It appeared that the matrix was being pulled from around the wire. Figure 51 shows the resulting fringe pattern, where an extremely high fringe density is observed parallel to the fiber. Such high-density fringe concentrations may help explain the propagation of unbonding which was previously described in the beam and plate tests. More work is essential to confirm this correlation between the macro- and microspecimen behavior and quantitative examination of the high-density fringe areas.

The disk subjected to diametral compression along a filament is a variation on the well-known experiment with a nonreinforced disk (Ref. 10).
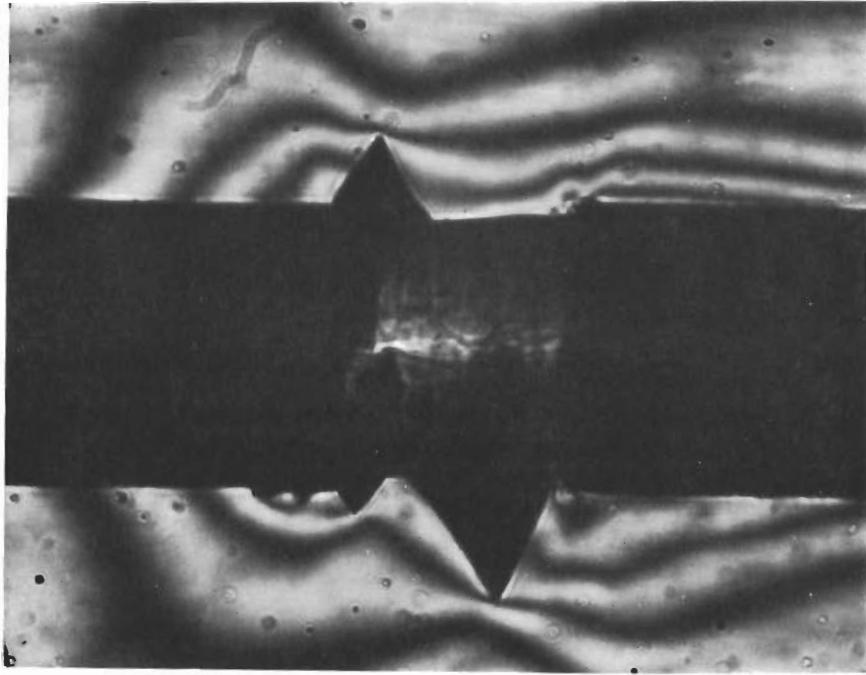
Figure 49. Detail of Flaw in Microspecimen
Subjected to Compression
(Mercury Green Monochromatic
Light With Crossed Quarter-Wave
Plates) 320X

Figure 50. Microspecimen Subjected to Tension (Mercury Green Monochromatic Light With Crossed Quarter-Wave Plates) 25X

Figure 51. Unbonding in Microspecimen Subjected to Tension (Mercury Green Monochromatic Light With Crossed Quarter-Wave Plates) 35X

There is a biaxial field at the center of the disk, of compressive stress along the axis of applied compression and tensile stress in the perpendicular direction. As a result of the normal tensile stress in the biaxial field, the steel wire unbonded, as can be seen in Fig. 52. The isochromatic pattern which exists in the vicinity of the center of the disk, the region of greatest variation from the nonreinforced disk and consequently the region of greatest interest, is shown under a higher magnification in Fig. 53. To further compare this specimen with the experimental results on a nonreinforced disk, the system of isoclinic lines was determined and these are plotted in Fig. 54. In the regions distant from the unbonded part of the wire, the isoclinics are very similar to those of the nonreinforced disk. However, the unbonding causes an extremely complex situation to exist.
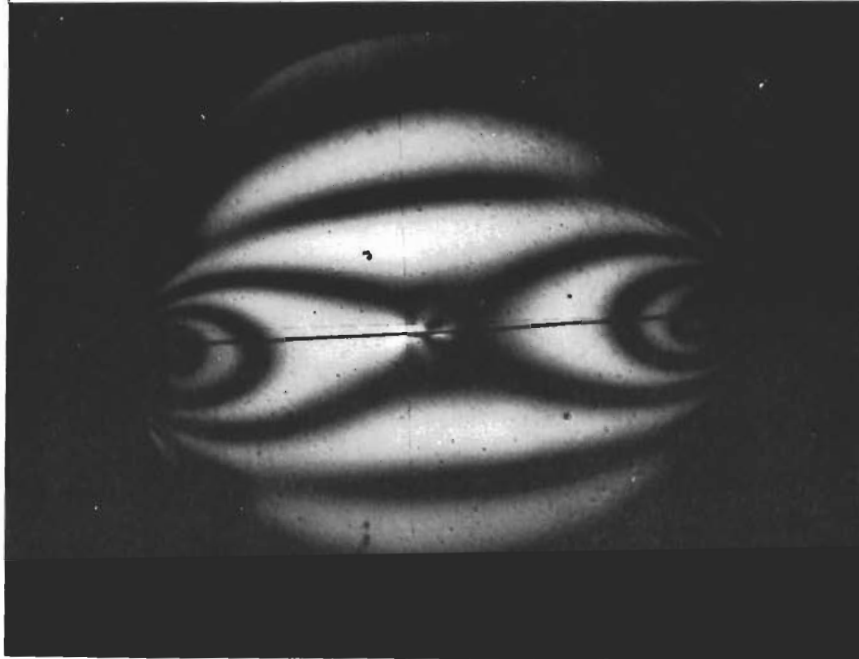
Figure 52.   Reinforced Disk Subjected to Diametral
Compression (Mercury Green Mono-
chromatic Light With Crossed Quarter-
Wave Plates) 4.5X

Figure 53.   Detail of Reinforced Disk Subjected to
Diametral Compression (Mercury Green
Monochromatic Light With Crossed
Quarter-Wave Plates) 35X

102
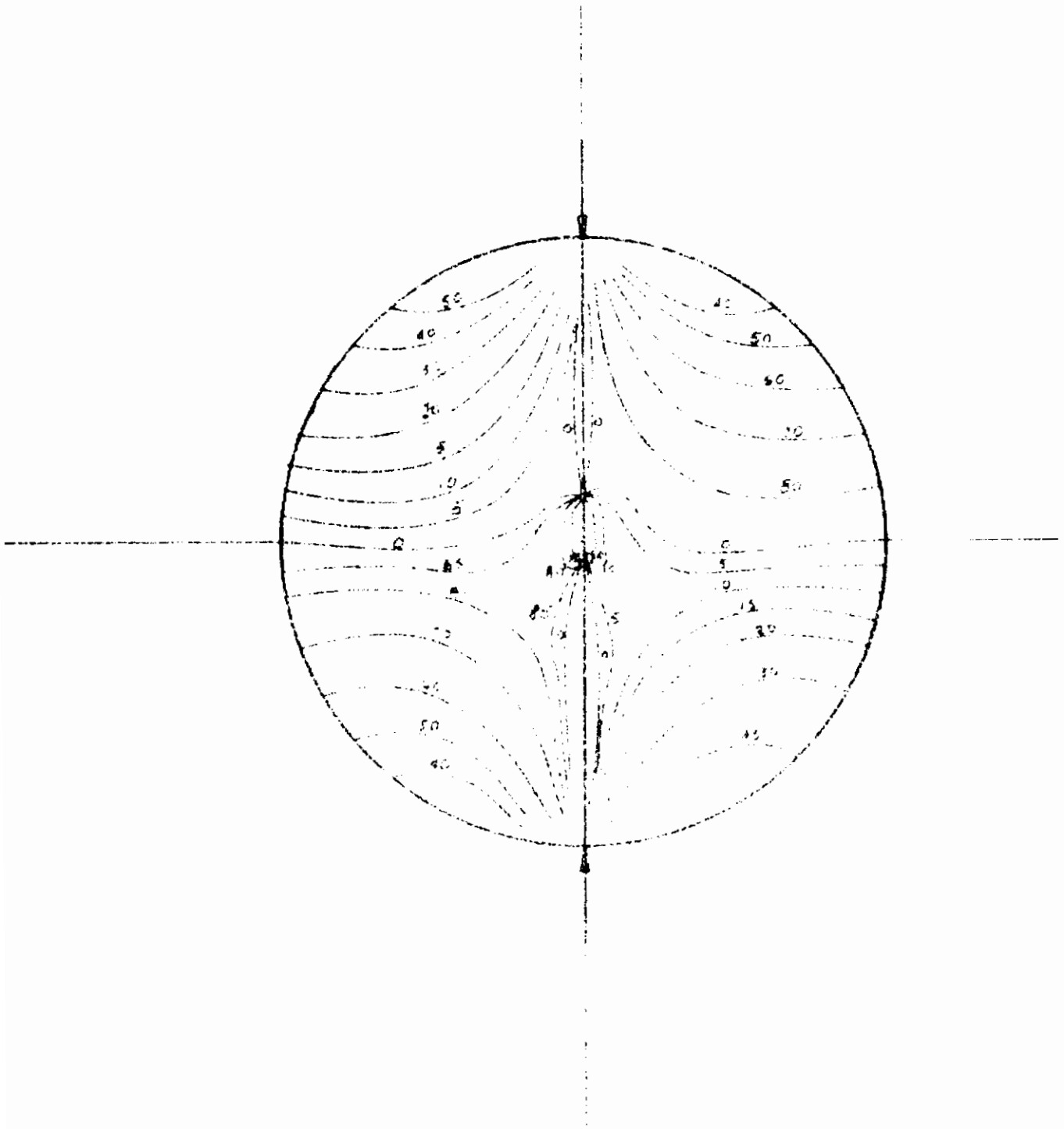
Figure 54. Isoclinics in Disk Under Diametral Compression

103

RESULTS AND CONCLUSIONS

BEAMS

The effect of filament modulus on beam stiffness in four-point flexure was investigated. Boron fibers provided significantly greater stiffening effect in comparison with all other fibers which were evaluated in the beams. This conclusion is somewhat surprising in view of the fact that the moduli of the boron filaments and tungsten wire were essentially the same. Apparently, the ratio of filament to matrix moduli or the modulus of the filament itself is not sufficient to explain the observed increase in beam stiffness. However, due to a redirection of the program with increasing emphasis on microphotoelastic studies, no subsequent beam tests were performed. It is suggested that further work along these lines would be desirable in order to gain an insight into the causes of this observation. The effects of filament modulus, elongation, and volume loading on the modes of failure in mid-point loading were also investigated.

These parameters were shown to have considerable influence on the nature of the fracture.

The internal strain wire technique was applied to reinforced beams. The technique was shown to be effective and a potentially powerful research tool for reinforced composite investigations.

PLATES

Plates with boron and steel filament reinforcements were tested in a biaxial strip test and observed by photoelastic techniques. A stepwise stress transfer process was noted in both plates. Buckling and unbonding

105

of wires was observed in the steel-reinforced plate, whereas only unbonding occurred in the boron-reinforced plate. The observations indicate that this technique would be useful in investigating structural problems such as the best manner of joining reinforced composite plates.

MICROPHOTOELASTIC ANALYSIS OF THREE-DIMENSIONAL MODELS

Three-dimensional models representing fiber configurations in laminates were loaded and photoelastic observations were obtained. Techniques were developed that provided excellent resolution of fringe patterns.

Initiation of flaws in the filament and resin was observed. Extremely high fringe gradients near the flaws were recorded. The field of influence of these flaws was observed to extend for a distance of many fiber diameters. These observations on flaws offer a starting point for a possible failure hypothesis which could have direct applications in laminates and other reinforced composites. Development and propagation of unbonding in a three-dimensional microspecimen under tension was observed. This was in some respects similar to the unbonding noted in the beams and plates. A correlation of the behavior of the micro- and macro-models should be important. Unbonding of a filament in a biaxial field (compression along wire, tension normal to wire) was observed. This type of stress situation is frequently encountered in larger structures. It is important to understand this mode of structural failure because such unbonding could adversely affect the structure.

106

APPENDIX A

FILAMENT ELONGATION MEASUREMENTS

In calculating the fiber modulus an accurate measure of the true elongation of the fiber is essential. Because there is fiber strain transmitted into the grips, the grip separation is not the actual gage length on which to base strain (or modulus) calculations. Among the several techniques utilized to account for the strain in the grips, the method of extrapolating to zero elongation (Ref. 11) was found to be very effective.

The determination of effective gage length is based on the repeatable performance of the test machine, gripping devices, and filaments at zero-inch grip separation. It is assumed that the strain transmitted back into the grips will be the same at zero grip separations as for other grip separations. Gross specimen slippage or premature sample fracture within the vise jaws is readily detectable, and serves as a basis to reject results of the test. These ground rules were justified by the consistent performance demonstrated by all the ductile materials tested in this program. Brittle materials produced wide scattering in tensile forces, but invariably followed the same stress-strain pattern to fracture, independent of gage length. The procedure used to determine the effective gage length (Ref. 11), involves extrapolation to zero elongation according to the following:

1. Various samples are tested at different initial grip separations.

2. For a given value of load, the elongation is plotted for the different initial grip separations.

3. Extrapolating to the gage length axis (zero elongation), the intercept gives a value representing elongation within the grip.

4. The effective gage length is obtained by adding the elongation within the grip to the initial grip separation.

107

This method is based on two major assumptions which require experimental verification. One is that the elongation transmitted into the grips is the same for all initial grip separations at a given stress level. The second is that the elongation transmitted into the grips is, for practical purposes, the same for different stress levels. To show how the extrapolation to zero elongation is related to the elongation transmitted into the grips we define

$$L_i \quad = \quad \text{initial separation of grips}$$

$$\Delta \quad = \quad \text{total elongation transmitted into the grips } (\Delta/2 \text{ into each grip})$$

$$\delta L_i \quad = \quad \text{change of grip separation}$$

Then the original fiber length being tested (the effective gage length) is

$$L_i + \Delta$$

The strain is given by

$$\epsilon_i \quad = \quad \frac{\delta L_i}{L_i + \Delta}$$

Using the subscript $_o$ to represent the experimental results for a given initial grip separation, and considering a particular stress level, then

$$\sigma \quad = \quad E \; \frac{\delta L_o}{L_o + \Delta} \quad = \quad E \; \frac{\delta L_i}{L_i + \Delta}$$

from which we can obtain

$$L_i \quad = \quad \delta L_i \; \frac{(L_o + \Delta)}{\delta L_o} \quad - \quad \Delta$$

This is a linear equation which can be expressed by a plot of the variables L_i vs δL_i. Therefore, if $\delta L_i \rightarrow 0$, i.e., we consider zero elongation, then

$$L_i = -\Delta$$

If the experimentally determined plot of L_i vs δL_i is a straight line, then our first assumption is justified and the intercept on the $\delta L_i = 0$ line is equal to the elongation transmitted into the grips.

Now consider the above argument for two different stress levels, and consider the possibility that the elongation transmitted into the grips is different at the new stress level. Using the second subscripts α and β to distinguish two different stress levels, the following expression is obtained:

$$L_{i\alpha} = \delta L_{i\alpha} \frac{(L_{o\alpha} + \Delta_\alpha)}{\delta L_{o\alpha}} - \Delta_\alpha$$

and

$$L_{i\beta} = \delta L_{i\beta} \frac{(L_{o\beta} + \Delta_\beta)}{\delta L_{o\beta}}$$

As $\delta L_{i\alpha}, \delta L_{i\beta} \rightarrow 0$,

$$L_{i\alpha} = -\Delta_\alpha$$
$$L_{i\beta} = -\Delta_\beta$$

If $\Delta_\alpha = \Delta_\beta = \Delta$, i.e., the lines for the two different stress levels intersect at zero elongation, then the amount of elongation transmitted into the grips is the same.

When the experimentally determined curves intersect at the same point on the $\delta L_i = 0$ line, then the second assumption is justified within experimental error. The specimens on which these calculations were performed satisfied the two assumptions as can be seen in the example shown below.

Using the tungsten data in Fig. 55, elongation values are calculated in the following manner:

1. Using point-to-point correction at 7 pounds force,
   the resultant grip separation at 7 pounds and 0.1-inch
   initial grip separation $\qquad$ $e_{0.1}$ = 0.0100 inch

   the resultant grip separation at 7 pounds and 10-inch
   initial grip separation $\qquad$ e_{10} = 0.0796 inch

   Percent elongation = $e_{\%}$ = $\dfrac{\Delta e \times 100}{10}$ = $\dfrac{(e_{10} - e_{0.1}) \times 100}{10}$

   $\qquad\qquad$ = 0.696 percent

2. Using the graphical solution
   Effective gage length $\quad$ = $\quad$ 11.3 inches
   Percent elongation = $\dfrac{\Delta e \times 100}{11.3}$ = $\dfrac{0.0796 \times 100}{11.3}$ = 0.705 percent

3. If the apparent gage length (grip separation) was assumed equal
   to the effective gage length

   $$\dfrac{\Delta e \times 100}{10} = 0.796 \text{ percent or 13.7 percent}$$
   $$\text{difference.}$$
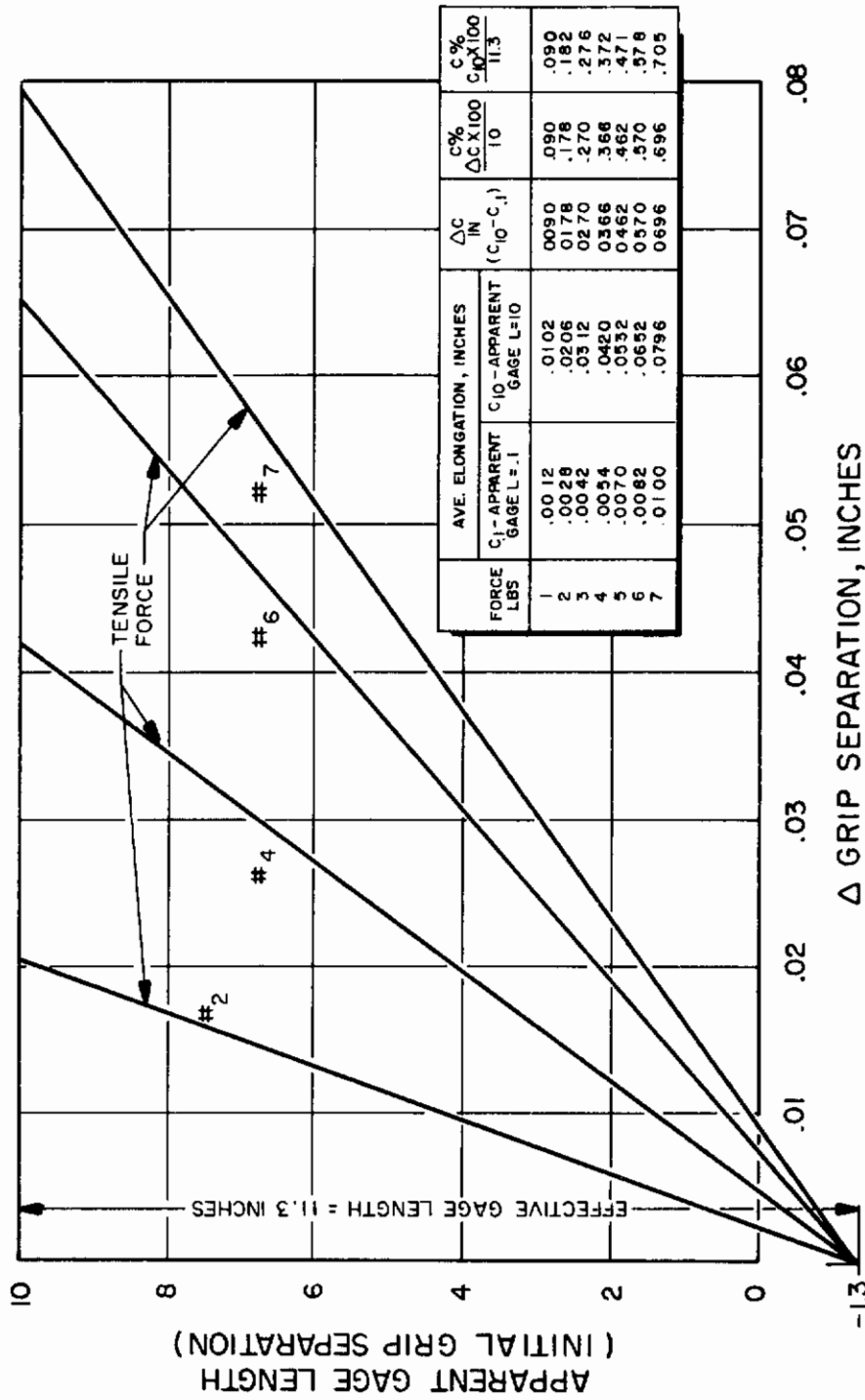
Figure 55. Filament Elongation Measurements
(5-mil Tungsten Wire)

111

APPENDIX B

DATA TABLES FROM REINFORCED-BEAM FLEXURE TESTING

EXPLANATION OF SPECIMEN DESIGNATION

An example follows:

```
                                    Specimen Within Lot
              *
      41941-2B-PL1-2
                                    Matrix Resin

                                    Type of Reinforcing Element
         Lot Number
                      Number of Reinforcing Elements
```
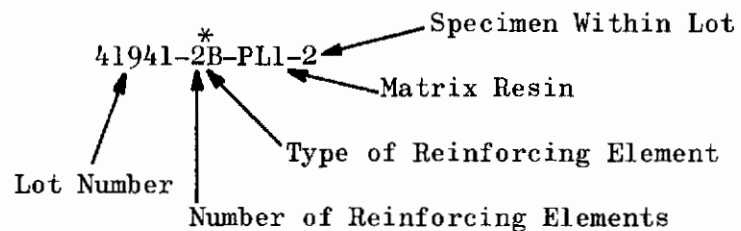
The reinforcing elements are:

1. HSS   high-strength steel

2. R   Rene' 41

3. B   boron

4. Be   beryllium

5. W   tungsten

6. Al   aluminum

7. K   Karma strain-gage wire

8. G   glass

---

*If 0 appears it indicates there is no reinforcement.

Specimen: 41927-4HSS-PL1-1

$I = 0.001189$ in.^{4} $E_R = 491,000$ psi

Load, pounds	$P/IE_R \times 10^5$	Deflection, mils
0.5	86	0
2.8	480	22
5.0	859	42
6.5	1115	55.5
8.9	1524	77
11.0	1889	97
13.2	2248	117
15.0	2575	134.5
17.4	2984	157
19.9	3415	180

Specimen: 41927-4HSS-PL1-2

$I = 0.001477$ in.^{4} $E_R = 491,000$ psi

0.6	43	0
3.0	414	18
6.4	884	43
8.3	1145	56.5
11.2	1545	78
13.9	1920	98
16.5	2278	118
18.8	2600	135.5
21.9	3025	158
24.8	3420	180

Specimen: 41927-4B-PL1-1

$$I = 0.001181 \text{ in.}^4 \qquad E_R = 491,000 \text{ psi}$$

Load, pounds	$P/IE_R \times 10^5$	Deflection, mils
0.5	86	0
2.9	499	21
4.9	845	38
7.5	1292	61
10.0	1725	80
11.0	1895	91
13.4	2310	111
15.7	2700	131
17.5	3020	147
19.3	3328	161
21.5	3704	181

Specimen: 41927-4B-PL1-2

$$I = 0.001136 \text{ in.}^4 \qquad E_R = 491,000 \text{ psi}$$

Load, pounds	$P/IE_R \times 10^5$	Deflection, mils
0.5	90	0
2.3	414	17
4.6	824	37
6.2	1111	52
8.3	1489	72
10.5	1882	92
12.0	2150	107
14.3	2565	127
15.8	2832	142
17.6	3175	157
20.3	3640	181

115

Specimen: 41927-5B-PL1-1

$I = 0.001283$ in.^{4} $E_R = 491,000$ psi

Load, pounds	$P/IE_R \times 10^5$	Deflection, mils
0.5	79	0
2.6	417	19
5.0	794	39
7.5	1189	59
9.3	1475	74
11.6	1840	93
12.6	2000	102
14.6	2316	119
17.0	2700	139
19.4	3074	159
22.0	3490	181

Specimen: 41927-5HSS-PL1-1

$I = 0.001271$ in.^{4} $E_R = 491,000$ psi

Load, pounds	$P/IE_R \times 10^5$	Deflection, mils
0.6	96	0
3.2	512	21.5
5.2	831	38
7.4	1184	56.5
9.9	1581	78
12.1	1939	98
14.5	2320	118
16.5	2640	135.5
19.0	3040	158
21.5	3440	180
18.5	....	158

Specimen: 41928-4R-PL1-1

$I = 0.00148$ in.^{4} $E_R = 565,000$ psi

Load, pounds	P/IE_R x 10^5	Deflection, mils
0.4	48	0
4.8	325	30
5.6	670	36
9.2	1100	60
13.6	1625	90.5
17.9	2140	120
21.6	2580	145
26.9	>3215	180

Specimen: 41928-4W-PL1-2

$I = 0.001261$ in.^{4} $E_R = 565,000$ psi

0.4	56	0
3.8	534	25.5
7.0	985	50.5
8.0	1141	57.5
10.4	1459	75.5
13.6	1905	100.5
16.9	2525	133.5
20.2	2845	150.5
22.2	3120	163.5
19.6	2750	150.5

117

Specimen: 41928-5R-PL1-1

$I = 0.001733$ in.^{4} $E_R = 565,000$ psi

Load, pounds	$P/IE_R \times 10^5$	Deflection, mils
0.4	41	0
5.6	572	30
6.8	694	37
10.8	1101.0	60
16.0	1633	90
21.2	2165	120
25.6	2613	134
26.6	2719	150
31.8	3245	180

Specimen: 41928- 5W-PL1

$I = 0.001168$ in.^{4} $E_R = 565,000$

0.4	61	0
3.2	485	25
5.2	789	41
6.2	939	50
9.1	1379	75
12.1	1833	100
13.0	1970	107
15.2	2304	125
18.2	2755	150
21.2	3210	175
21.6	3267	177

Specimen: 41930-2G-PL1-1

$I = 0.00089$ in.^{4} $\qquad$ $E_R = 557,000$ psi

Load, pounds	$P/IE_R \times 10^5$	Deflection, mils
0.4	81	0
2.6	524	25
4.8	966	50
7.8	1431	75
8.0	1611	86
9.2	1855	100
11.6	2340	125
13.8	2783	150
14.6	2942	159

Specimen: 41930-2G-PL1-2

$I = 0.00108$ in.^{4} $\qquad$ $E_R = 557,000$ psi

Load, pounds	$P/IE_R \times 10^5$	Deflection, mils
0.4	61	0
3.0	497	25
5.8	964	50
8.5	1413	75
9.5	1578	83
11.4	1891	100
14.1	2430	125
16.9	2805	150
19.2	3180	169
16.6	--	159

Specimen: 41927-3B-PL1-1

$I = 0.00129$ in.^{4} $E_R = 491,000$ psi

Load, pounds	$P/IE_R \times 10^5$	Deflection, mils
0.50	79	0
3.0	473	20
5.5	869	40
7.8	1230	60
9.4	1484	73
11.6	1830	90
13.7	2162	108
15.1	2385	120
17.5	2760	140
18.8	2965	150
21.1	3330	170

Specimen: 41927-3HSS-PL1-1

$I = 0.001284$ in.^{4} $E_R = 491,000$ psi

Load, pounds	$P/IE_R \times 10^5$	Deflection, mils
0.50	79.1	25
3.3	524	25
5.6	889	44
8.0	1269	65
10.3	1631	85
12.5	1980	105
14.9	2368	125
16.3	2580	137.5
19.4	3075	165
21.0	3325	180

Specimen: 41928-3R-PL1-1

$I = 0.001385$ in.^{4} $E_R = 565,000$ psi

Load, pounds	$P/IE_R \times 10^5$	Deflection, mils
0.4	51.2	0
4.4	562	30
6.6	844	45
8.6	1100	60
12.8	1635	90
16.0	2045	114
16.9	2160	120
21.0	2785	150
25.4	3250	180

Specimen: 41928-3W-PL1-1

$I = 0.00138$ in.^{4} $E_R = 565,000$ psi

Load, pounds	$P/IE_R \times 10^5$	Deflection, mils
0.4	51.4	0
4.6	589	30
7.6	975	51
8.8	1129	60
13.2	1709	90
17.6	2259	121
21.8	2795	150
26.2	3360	180

Specimen: 41925-00-PL1-1

$I = 0.001419$ in.^{4} $E_R = 543,000$ psi

Load, pounds	$P/IE_R \times 10^5$	Deflection, mils
0.4	52	0
8.8	1141	63
14.9	1935	107
19.0	2468	137
26.1	3388	191

Specimen: 41927-00-PL1-1

$I = 0.000791$ in.^{4} $E_R = 491,000$ psi

0.5	129	0
1.7	438	18
3.0	774	38
4.5	1159	58
5.9	1521	78
7.2	1859	98
8.5	2190	118
9.9	2555	138
11.3	2914	158
12.7	3268	180

Specimen: 41928-00-PL1-1

$I = 0.001309$ in.^{4} $E_R = 565,000$ psi

0.3	41	0
4.0	540	30
6.6	892	50
7.8	1047	60
11.6	1570	90
14.0	1889	110
15.4	2080	120
19.2	2595	150
22.4	3030	176
23.0	3110	180

Specimen: 41930-00-PL1-2

$I = 0.001499$ in.^{4} $E_R = 557,000$ psi

Load, pounds	$P/IE_R \times 10^5$	Deflection, mils
0.4	49	0
4.2	502	25
6.8	811	44
7.8	933	50
11.4	1363	75
14.0	1674	92
15.2	1865	100
19.0	2270	125
22.3	2665	148
22.8	2730	150
23.4	2800	154

APPENDIX C

MAXIMUM SHEAR STRESS PLATES

This appendix contains plots of maximum shear stress along two vertical planes of beam composites subjected to three-poing loading (Fig. 56 through 66). Data obtained from photoelastic stress patterns (Fig. 56 through 66) are included in tabular form. The vertical planes considered are located 0.04 and 0.10 inch from midspan of beam.

Please refer to the first page of Appendix B for specimen designation nomenclature.
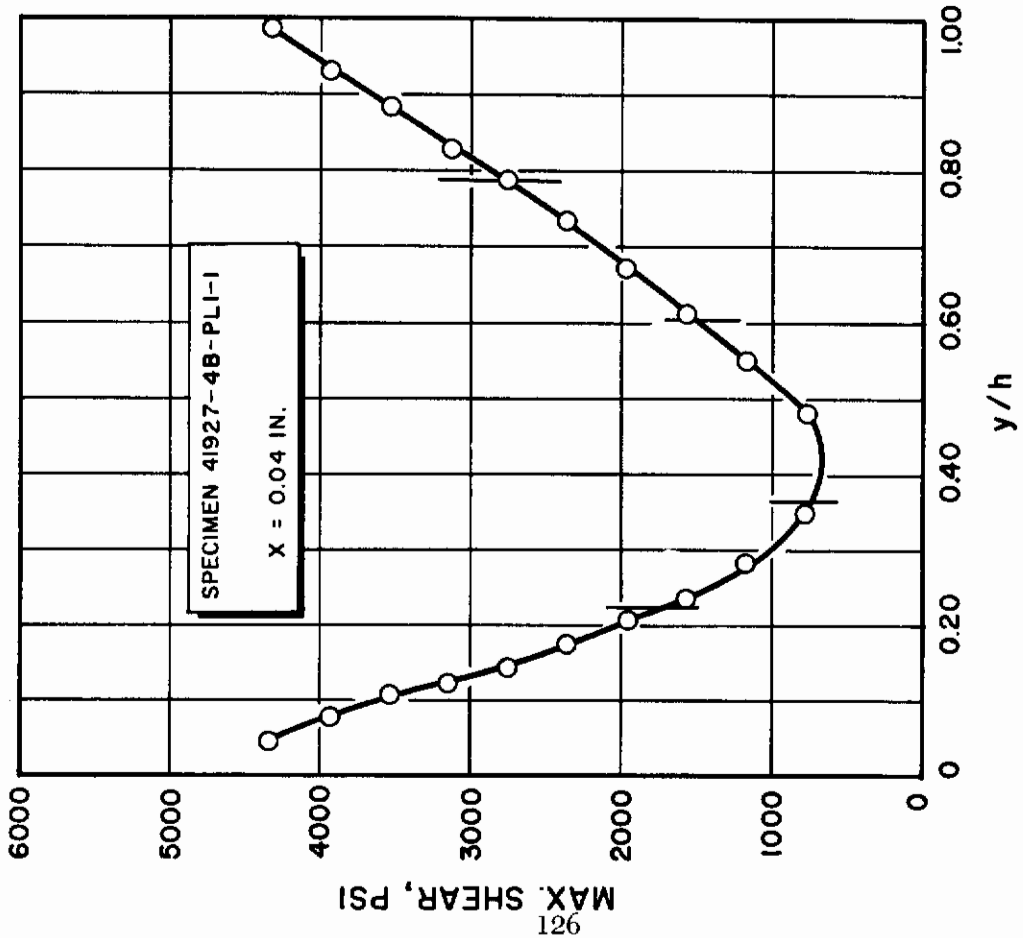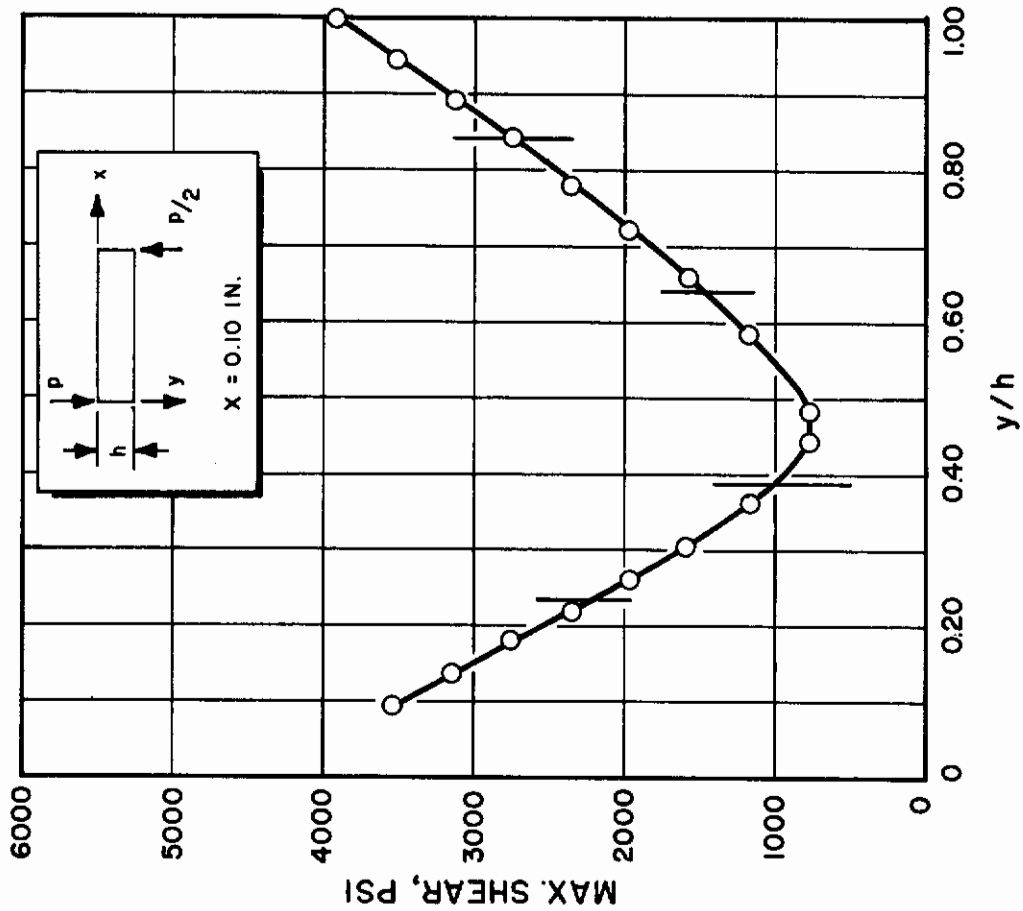
Figure 56.   Maximum Shear Stress Along Vertical Planes
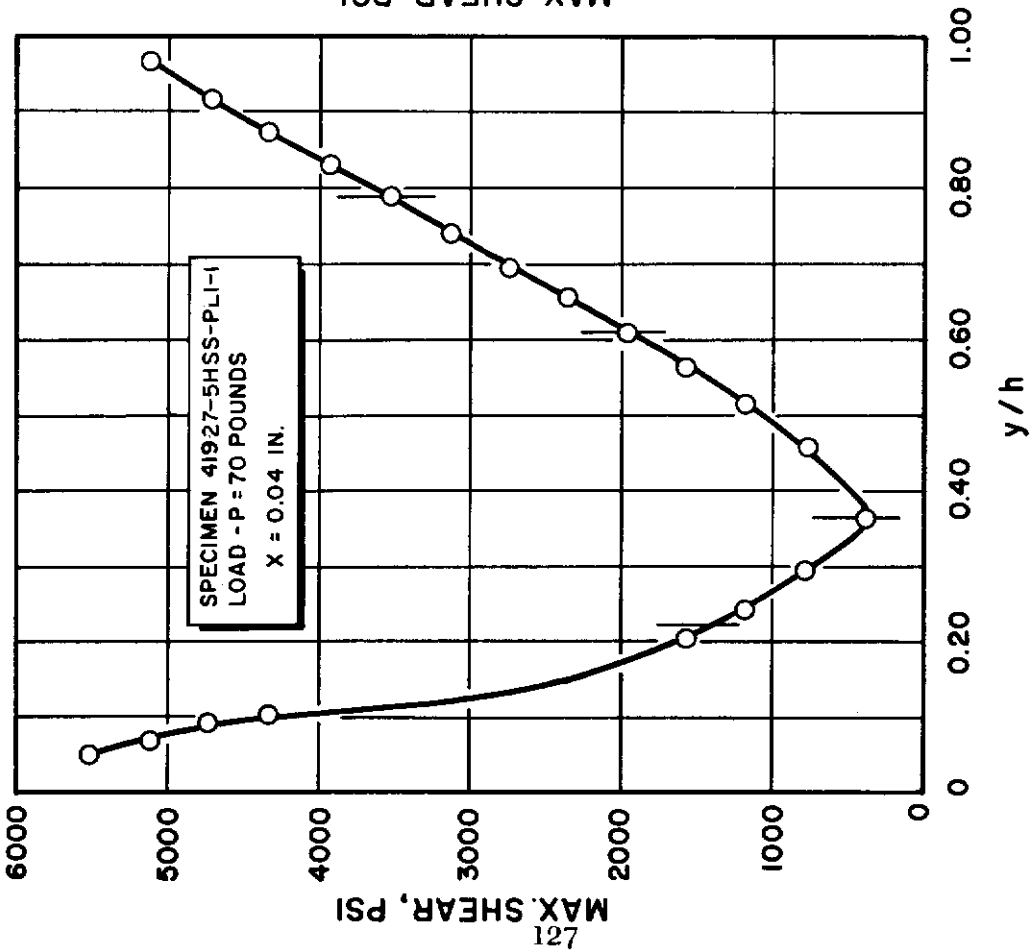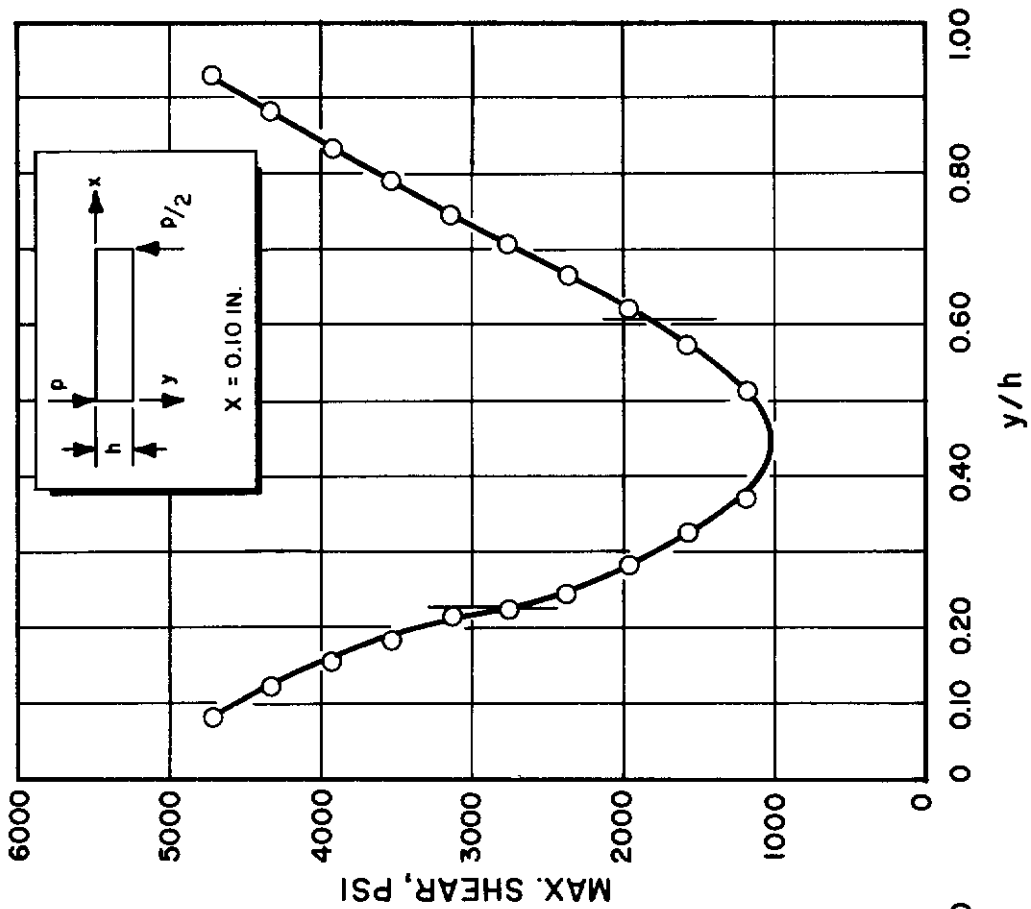
Figure 57. Maximum Shear Stress Along Vertical Planes
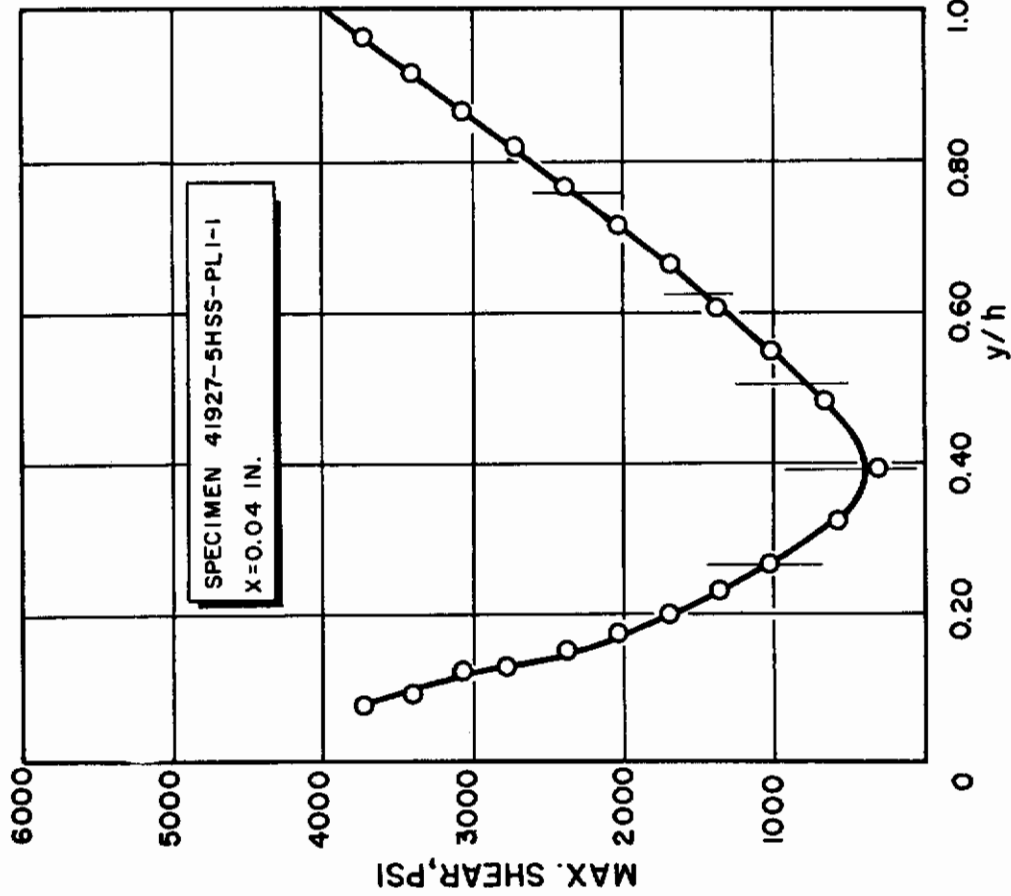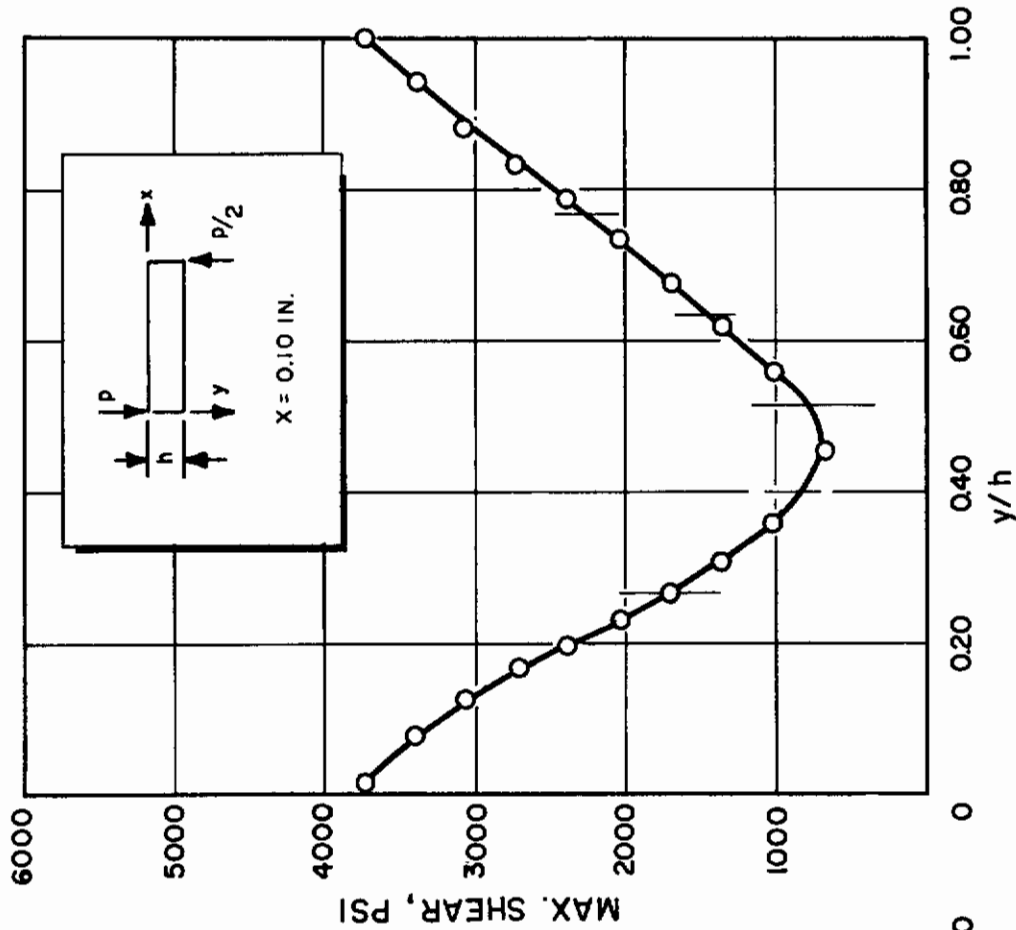
Figure 58. Maximum Shear Stress Along Vertical Planes

128
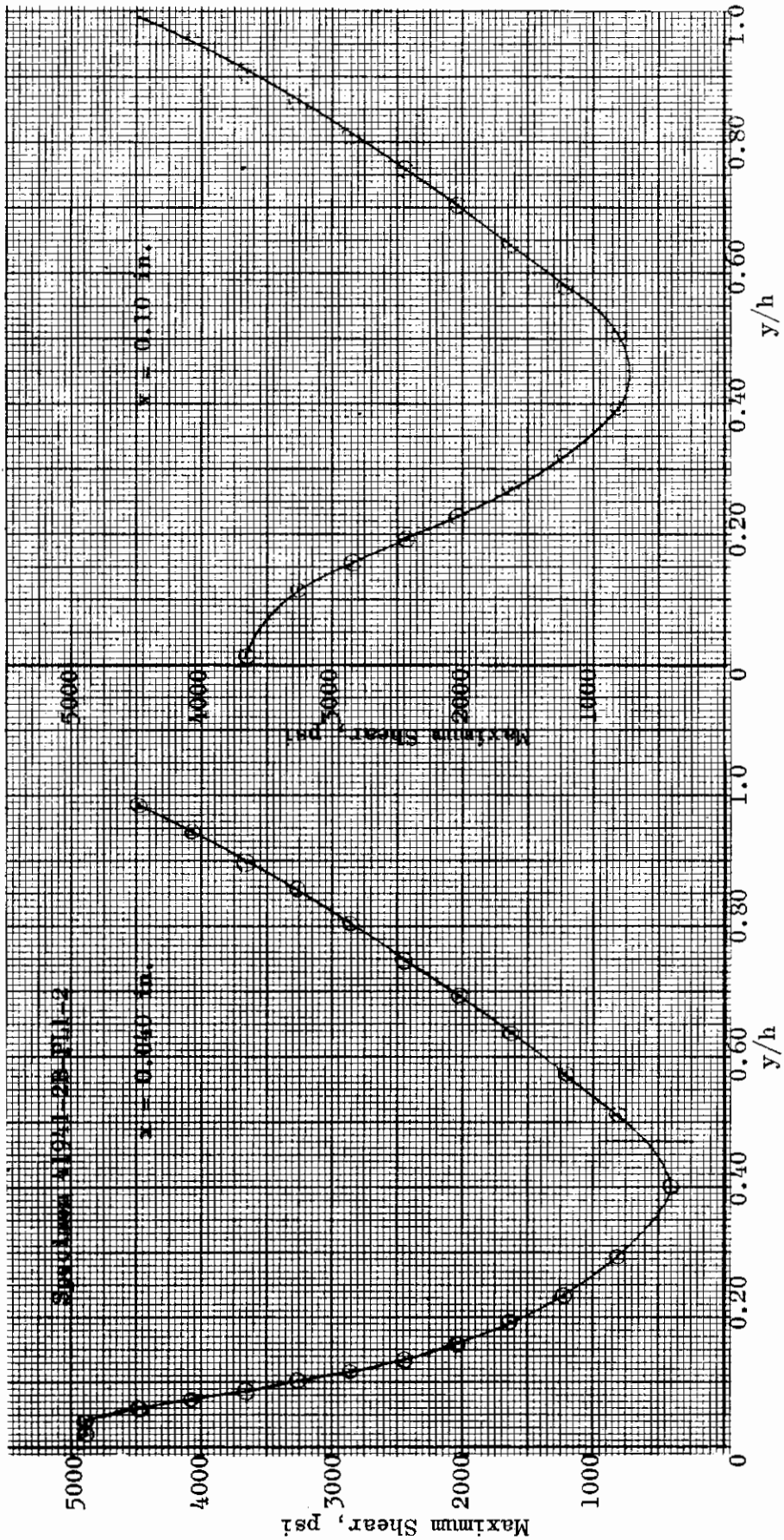
Figure 59.   Maximum Shear Stress Along Vertical Planes

129
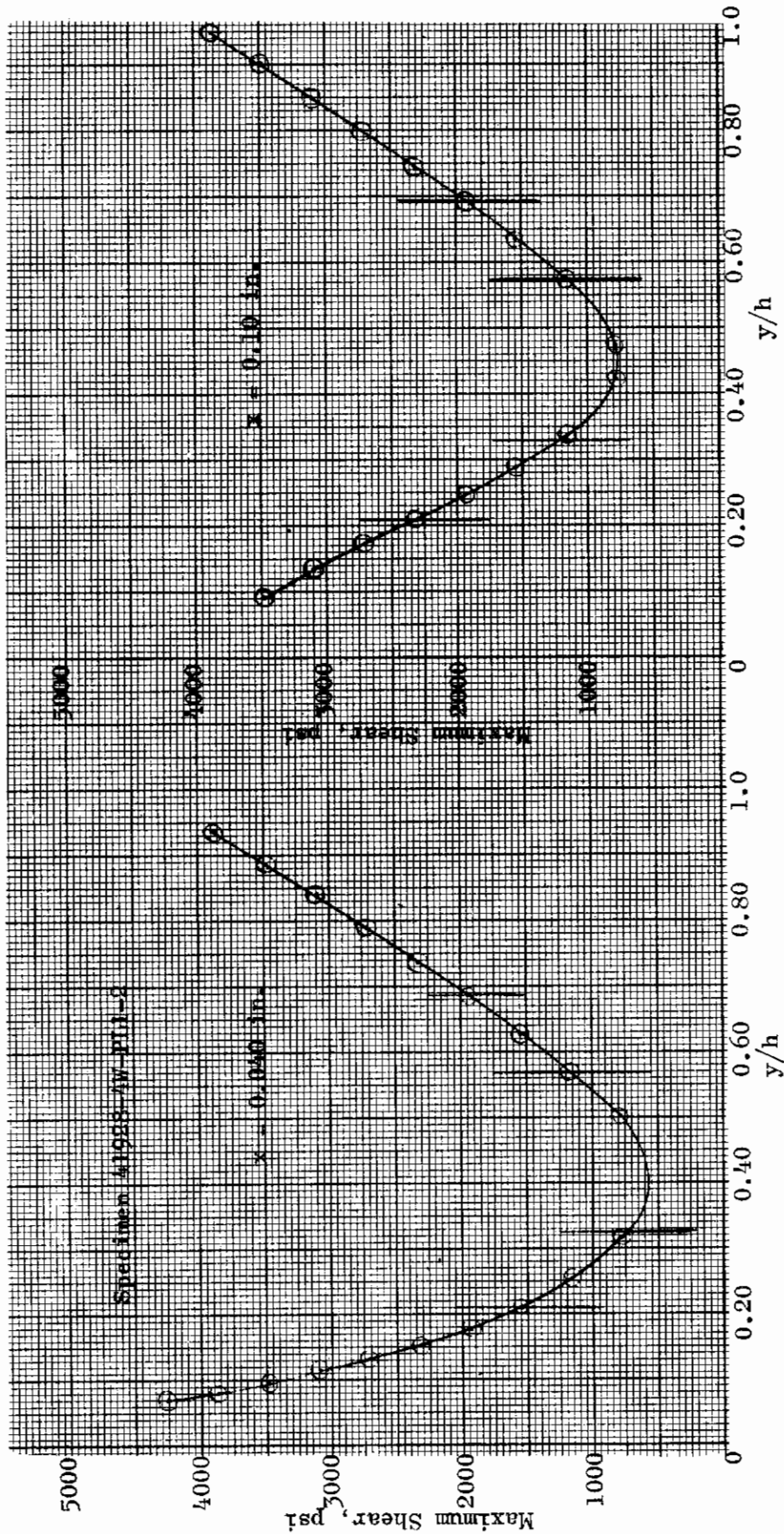
Figure 60. Maximum Shear Stress Along Vertical Planes

130
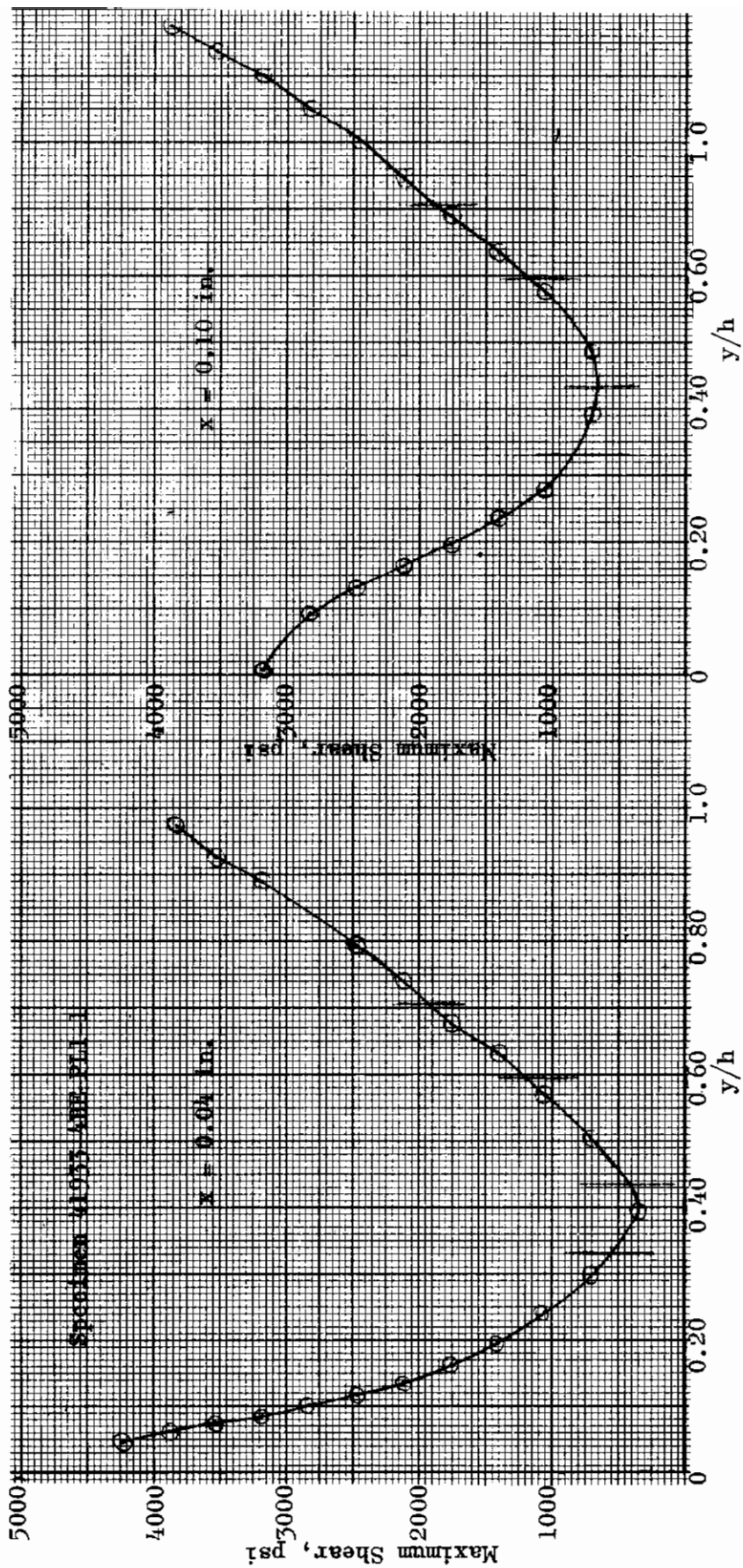
Figure 61. Maximum Shear Stress Along Vertical Planes

131
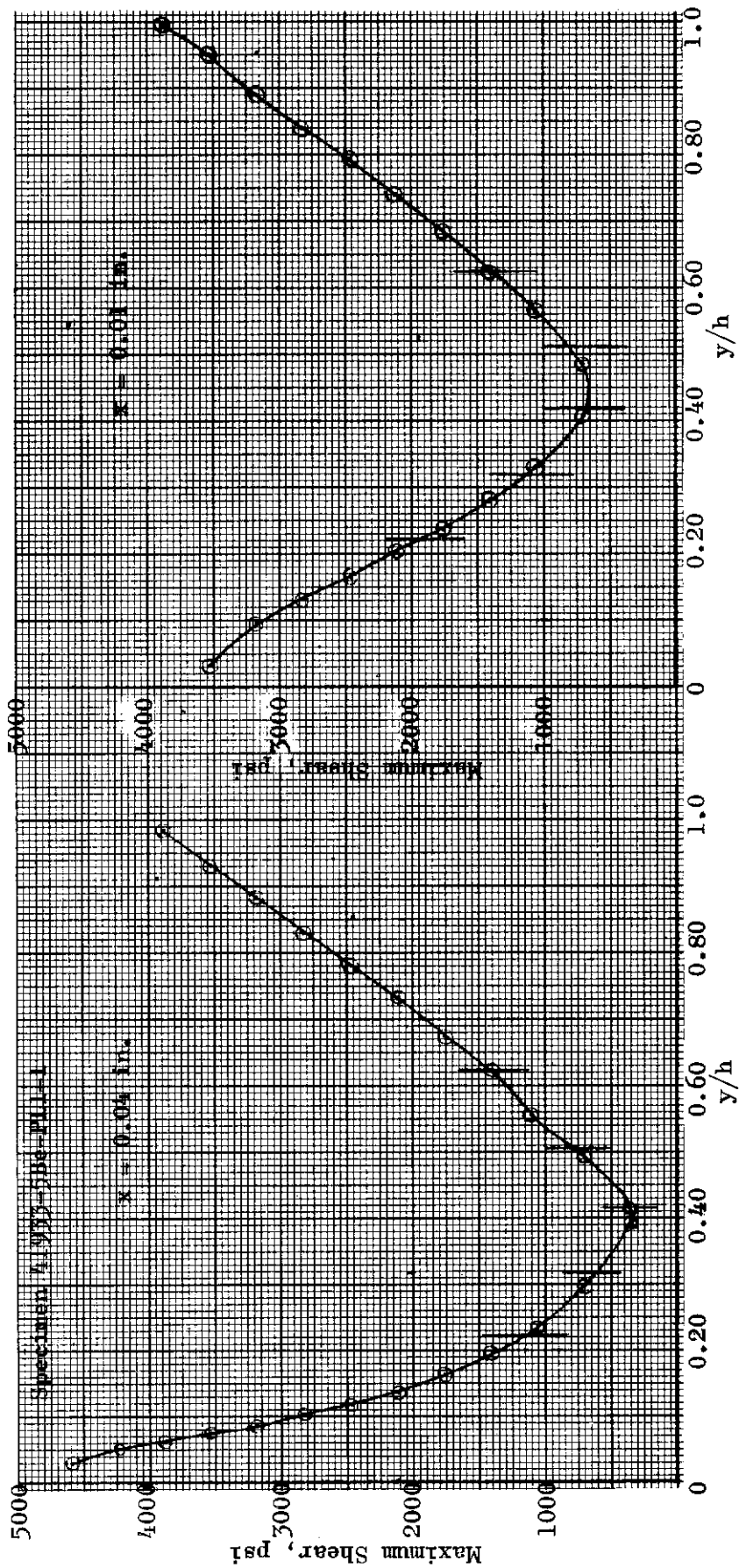
Figure 62. Maximum Shear Stress Along Vertical Planes
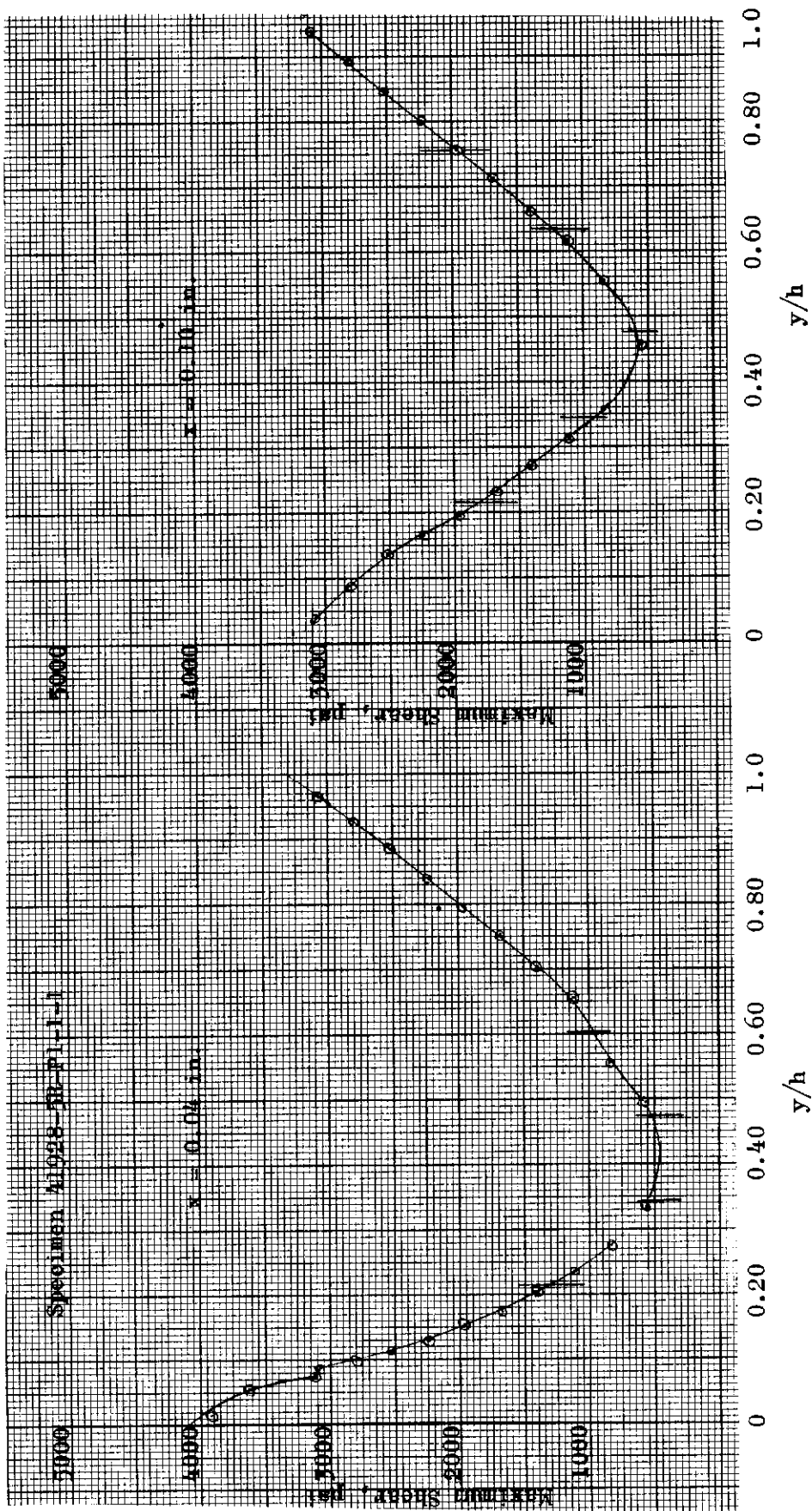
Figure 63. Maximum Shear Stress Along Vertical Planes
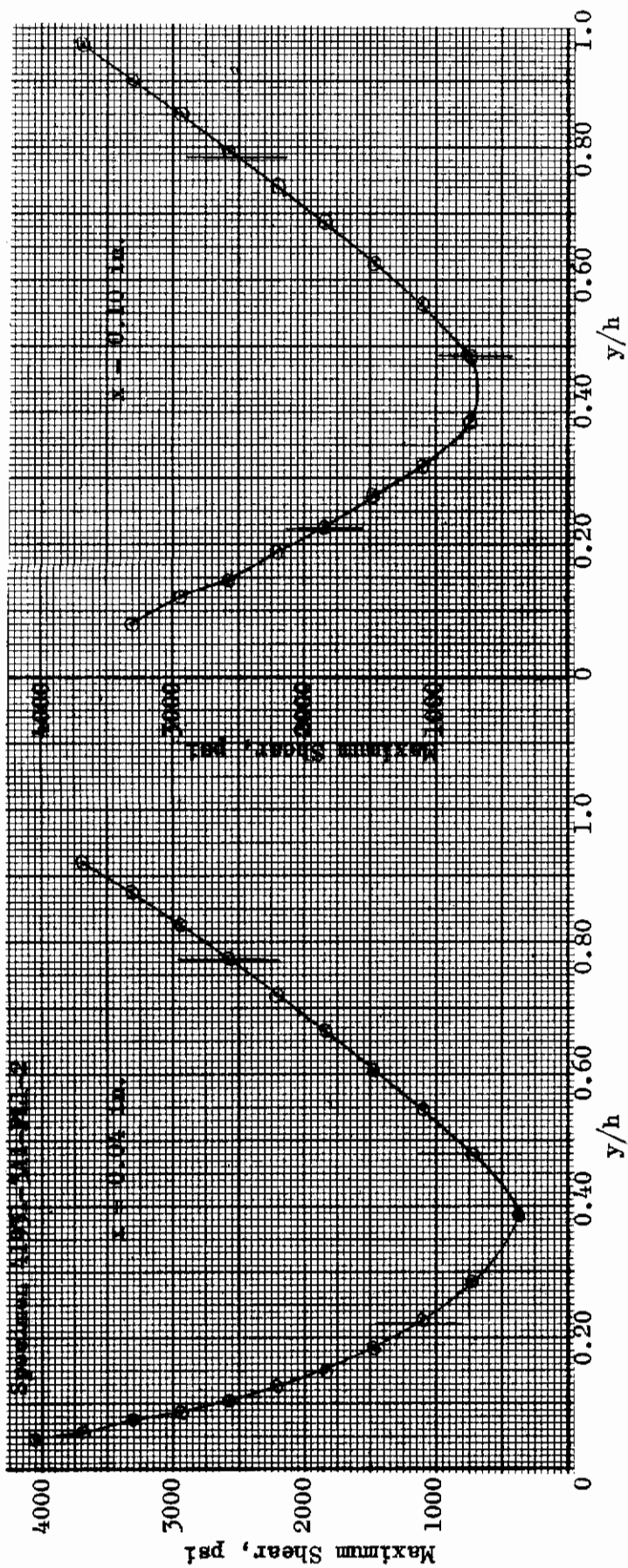
Figure 64. Maximum Shear Stress Along Vertical Planes

134
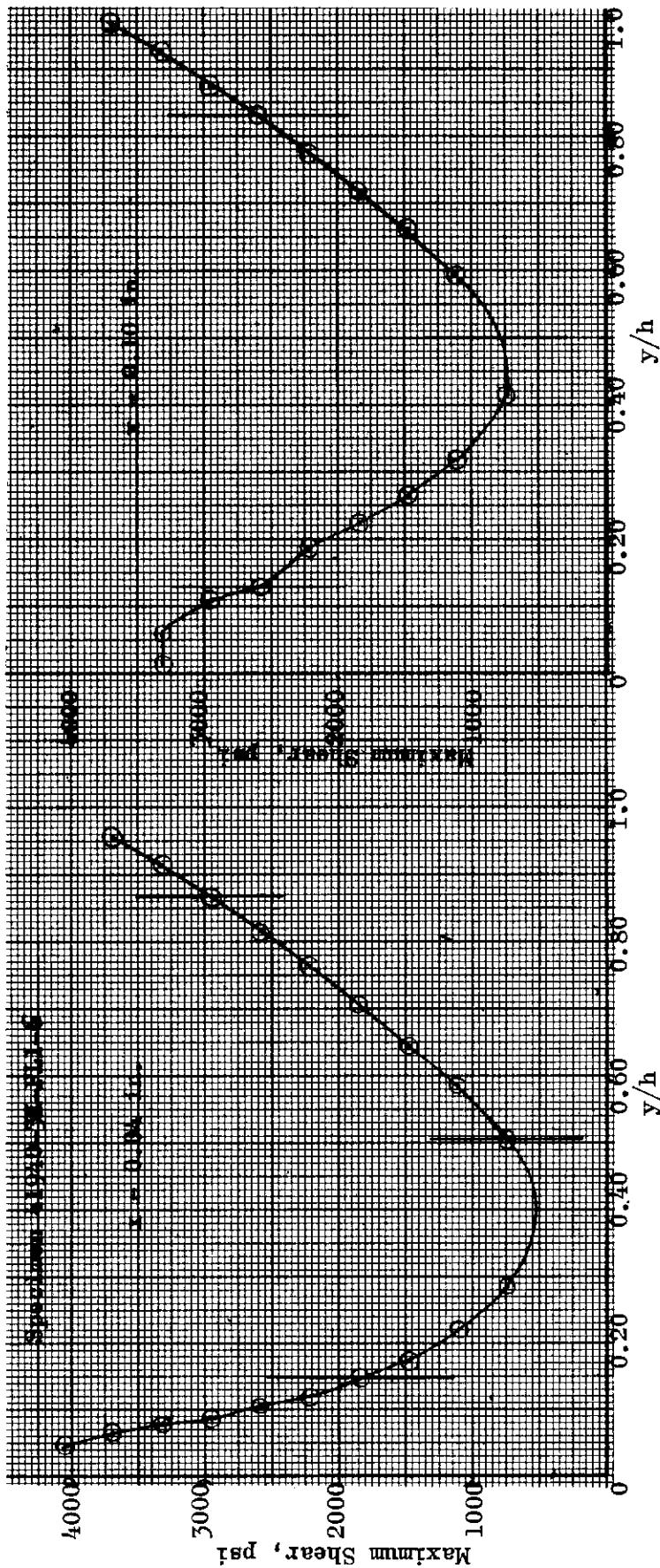
Figure 65. Maximum Shear Stress Along Vertical Planes
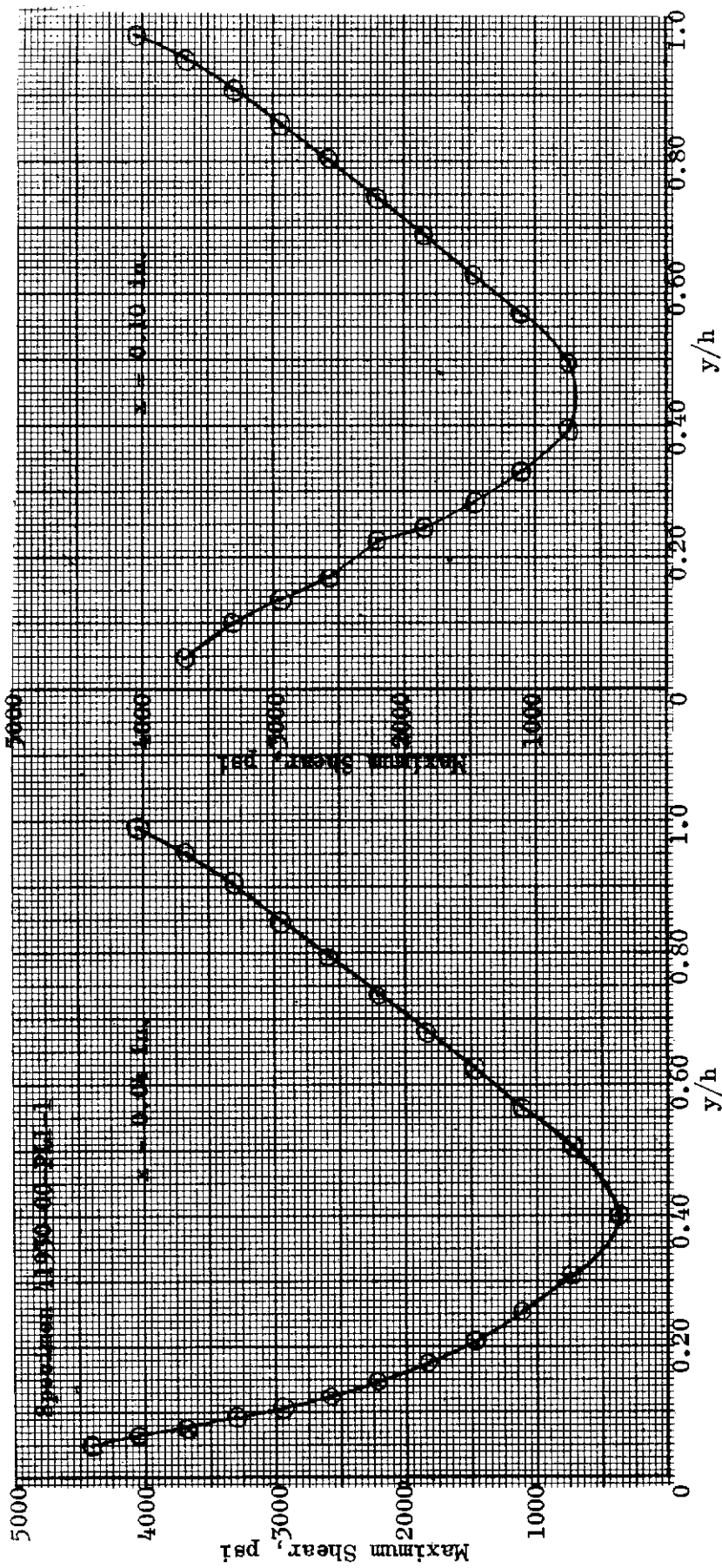
Figure 66. Maximum Shear Stress Along Vertical Planes

136

Specimen 41928-5R-PL1-1

3-Point Loading
Load   60 Pounds
$k = 0.240 \times 10^{-6}$ fringe/psi
$f = 560$ psi/fringe

Distance From Center 0.04 Inch				Distance From Center 0.10 Inch			
y/h	N	N·f	N·f/2	y/h	N	N·f	N·f/2
0.0160	14	7840	3920	0.03987	≈1	6160	3080
0.0559	13	7270	3635	0.09245	10	5600	2800
0.0725	12	6220	3110	0.1360	9	5040	2520
0.0893	11	6160	3080	0.1670	8	4480	2240
0.0995	10	5600	2800	0.1980	7	3920	1960
0.1132	9	5040	2520	0.2135	*	– –	– –
0.1310	8	4480	2240	0.2306	6	3360	1680
0.1518	7	3920	1960	0.2705	5	2800	1400
0.1749	6	3360	1680	0.3110	4	2240	1120
0.2030	5	2800	1400	0.3470	*	– –	– –
0.2160	*	– –	– –	0.3550	3	1680	840
0.2379	4	2240	1120	0.4580	2	1120	560
0.2775	3	1680	840	0.4755	*	– –	– –
0.3335	2	1120	560	0.5560	3	1680	840
0.3440	*	– –	– –	0.6140	4	2240	1120
0.407	≈1	560	280	0.6350	*	– –	– –
0.4730	*	– –	– –	0.660	5	2800	1400
0.496	2	1120	560	0.7105	6	3360	1680
0.554	3	1680	840	0.7545	7*	3920	1960
0.604	*	– –	– –	0.803	8	4480	2240
0.655	4	2240	1120	0.848	9	5040	2520
0.702	5	2800	1400	0.893	10	5600	2800
0.753	6*	3360	1680	0.940	11	6160	3080
0.795	7	3920	1960	0.972	12	6220	3110
0.840	8	4480	2240	1.00	––		
0.885	9	5040	2520				
0.927	10	5600	2800				
0.966	11	6160	3080				
1.00							

*Wire

137

Specimen 41927-5HSS-PL1-1

3-Point Loading
Load   60 Pounds
$k = 0.240 \times 10^{-6}$ fringe/psi
$f = 786$ psi/fringe

Distance From Center 0.04 Inch				Distance From Center 0.10 Inch			
y/h	N	N·f	N·f/2	y/h	N	N·f	N·f/2
0.0799	11	7480	3740	0.0169	11	7480	3740
0.0965	10	6800	3400	0.0819	10	6800	3400
0.1247	9	6120	3060	0.1240	9	6120	3060
0.1301	8	5440	2720	0.1590	8	5440	2720
0.1508	7	4760	2380	0.1939	7	4760	2380
0.1730	6	4080	2040	0.2300	6	4080	2040
0.1997	5	3400	1700	0.2680	5*	3400	1700
0.2325	4	2720	1360	0.3060	4	3720	1360
0.2648	3*	2040	1020	0.3550	3	2040	1020
0.3217	2	1360	680	0.4010	*	- -	- -
0.3917	≈1*	≈680	≈340	0.4530	≈2	1360	≈680
0.4860	2	1360	680	0.5160	*	- -	- -
0.5050	*	- -	- -	0.5600	3	2040	1020
0.5500	3	2040	1020	0.6200	4	2720	1360
0.6070	4	2720	1860	0.6330	*	- -	- -
0.6250	*	- -	- -	0.6760	5	3400	1700
0.6630	5	3400	1700	0.7320	6	4080	2040
0.7145	6	4080	2040	0.7640	*	- -	- -
0.7595	*	- -	- -	0.7850	7	4760	2380
0.7660	7	4760	2380	0.8350	8	5440	2720
0.8190	8	5440	2720	0.8810	9	6120	3060
0.8640	9	6120	3060	0.9430	10	6800	3400
0.9155	10	6800	3400	1.000	11	7480	3740
0.9660	11	7480	3740				
1.00							

*Wire

138

Specimen 41927-4B-PL1-1

3-Point Loading
Load 71 Pounds
$k = 0.240 \times 10^{-6}$ fringe/psi
$f = 786$ psi/fringe

Distance From Center 0.04 Inch				Distance From Center 0.10 Inch			
y/h	N	N·f	N·f/2	y/h	N	N·f	N·f/2
0.05210	14	11,000	5500	0.824	12	9430	4715
0.0700	13	10,210	5105	0.1231	11	8650	4325
0.0944	12	9,430	4715	0.1574	10	7860	3930
0.1051	11	8,650	4325	0.1875	9	7060	3530
0.2040	4	3,140	1570	0.2180	8	6290	3145
0.2255	*	- -	- -	0.2274	7*	5500	2750
0.2455	3	2,360	1180	0.2488	6	4710	2355
0.2990	2	1,570	785	0.2860	5	3930	1965
0.3680	1*	786	393	0.3275	4	3140	1570
0.4590	2	1,570	785	0.3729	3	2360	1180
0.5150	3	2,360	1180	0.5140	3	2360	1180
0.5650	4	3,140	1570	0.5750	4	3140	1570
0.6100	5*	3,930	1965	0.6070	*	- -	- -
0.6550	6	4,710	2355	0.6210	5	3930	1965
0.6980	7	5,500	2750	0.6670	6	4710	2355
0.7400	8	6,290	3145	0.7090	7	5500	2750
0.7901	9*	7,060	3530	0.749	8	6290	3145
0.8290	10	7,860	3930	0.793	9	7060	3530
0.8740	11	8,650	4325	0.835	10	7860	3930
0.9195	12	9,430	4715	0.885	11	8650	4325
0.9640	13	10,210	5105	0.930	12	9430	4715
1.00	**			1.00			

*Wire
**Boundary

Specimen 41928-4W-PL1-2

3-Point Loading
Load   60 Pounds
$k = 0.240 \times 10^{-6}$ fringe/psi
$f = 774$ psi/fringe

Distance From Center 0.04 Inch				Distance From Center 0.10 Inch			
y/h	N	N·f	N·f/2	y/h	N	N·f	N·f/2
0.0703	11	8514	4257	0.0911	9	6966	3483
0.0804	10	7740	3870	0.1353	8	6192	3096
0.0958	9	6966	3483	0.1723	7	5418	2709
0.1135	8	6192	3096	0.2085	6*	4644	2322
0.1311	7	5418	2709	0.2486	5	3870	1935
0.1514	6	4644	2322	0.2894	4	3096	1548
0.1777	5	3870	1935	0.3291	–*	– –	– –
0.2095	4*	3096	1548	0.3365	3	2322	1161
0.2530	3	2322	1161	0.4222	2	1548	774
0.3170	2	1548	774	0.4752	2	1548	774
0.3264	–*	– –	– –	0.5728	3*	2322	1161
0.5013	2	1548	774	0.6351	4	3096	1548
0.5685	3*	2322	1161	0.6931	5*	3870	1935
0.6269	4	3096	1548	0.7462	6	4644	2322
0.6869	5*	3870	1935	0.7991	7	5418	2709
0.7382	6	4644	2322	0.8498	8	6192	3096
0.7896	7	5418	2709	0.9020	9	6966	3483
0.8402	8	6192	3096	0.9491	10	7740	3870
0.8878	9	6966	3483	1.00	**		
0.9359	10	7740	3870				
1.00	**						

*Wire
**Boundary

140

Specimen 41930-00-PL1-1

3-Point Loading
Load   60 Pounds
$k = 0.240 \times 10^{-6}$ fringe/psi
$f = 735$ psi/fringe

Distance From Center 0.04 Inch				Distance From Center 0.10 Inch			
y/h	N	N·f	N·f/2	y/h	N	N·f	N·f/2
0.0498	12	8810	4405	0.0476	10	7350	3675
0.0652	11	8090	4045	0.100	9	6610	3305
0.0749	10	7350	3675	0.1368	8	5890	2945
0.0905	9	6610	3305	0.1709	7	5145	2573
0.1069	8	5890	2945	0.228	6	4410	2205
0.1240	7	5145	2573	0.242	5	3695	1843
0.1474	6	4410	2205	0.2825	4	2940	1470
0.1729	5	3695	1848	0.330	3	2205	1103
0.2075	4	2940	1470	0.3955	2	1470	735
0.2515	3	2205	1103	0.4940	2	1470	735
0.3085	2	1470	735	0.5690	3	2205	1103
0.400	1	735	368	0.5690	3	2205	1103
0.400	1	735	368	0.6290	4	2940	1470
0.504	2	1470	735	0.6890	5	3695	1848
0.566	3	2205	1103	0.7430	6	4410	2205
0.626	4	2940	1470	0.802	7	5145	2573
0.681	5	3695	1848	0.855	8	5890	2945
0.737	6	4410	2205	0.909	9	6610	3305
0.795	7	5145	2573	0.956	10	7350	3675
0.847	8	5890	2945	0.990	11	8090	4045
0.904	9	6610	3305	1.00	**		
0.952	10	7350	3675				
0.990	11	8090	4045				
1.00	**	– –					

**Boundary

141

Specimen 41931-3A1-PL1-2

3-Point Loading
Load 60 Pounds
$k = 0.230 \times 10^{-6}$ fringe/psi
$f = 735$ psi/fringe

Distance From Center 0.04 Inch				Distance From Center 0.10 Inch			
y/h	N	N·f	N·f/2	y/h	N	N·f	N·f/2
0.0446	11	8096	4048	0.0795	9	6624	3312
0.0575	10	7360	3680	0.1211	8	5888	2944
0.0752	9	6624	3312	0.1459	7	5152	2576
0.08840	8	5888	2944	0.1913	6	4416	2208
0.1030	7	5152	2576	0.2275	5*	3680	1840
0.1270	6	4416	2208	0.2735	4	2944	1472
0.1485	5	3680	1840	0.3180	3	2208	1104
0.1835	4	2944	1472	0.388	2	1472	736
0.2219	*	– –	– –	0.486	2*	1472	736
0.2275	3	2208	1104	0.565	3	2208	1104
0.2860	2	1472	736	0.626	4	2944	1472
0.3840	1	736	368	0.685	5	3680	1840
0.480	2*	1472	736	0.740	6	4416	2208
0.547	3	2208	1104	0.785	*	– –	– –
0.608	4	2944	1472	0.796	7	5152	2576
0.665	5	3680	1840	0.851	8	5888	2944
0.720	6	4416	2208	0.902	9	6624	3312
0.773	7*	5152	2576	0.955	10	7360	3680
0.825	8	5888	2944	1.00	**		
0.876	9	6624	3312				
0.920	10	7360	3680				
1.00	**						

*Wire
**Boundary

Specimen 41931-4A1-PL1-2

3-Point Loading
Load 60 Pounds
$k = 0.230 \times 10^{-6}$ fringe/psi
$f = 793$ psi/fringe

Distance From Center 0.04 Inch				Distance From Center 0.10 Inch			
y/h	N	N·f	N·f/2	y/h	N	N·f	N·f/2
0.0546	10	7930	3965	0.0814	9	7137	3569
0.0713	9	7137	3569	0.1273	8	6344	3172
0.0831	8	6344	3172	0.1622	7	5551	2776
0.0968	7	5551	2776	0.1966	6*	4758	2379
0.1127	6	4758	2379	0.2302	5	3965	1983
0.1316	5	3965	1983	0.2715	4	3172	1586
0.1582	4	3172	1586	0.3204	3	2379	1190
0.1910	*	- -	- -	0.3852	2	1586	793
0.2303	3	2379	1190	0.3930	*	- -	- -
0.2850	2	1586	793	0.4802	2	1586	793
0.3901	1*	793	397	0.5586	3	2379	1190
0.4882	2	1586	793	0.5768	*	- -	- -
0.5515	3	2379	1190	0.6232	4	3172	1586
0.5734	*	- -	- -	0.6814	5	3965	1983
0.6140	4	3172	1586	0.7355	6	4758	2379
0.6729	5	3965	1983	0.7495	*	- -	- -
0.7300	6	4758	2379	0.7912	7	5551	2776
0.7495	*	- -	- -	0.8460	8	6344	3172
0.7868	7	5551	2776	0.8960	9	7137	3569
0.8378	8	6344	3172	0.9421	10	7930	3965
0.8857	9	7137	3569	0.9911	11	8723	4362
0.9324	10	7930	3965	1.00	**		
0.9849	11	8723	4362				
1.00	**						

*Wire
**Boundary

143

Specimen 41933-4Be-PL1-1

3-Point Loading
Load   60 Pounds
$k = 0.240 \times 10^{-6}$ fringe/psi
$f = 706$ psi/fringe

Distance From Center 0.04 Inch				Distance From Center 0.10 Inch			
y/h	N	$N \cdot f$	$N \cdot f/2$	y/h	N	$N \cdot f$	$N \cdot f/2$
0.0461	12	8472	4236	0.0079	9	6354	3177
0.0606	11	7766	3883	0.0931	8	5648	2824
0.0746	10	7060	3530	0.1310	7	4942	2471
0.0865	9	6354	3177	0.1641	6	4236	2118
0.1015	8	5648	2824	0.1980	5	3530	1765
0.1170	7	4942	2471	0.2355	4	2824	1412
0.1385	6	4236	2118	0.2785	3	2118	1059
0.1620	5	3530	1765	0.3313	*	- -	- -
0.1961	4	2824	1412	0.3910	2	1412	706
0.2410	3	2118	1059	0.4330	*	- -	- -
0.2990	2	1412	706	0.4870	2	1412	706
0.3314	*	- -	- -	0.5750	3	2118	1059
0.3960	1	706	353	0.5960	*	- -	- -
0.435	*	- -	- -	0.6360	4	2824	1412
0.504	2	1412	706	0.6900	5	3530	1765
0.570	3	2118	1059	0.7060	*	- -	- -
0.596	*	- -	- -	0.7460	6	4236	2118
0.631	4	2824	1412	0.8060	7	4942	2471
0.675	5	3530	1765	0.850	8	5648	2824
0.706	*	- -	- -	0.900	9	6354	3177
0.740	6	4236	2118	0.937	10	7060	3530
0.793	7	4942	2471	0.974	11	7766	3883
0.813	8	5648	2824	1.00	**		
0.890	9	6354	3177				
0.926	10	7060	3530				
0.977	11	7766	3883				
1.00	**						

*Wire
**Boundary

144

Specimen 41940-3K-PL1-6

3-Point Loading
Load   60 Pounds
$k = 0.230 \times 10^{-6}$ fringe/psi
$f = 739$ psi/fringe

Distance From Center 0.04 Inch				Distance From Center 0.10 Inch			
y/h	N	N·f	N·f/2	y/h	N	N·f	N·f/2
0.0477	11	8110	4055	0.0141	9	6640	3320
0.0640	10	7390	3695	0.0612	9	6640	3320
0.0785	9	6640	3320	0.1100	8	5900	2950
0.0880	8	5900	2950	0.1297	7*	5160	2580
0.1040	7	5160	2580	0.1854	6	4430	2215
0.1214	6	4430	2215	0.2234	5	3690	1845
0.1491	5*	3690	1845	0.2660	4	2950	1475
0.1739	4	2950	1475	0.319	3	2215	1108
0.2209	3	2215	1108	0.416	2	1475	738
0.2840	2	1475	738	0.5005	*	– –	– –
0.506	2*	1475	738	0.592	3	2215	1108
0.585	3	2215	1108	0.661	4	2950	1475
0.646	4	2950	1475	0.719	5	3690	1845
0.705	5	3690	1845	0.776	6	4430	2215
0.763	6	4430	2215	0.830	7*	5160	2580
0.816	7	5160	2580	0.873	8	5900	2950
0.868	8*	5900	2950	0.925	9	6640	3320
0.914	9	6640	3320	0.969	10	7390	3695
0.954	10	7390	3695	1.00	**		
1.00	**						

*Wire
**Boundary

Specimen 41941-2B-PL1-2

3-Point Loading
Load   60 Pounds
$k = 0.230 \times 10^{-6}$ fringe/psi
$f = 814$ psi/fringe

Distance From Center 0.04 Inch				Distance From Center 0.10 Inch			
y/h	N	N·f	N·f/2	y/h	N	N·f	N·f/2
0.0197	12	9768	4884	0.0700	9	7326	3663
0.0409	12	9768	4884	0.1184	8	6512	3256
0.0602	11	8954	4477	0.1556	7	5698	2849
0.0733	10	8140	4070	0.1916	6	4884	2442
0.0855	9	7326	3663	0.2283	5	4070	2035
0.1005	8	6512	3256	0.2700	4	3256	1628
0.1178	7	5698	2849	0.3197	3	2442	1221
0.1359	6	4884	2442	0.3937	2	1628	814
0.1602	5	4070	2035	0.4646	*	- -	- -
0.1936	4	3256	1628	0.4747	*	- -	- -
0.2350	3	2442	1221	0.5087	2	1628	814
0.2935	2	1628	814	0.5802	3	2442	1221
0.4006	1	814	407	0.6415	4	3256	1628
0.4699	*	- -	- -	0.7020	5	4070	2035
0.5112	2	1628	814	0.7585	6	4884	2442
0.5747	3	2442	1221	0.8105	7	5698	2849
0.6374	4	3256	1628	0.8614	8	6512	3256
0.6934	5	4070	2035	0.9076	9	7326	3663
0.7493	6	4884	2442	0.9517	10	8140	4070
0.8042	7	5698	2849	0.9898	11	8954	4477
0.8555	8	6512	3256	1.00	**		
0.8991	9	7326	3663				
0.9445	10	8140	4070				
0.9854	11	8954	4477				
1.00	**						

*Wire
**Boundary

146

Specimen 41927-4B-PL1-1

3-Point Loading
$k = 0.240 \times 10^{-6}$ fringe/psi
$f = 785$ psi/fringe

Distance From Center 0.40 Inch				Distance From Center 0.10 Inch			
y/h	N	N·f	N·f/2	y/h	N	N·f	N·f/2
0.0436	11	8650	4325	0.0941	9	7070	3535
0.0786	10	7860	3930	0.1404	8	6290	3145
0.1029	9	7070	3535	0.1820	7	5500	2750
0.1258	8	6290	3145	0.2200	6	4910	2350
0.1484	7	5500	2750	0.2380	*	- -	- -
0.1780	6	4710	2355	0.2595	5	3930	1965
0.2082	5	3930	1965	0.3075	4	3145	1573
0.2235	*	- -	- -	0.3667	3	2358	1179
0.2360	4	3145	1578	0.3900	*	- -	- -
0.2850	3	2358	1179	0.4450	2	1571	786
0.3500	2	1571	786	0.4860	2	1571	786
0.3680	*	- -	- -	0.5870	3	2358	1179
0.4820	2	1571	786	0.6450	*	- -	- -
0.5510	3	2358	1179	0.6610	4	3145	1573
0.6050	*	- -	- -	0.7200	5	3930	1965
0.6130	4	3145	1573	0.7800	6	4710	2350
0.6730	5	3930	1965	0.8450	7*	5500	2750
0.7250	6	4710	2355	0.8920	8	6290	3145
0.789	7*	5500	2750	0.9460	9	7070	3535
0.83	8	6290	3145	1.00	10	7860	3930
0.8830	9	7070	3535				
0.930	10	7860	3930				
0.9880	11	8650	4325				
1.0							

*Wire
**Boundary

3-Point Loading
Load   60 Pounds
$k = 0.240 \times 10^{-6}$ fringe/psi
$f = 706$ psi/fringe

Distance From Center 0.04 Inch				Distance From Center 0.10 Inch			
y/h	N	N·f	N·f/2	y/h	N	N·f	N·f/2
0.0285	13	9178	4589	0.0318	10	7060	3530
0.0514	12	8472	4236	0.0945	9	6354	3177
0.0615	11	7766	3883	0.1314	8	5648	2824
0.0741	10	7060	3530	0.1664	7	4942	2471
0.0877	9	6354	3177	0.2028	6	4236	2118
0.1029	8	5648	2824	0.2220	*	--	--
0.1189	7	4942	2471	0.2382	5	3530	1765
0.1362	6	4236	2118	0.2810	4	2824	1412
0.1630	5	3530	1765	0.3185	*	--	--
0.1960	4	2824	1412	0.330	3	2118	1059
0.2220	*	--	--	0.405	2	1412	706
0.2365	3	2118	1059	0.419	*	--	--
0.2990	2	1412	706	0.485	2	1412	706
0.3168	*	--	--	0.511	*	--	--
0.3945	1	706	353	0.565	3	2118	1059
0.416	1*	706	353	0.624	4*	2824	1412
0.493	2	1412	706	0.685	5	3530	1765
0.505	*	--	--	0.740	6	4236	2118
0.557	3	2118	1059	0.794	7	4942	2471
0.623	4*	2824	1412	0.840	8	5648	2824
0.675	5	3530	1765	0.890	9	6354	3177
0.734	6	4236	2118	0.950	10	7060	3530
0.781	7	4942	2471	0.9930	11	7766	3883
0.830	8	5648	2824	1.00	**		
0.884	9	6354	3177				
0.931	10	7060	3530				
0.986	11	7766	3883				
1.00							

*Wire
**Boundary

Specimen 41933-00-PL1-1

$A = 0.072 \text{ in.}^2$

Tension Loading

Load, pounds	Stress, psi	ΔR (r)	R (r)	Strain, inches	Fringe Order
First Cycle					
0	0	0	119.6		–
42	584	0.20	119.8	0.00081	1
76	1059	0.40	120.0	0.00161	
92	1279				2
108	1500	0.60	120.2	0.00242	
136	1890				3
144	2000	0.80	120.4	0.00322	
177	2460	1.00	120.6	0.00402	
185	2570				4
206	2860	1.20	120.8	0.00483	
210	2920				4.55
183	2540				4
171	2375	1.00	120.6	0.00402	
140	1945	0.80	120.4	0.00322	
130	1808				3
98	1361	0.60	120.2	0.00242	
83	1154				2
70	973	0.40	120.0	0.00161	
36	500				1
31	431	0.20	119.8	0.00081	
0	0	0	119.6		–
Second Cycle					
0	0	0	119.6	– –	–
35	486	0.2	119.8	0.00081	
40	556				1
75	1042	0.4	120.0	0.00161	
85	1180				2

149

Specimen 41933-00-PL1-1

(Concluded)

Load, pounds	Stress, psi	ΔR (r)	R (r)	Strain, inches	Fringe Order
Second Cycle (Continued)					
105	1460	0.6	120.2	0.00242	
132	1835				3
140	1945	0.8	120.4	0.00322	
170	2360	1.0	120.6	0.00402	
237	3295	1.4	121.0	0.00564	
295	3960	1.8	121.4	0.00725	
327	4540	2.0	121.6	0.00805	
360	5000	2.2	121.8	0.00885	
391	5430	2.4	122.0	0.00965	

Specimen 41930-00-PL1-2
A = 0.0619 in.^{2}
Tension Loading

Load, pounds	Stress, psi	ΔR (r)	R (r)	Strain, inches	Fringe Order
First Cycle					
0		0	119.8		
31	501	0.2	120.0	0.00081	
35	566				1
61	986	0.4	120.2	0.00161	
78	1261				2
98	1585	0.6	120.4	0.00242	
130	2100				3
135	2183	0.8	120.6	0.00322	
168	2719	1.0	120.8	0.00402	
174	2814				4
200	3215	1.2	121.0	0.00483	4.53
Second Cycle					
0	0	0	119.8	0	
37	436				1
66	1068	0.4	120.2	0.00161	
86	1390				2
134	2165	0.8	120.6	0.00322	
136	2200				3
177	2860				4

Specimen 41928-00-PL1-1

A = 0.0623 in.
Tension Loading

Load, pounds	Stress, psi	ΔR (r)	R (r)	Strain, inches	Fringe Order
First Cycle					
0	0	0	119.7		
20	323	0.2	119.9	0.00081	
45	726				1
51	824	0.4	120.1	0 00161	1
75	1210	0.6	120.3	0.00242	
88	1420				2
105	1694	0.8	120.5	0.00322	
125	2018	1.00	120.7	0.00402	
137	2210				3
150	2420	1.20	120.9	0.00483	3.13
Second Cycle					
0	0	0	119.7	0	- -
40	645				1
45	726	0.40	120.1	0.00161	
85	1371				2
94	1518	0.80	120.5	0.00322	
129	2080				3
150	2420	1.20	120.9	0.00483	
175	2822				4
203	3275	1.60	121.3	0.00644	
226	3645				5

152

Specimen 41941-00-PL1-1

4-Point Loading
Load 31 Pounds
$M = 23.25$ in.-lb
$I_{xx} = 0.001254$ in.^{4}

Fringe Order	y/h	Distance From Neutral Axis = C	Stress, psi $\sigma = \frac{MC}{I}$
Boundary			4650
5	0.0663	0.218	4045
4	0.1502	0.176	3270
3	0.2315	0.135	2525
2	0.3350	0.0829	1538
1	0.4240	0.0382	709
0	0.5100	0.0052	97
1	0.6000	0.0520	965
2	0.6850	0.0929	1722
3	0.774	0.1372	2548
4	0.856	0.1788	3310
5	0.940	0.221	4100
Boundary	1.00	0.251	4650

REFERENCES

1. Goldberg, R. S. and Chu, H. N.: "Fiber Mechanics of Reinforced Structures," Bulletin of the 3rd Meeting, Working Group on Mechanical Behavior, Volume I, CPIA, November 1964.

2. Frocht, M. M.: Photoelasticity, John Wiley & Sons, Inc., New York.

3. Schmitz, G. K.: Exploration and Evaluation of New Glasses in Fiber Form, Solar San Diego FR No. 2, RDR 1343-6, January-December 1963.

4. ABL/QPR-37 and 39, Status of Research and Engineering Projects, Allegany Ballistics Laboratory, NOrd 1664, March-August 1962.

5. Rosen, B. W.: Tensile Failure of Fibrous Composites, General Electric Co., Missile & Space Division, AIAA, Aerospace Sciences Meeting, Preprint 64-73, NASw-470, New York, New York, January 1964.

6. Schulman, S. E. and J. Epting: A Survey of Test Procedures for Evaluating Short Brittle Fibers, WPAFB--Aeronautical Systems Division, Report ASD-TDR-63-92, May 1963.

7. Hughel, T. J.: "Beryllium - A Space Age Metal," Metals Engineering Quarterly, Volume 2, No. 2, May 1962.

8. Islinger, J. S., K. Gutfreund, I. M. Daniel, and A. J. Durelli: Mechanism of Reinforcement of Fiber-Reinforced Structural Plastics and Composites, Armour Research Foundation, Chicago, Illinois, WADC TR 59-600, Part III, April 1961.

9. R-5853, Technical Summary Report, Research on the Response of Reinforced Solid Propellants, E. L. Alexander, et al., Nonr 3858(00), Prog. NR0064-469, Rocketdyne, a Division of North American Aviation, Inc., Canoga Park, California, September 1964, CONFIDENTIAL.

10. Jessop, H. T. and F. C. Harris: Photoelasticity: Principles and Methods, Cleaver-Hume Press, Ltd., London, 1949.

11. "Graphical and Operational Techniques in Interpreting Stress-Strain Data," Instron Engineering Corporation.

DOCUMENT CONTROL DATA - R&D

(Security classification of title, body of abstract and indexing annotation must be entered when the overall report is classified)

1. ORIGINATING ACTIVITY (Corporate author)	2a. REPORT SECURITY CLASSIFICATION
Rocketdyne	UNCLASSIFIED
A Division of North American Aviation, Inc.	2b. GROUP
Canoga Park, California	N/A

3. REPORT TITLE

Micromechanics of Fiber-Reinforced Composites

4. DESCRIPTIVE NOTES *(Type of report and inclusive dates)*

Technical Report, AFML-TR-65-283, July 1, 1964 to June 30, 1965

5. AUTHOR(S) *(Last name, first name, initial)*

Alexander, E. L.   Hilzinger, J. E.
Caputo, A. A.
Prado, M. E.

6. REPORT DATE	7a. TOTAL NO. OF PAGES	7b. NO. OF REFS
September 1965	155	11

8a. CONTRACT OR GRANT NO.	9a. ORIGINATOR'S REPORT NUMBER(S)
AF 33(615)-1627	
b. PROJECT NO. 7340	AFML-TR-65-283
c. Task 734003	9b. OTHER REPORT NO(S) *(Any other numbers that may be assigned this report)*
d.	

10. AVAILABILITY/LIMITATION NOTICES

Distribution of this report is unlimited.

11. SUPPLEMENTARY NOTES	12. SPONSORING MILITARY ACTIVITY
	Air Force Materials Laboratory
	Plastics & Composites Branch
	Wright-Patterson Air Force Base, Ohio

13. ABSTRACT

Research on the micromechanical behavior of composites reinforced with boron and other fibers is reported. A wide variety of reinforcing elements were used in photoelastic matrix materials to form beams, plates, and three-dimensional microspecimens of varied configurations. The effects of reinforcing element modulus and elongation were investigated in beams in four- and three-point loading. The degree of stiffening derived from various filament reinforcing materials was defined, and different failure mechanisms were investigated.

Reinforced plates were biaxially tested, and fiber unbonding, buckling, and the subsequent stress redistribution were observed photoelastically.

Significant advances in microphotoelasticity are reported. Very small specimens were loaded, and sharp microscopic photoelastic stress patterns (including induced flaw points) were photographed. The filament configurations represent typical laminate geometries, and small flaws were seen to have a remarkably wide field of influence.

DD FORM 1 JAN 64 **1473**

14. KEY WORDS	LINK A		LINK B		LINK C	
	ROLE	WT	ROLE	WT	ROLE	WT
Micromechanics						
Photoelasticity						
Boron reinforced composites						
Biaxial load						
Fiber unbonding and buckling						
Stress distribution						

INSTRUCTIONS

1. ORIGINATING ACTIVITY: Enter the name and address of the contractor, subcontractor, grantee, Department of Defense activity or other organization (corporate author) issuing the report.

2a. REPORT SECURITY CLASSIFICATION: Enter the overall security classification of the report. Indicate whether "Restricted Data" is included. Marking is to be in accordance with appropriate security regulations.

2b. GROUP: Automatic downgrading is specified in DoD Directive 5200.10 and Armed Forces Industrial Manual. Enter the group number. Also, when applicable, show that optional markings have been used for Group 3 and Group 4 as authorized.

3. REPORT TITLE: Enter the complete report title in all capital letters. Titles in all cases should be unclassified. If a meaningful title cannot be selected without classification, show title classification in all capitals in parenthesis immediately following the title.

4. DESCRIPTIVE NOTES: If appropriate, enter the type of report, e.g., interim, progress, summary, annual, or final. Give the inclusive dates when a specific reporting period is covered.

5. AUTHOR(S): Enter the name(s) of author(s) as shown on or in the report. Enter last name, first name, middle initial. If military, show rank and branch of service. The name of the principal author is an absolute minimum requirement.

6. REPORT DATE: Enter the date of the report as day, month, year; or month, year. If more than one date appears on the report, use date of publication.

7a. TOTAL NUMBER OF PAGES: The total page count should follow normal pagination procedures, i.e., enter the number of pages containing information.

7b. NUMBER OF REFERENCES: Enter the total number of references cited in the report.

8a. CONTRACT OR GRANT NUMBER: If appropriate, enter the applicable number of the contract or grant under which the report was written.

8b, 8c, & 8d. PROJECT NUMBER: Enter the appropriate military department identification, such as project number, subproject number, system numbers, task number, etc.

9a. ORIGINATOR'S REPORT NUMBER(S): Enter the official report number by which the document will be identified and controlled by the originating activity. This number must be unique to this report.

9b. OTHER REPORT NUMBER(S): If the report has been assigned any other report numbers (either by the originator or by the sponsor), also enter this number(s).

10. AVAILABILITY/LIMITATION NOTICES: Enter any limitations on further dissemination of the report, other than those imposed by security classification, using standard statements such as:

(1) "Qualified requesters may obtain copies of this report from DDC."

(2) "Foreign announcement and dissemination of this report by DDC is not authorized."

(3) "U. S. Government agencies may obtain copies of this report directly from DDC. Other qualified DDC users shall request through

_____ ."

(4) "U. S. military agencies may obtain copies of this report directly from DDC. Other qualified users shall request through

_____ ."

(5) "All distribution of this report is controlled. Qualified DDC users shall request through

_____ ."

If the report has been furnished to the Office of Technical Services, Department of Commerce, for sale to the public, indicate this fact and enter the price, if known.

11. SUPPLEMENTARY NOTES: Use for additional explanatory notes.

12. SPONSORING MILITARY ACTIVITY: Enter the name of the departmental project office or laboratory sponsoring (paying for) the research and development. Include address.

13. ABSTRACT: Enter an abstract giving a brief and factual summary of the document indicative of the report, even though it may also appear elsewhere in the body of the technical report. If additional space is required, a continuation sheet shall be attached.

It is highly desirable that the abstract of classified reports be unclassified. Each paragraph of the abstract shall end with an indication of the military security classification of the information in the paragraph, represented as (TS), (S), (C), or (U).

There is no limitation on the length of the abstract. However, the suggested length is from 150 to 225 words.

14. KEY WORDS: Key words are technically meaningful terms or short phrases that characterize a report and may be used as index entries for cataloging the report. Key words must be selected so that no security classification is required. Identifiers, such as equipment model designation, trade name, military project code name, geographic location, may be used as key words but will be followed by an indication of technical context. The assignment of links, rules, and weights is optional.